THESIS APPROVAL

GRADUATE SCHOOL, KASETSART UNIVERSITY

Doctor of Engineering (Civil Engineering)

DEGREE

Civil Engineering	Civil Engineering
FIELD	**DEPARTMENT**

TITLE: Modeling Approach for LNAPL Migration Containment using Soil Cement Column

NAME: Mr. Chusak Kererat

THIS THESIS HAS BEEN ACCEPTED BY

_____ **THESIS ADVISOR**

(Associate Professor Suttisak Soralump, Ph.D.)

_____ **THESIS CO-ADVISOR**

(Assistant Professor Apiniti Jotisankasa, Ph.D.)

_____ **THESIS CO-ADVISOR**

(Associate Professor Sanya Sirivithayapakorn, Ph.D.)

_____ **DEPARTMENT HEAD**

(Assistant Professor Wanchai Yodsudjai, D.Eng.)

APPROVED BY THE GRADUATE SCHOOL ON _____

_____ **DEAN**

(Associate Professor Gunjana Theeragool, D.Agr.)

THESIS

MODELING APPROACH FOR LNAPL MIGRATION CONTAINMENT USING SOIL CEMENT COLUMN

CHUSAK KERERAT

A Thesis Submitted in Partial Fulfillment of
the Requirements for the Degree of
Doctor of Engineering (Civil Engineering)
Graduate School, Kasetsart University
2014

Chusak Kererat 2014: Modeling Approach for LNAPL Migration Containment using Soil Cement Column. Doctor of Engineering (Civil Engineering), Major Field: Civil Engineering, Department of Civil Engineering. Thesis Advisor: Associate Professor Suttisak Soralump, Ph.D. 181 pages.

The leakage of hydrocarbons from the underground storage tanks is a significant problem which affects human health and environment. Light nonaqueous phase liquid (LNAPL) migration can widely spread in subsurface, especially in sandy soil layer. Therefore, this study focuses on the behavior of LNAPL migration which is under with and without containment for the case of flow and no flow conditions. The physical models and numerical models were performed to evaluate the performance of a soil cement wall used as containment barrier, the effects of groundwater flow on LNAPL migration and to investigate an appropriated pattern of containment. Gasoline and paraffin liquid were used to represent LNAPL. The 1 g model tests and centrifuge modeling experiments at 30 g were performed as the physical model. Numerical simulations were used for comparing to the physical models and to investigate the appropriated pattern of containment. The model parameters for numerical simulation were determined from laboratory testing.

The results from the 1 g model tests show the correlations of the horizontal distance and the contaminated area between gasoline and paraffin liquid. All tests from centrifuge models show that the water level was depressed due to the large volume of LNAPL confined between the walls. The depth of a soil cement wall should be designed to a greater maximum depth to account for the self-weight of the contaminants and the groundwater flow effects. In addition, numerical simulations were performed and validated with the physical model test results. Both methods showed a good agreement as they provided similar behavior of the LNAPL migration and confirmed the effective performance of the soil cement wall as a containment barrier.

_____ _____ __ / __ / __

Student's signature Thesis Advisor's signature

ACKNOWLEDGEMENTS

I would like to grateful thank and deeply indebted to Assoc.Prof.Dr.Suttisak Soralump my thesis advisor for advice, encouragement and valuable suggestion for completely writing of thesis. I would sincerely like to thank Asst.Prof.Dr. Apiniti Jotisankasa, and Assoc.Prof.Dr.Sanya Sirivithayapakorn, and also Asst.Prof.Dr.Thanadol Kongsomboon and Assoc.Prof.Dr.Supakij Nontananandh from Graduate School for their valuable comments and suggestion. I grateful thank Assst.Prof.Dr.Cheema Soralump for kindly providing the 1g model (tank model) for using in this research and her valuable advice for contamination testing.

I would like to sincerely thank Dr.Inthuorn Sasanakul for kindly providing the RPI centrifuge model test and her suggestion during research work. I would like to grateful indebted to staff of the RPI centrifuge lab for their help with the model design and testing. I am heartfelt thank Alfredo Battitelli for his suggestion about the use of TMVOC simulation and also thank Mr.Wasan Sutthinun and Ms.Jitima Tappanich for their suggestion about the suction test.

The authors would like to thank the Office of the Higher Education Commission, Thailand for the grant fund support under the program Strategic Scholarships for Frontier Research Network for the Joint Ph.D. Program Thai Doctoral degree for this research and also thank Rajamangala University of Technology Rattanakosin for providing funding for this research.

I am especially my parents, my sister, my wife for their continuing encouragements and also my daughter who always gives me heartfelt love during my graduate study.

Chusak Kererat

July, 2014

TABLE OF CONTENTS

Page

LIST OF TABLES

LIST OF TABLES (Continued)

LIST OF FIGURES

LIST OF FIGURES (Continued)

LIST OF FIGURES (Continued)

LIST OF FIGURES (Continued)

LIST OF ABBREVIATIONS

A	=	cross-section of the soil perpendicular to the direction of flow
A_m	=	the area of flow
C_R	=	specific heat of the rock
DM	=	deep mixing
DNAPL	=	dense nonaqueous phase liquid
DSM	=	deep soil mixing
D_{nm}	=	the distance between the nodal points n and m
D_β^κ	=	the molecular diffusion coefficient of κ in the β phase
LNAPL	=	light nonaqueous phase liquid
F_{nm}	=	the average value of the (inward) normal component of F over the surface segment A_{nm} between volume elements V_n and V_m
F^κ	=	the flux of κ through the surface area A_n of V_n
g	=	acceleration due to gravity, cm/s^2
g-level	=	acceleration due to gravity –level
g_{nm}	=	the component of gravitational acceleration in the direction from m to n
i	=	hydraulic gradient
k	=	coefficient of hydraulic conductivity
k-function	=	hydraulic conductivity function
$k_{r\beta}$	=	relative permeability in phase β
K	=	intrinsic (or absolute) permeability, cm^2
K_d	=	the aqueous phase distribution coefficient
K_t	=	the overall heat conductivity coefficient
KU	=	Kasetsart University
M	=	the mass or energy components κ (air, water, chemical or heat) per unit porous media volume (V_n)
M_n	=	the average value of M over V_n
M_V	=	a volume-normalized extensive quantity

LIST OF ABBREVIATIONS (Continued)

n	=	porosity
nm	=	a suitable average at the interface between grid blocks n and m
P	=	the pressure
PCEs	=	polychlorinated biphenyls
q^{κ}	=	the mass or heat generation per unit volume
SM	=	silty sandy soil
SP	=	poorly-graded sandy soil
SSM	=	shallow soil mixing
SWCC	=	soil water characteristic curve
S_{β}	=	the saturation of phase β (i.e., the fraction of pore volume occupied by phase β)
T	=	temperature
TCE	=	trichloroethylene
TMVOC	=	Three-Phase Non-isothermal Flows of multicomponent mixtures of volatile organic chemicals
TOUGH	=	Transport Of Unsaturated Groundwater and Heat
VOCs	=	volatile organic chemicals
V_s	=	volume of solid
V_v	=	volume of void
w/c	=	water cement ratio
X_{β}^{κ}	=	the mole fraction of component κ present in phase β
x_w^{κ}	=	the mole fraction of VOC component κ in the aqueous phase
ρ	=	mass density of the fluid, g/cm^3
ρ_R	=	the density of the rock grains
ρ_w	=	the density of the aqueous phase
ρ_{β}	=	the density of phase β
μ	=	absolute viscosity of the fluid, g/(cm.s)

LIST OF ABBREVIATIONS (Continued)

u_β	=	specific internal energy in phase β (in TMVOC, specific internal energy and enthalpy are expressed in units of J/mole).
Θ	=	Normalized (or Dimensionless) water content
θ_s	=	Saturated volumetric water content
θ_r	=	Residual volumetric water content
ψ	=	Suction
ψ_b	=	Air entry value
λ	=	Pore-size distribution index
α, n, m	=	Three different soil parameters
ϕ	=	porosity

MODELING APPROACH FOR LNAPL MIGRATION CONTAINMENT USING SOIL CEMENT COLUMN

INTRODUCTION

Subsurface contamination is the major public problem caused the geoenvironmental damage. Gas stations, chemical manufacturing and processing facilities, and other facilities which have the underground storage tanks (USTs) for storing hazardous chemicals are resources of contaminants. Many USTs which exceeded or closed to the end of useful life are likely to risk to leakage of toxic constituents. Petroleum hydrocarbons leaking from USTs will likely be found in soils and also in shallow groundwater that they are probably and possibly carcinogenic to humans. They are nearly immiscible in water, namely nonaqueous phase liquids (NAPLs). LNAPLs which have densities less than that of water, always transport through the unsaturated zone and move downward under the gravitational force. If a small volume of LNAPLs is released to the subsoil, it will be retained by capillary forces in the soil pores and may spread laterally as a continuous until movement ceases. If sufficient LNAPL is release, not only retained in the soil pores but also depress the capillary fringe and water table. The retained LNAPL can migrate laterally because some of the LNAPL components can dissolve in the groundwater and move by diffusion and advection with groundwater flow. Additionally, rainfall is a factor to influence LNAPL migration. When it move downward and reach the top capillary fringe or groundwater table, it spread out laterally together with LNAPL migration due to advection process. As the above reason, many remediation methods are proposed to control the releases from leaking USTs and to minimize the risks to human health and the environment. One of these is containment which is a main focus of this study.

Soil cement walls are the structures which are often used to improve the geotechnical properties of soft soil. They can be constructed by two methods as follows: (1) the rotary mixed method, which is the technique preferred for cohesive

soil, with a widespread use in Japan and (2) the jet grouting method, which is a technique used for both cohesive soil and cohesionless soil. The latter method can be used especially for sandy soil where the injection of cement slurry is more effective than in clay. This approach offers the advantage of building wall columns in both vertical and inclined directions by cement based grout. Several researchers (e.g., Gazaway and Jasperse 1992; Dwyer 1997; Bruce 2000; Gurney 2001; Al-Tabbaa and Evans 2003; Kererat and Chaikaew 2009a) have proposed that the soil cement mixing can be used to form a number of containment and remediation systems in geoenvironmental applications. The focus of this study is to investigate the behavior of LNAPL migration in sandy soil deposits contained by soil cement barriers.

Previous studies of LNAPL migration in subsurface soil have been performed by laboratory studies, numerical simulations or field investigations. All of these approaches have their limitations. Laboratory studies are easy to perform but cannot simulate stress conditions and the long term monitoring of LNAPL migration. Numerical simulations have limitations due to a lack of realistic input parameters, while field investigations are costly and time consuming. The geotechnical centrifuge modeling test is a great alternative to these methods because stress conditions can be simulated and long-term migration can be accelerated in the centrifuge. The stress condition is a result of the self-weight of the soil layer involving subsurface transport in three aspects (Taylor, 1995). First, the stress level affects material properties such as porosity and permeability that result in the movement of liquid pollutants through soil. Second, transport problems always occur under gravitational force. Third, geo-environmental problems often involve flow in which capillary rise zones and total potential gradients are governed by gravity. Centrifuge modeling aims to reproduce identical stresses in a model and a corresponding prototype with a small scale, accelerated modeling time; in this manner, the self-weight effects in the prototype can be simulated in the centrifuge modeling, while they cannot be simulated in 1 g modeling (Nakajima *et al.* 1998). Furthermore, centrifuge tests are significantly less expensive than field investigations.

The state of stress in soil mass is a greater influence on permeability and soil water characteristic curve (SWCC) than other effects (Taylor, 1995; Zhou and Yu, 2005). The relative amounts and corresponding pressure of the pore water and pore air phase in soil have a direct impact on the state of stress acting at the particle-particle contacts (Lu and Likos, 2004). SWCC can be used to construct hydraulic conductivity function (k-function). Both SWCC and k-function are the important property for studying the movement of liquid pollutants through unsaturated soil. For saturated soil, the saturated hydraulic conductivity is the property affecting the movement of liquid pollutants. Therefore, the stress levels at different depths and under various gravitational forces affect the movement of liquid pollutants through soil. In addition, Newell *et al*. (1995) presents that the factors affecting the movement of liquid pollutants through soil are as follows: density and viscosity of pollutants, interfacial tension, wettability, capillary pressure, saturation of pores space, and relative permeability.

OBJECTIVES

1. To study the model parameters for numerical simulation and the correlation of LNAPL types between liquid paraffin and gasoline.

2. To study LNAPL migration behavior as a pure liquid in the soil pore in the saturated sandy soil with and without the soil cement barrier including the effect of groundwater flow by using physical model experiment and numerical modeling.

3. To investigate the modeling approach to study LNAPL migration by comparing the results of 1g and 30g simulation under groundwater flow conditions.

4. To investigate the appropriated pattern of containment for using to contain the migration of gasoline in sandy soil area.

Limitations of Work

1. LNAPLs used in small tank model experiment are 91-octane gasoline and paraffin liquid

2. LNAPL used in centrifuge model experiment is paraffin liquid.

3. KU (Kasetsart University) tensiometer is used as an instrument to measure suction of sandy soil and soil cement samples against moisture content.

4. Chonburi soil (SP) and Huahin soil (SM) are used as the representative samples of sandy soil layer for physical tank model experiment.

5. Nevada sand (SP) is used as the representative samples of sandy soil layer for centrifuge model experiment.

6. Soil cement mixing proportion is cement content of 220 kg/m^3 and a water cement ratio (w/c) of 2.

7. The g-level of 30 is used in centrifuge model experiment.

8. This study is not considering the results of evaporation, sorption and dissolution of LNAPL.

LITERATURE REVIEW

1. NAPL Characteristics and Behaviors

Non-Aqueous Phase Liquids (NAPLs) are an organic fluid with low solubility in water and can move as a separate phase. They are widely used in numerous industries, at waste disposal sites and in many locations where have been spilled either accidentally or on purpose. Contamination due to the presence of NAPLs causes an environmental problem and jeopardizes human health; thus, it is important to understand the process of migration of NAPLs to evaluate the potential impacts and to design effective control methods.

Because NAPLs have different chemical and physical characteristics, their behavior and transportation within subsurface also vary. Their density is the main property that influences migration behavior in the subsurface. NAPLs are common grouped into the following two categories based on density:

1.1 LNAPL: Light fluids with a density less than that of water. They float and migrate along the top of the saturated groundwater zone. Examples of LNAPL are gasoline, benzene, and xylene.

1.2 DNAPL: Dense fluids with a density greater than that of water. They can be moved through the groundwater level and progress deeper into the aquifer. Examples of DNAPL are trichloroethylene (TCE) and polychlorinated biphenyls (PCEs).

A NAPL may be a pure chemical or a mixture of substances with different chemical characteristics. Therefore, some NAPL components can be dissolved in the water phase and vaporized in the air phase. Although the concentrations of NAPL components are very small, their toxicity is high. NAPL migration in both water and air is critical. (Mayer and Hassanizadeh, 2005)

Figure 1(a) shows a schematic of LNAPL migration in an unsaturated zone after spills above groundwater level. In an unsaturated zone, it moves downward due to gravity until it reaches the capillary fringe, then it spreads laterally due to the capillary effect. The LNAPL will displace air during migration in an unsaturated zone because the air phase has high mobility due to its low density and viscosity. A contaminant is left as residual NAPL because of immobilization caused by disconnection. The residual contaminant is a long-term source of infiltrating precipitation or a fluctuating water table. If a LNAPL spill is sufficiently large, it may migrate below the capillary fringe and groundwater table. Initially, LNAPL starts accumulating on the capillary fringe under negative pressure relative to atmospheric pressure. If the contaminant continues to accumulate, the pressure becomes positive. When the amount of LNAPL is high enough to overcome the buoyancy and capillary force, it can displace water from the capillary and saturated zone and can penetrate the water table. Consequently, LNAPL can spread laterally along the direction of groundwater flow. Some contaminant may be left in a saturated zone due to the capillary trapping effect. This spreading behavior only occurs in idealized geological conditions. In addition, the configuration of LNAPL depends on various factors as follows: the spill history, liquids properties and geological setting.

Figure 1(b) shows a schematic of DNAPL migration in the unsaturated zone; the spreading behavior of DNAPL is similar to LNAPL migration. Because it has a different density and viscosity, the horizontal spreading is narrow, and it moves downward through groundwater to a less permeable boundary. Some contaminant is retained as residual saturation in both the unsaturated and saturated zones due to the capillary force. (Mayer and Hassanizadeh, 2005)

Table 1 shows the physicochemical composition of water, air and selected NAPLs. Their relative mobility compared to water demonstrates the ability of a liquid to migrate in the subsurface, and the mobility of DNAPL is about twice that of water, which indicates that these liquids are extremely mobile in the subsurface.

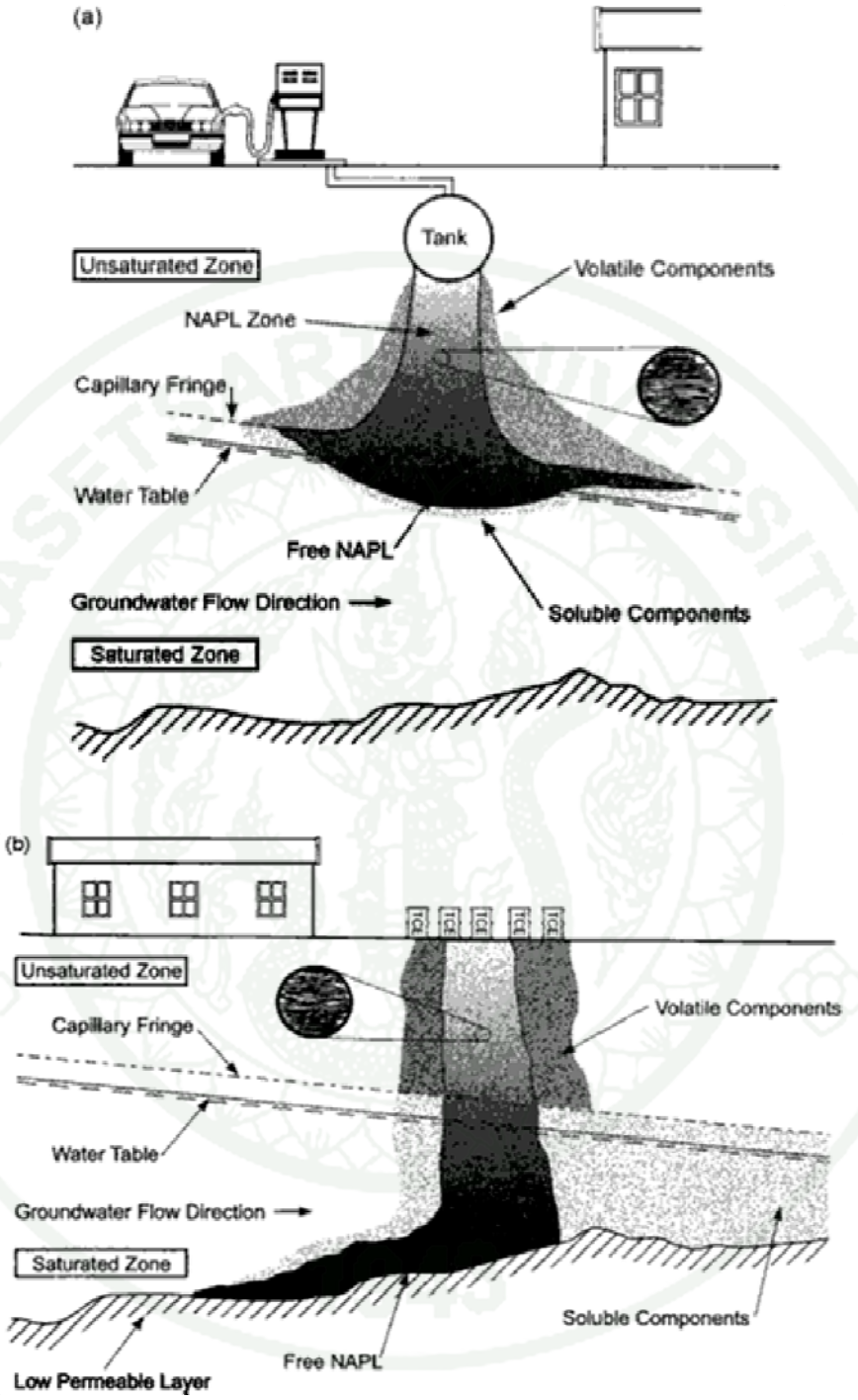

Figure 1 Idealized migration of (a) an LNPL plume and (b) a DNAPL plume

Source: Mayer and Hassanizadeh (2005)

Table 1 Physicochemical parameters for water, air and selected LNAPLs (light gray shading) and DNAPLs (dark gray shading) compounds for the temperature range 20-25 °C

	Density (g/cm^3)	Viscosity (cP)	Relative Mobility to Water	Boiling Point (°C)	Solubility in Water (mg/l)	Vapor pressure (mm Hg)
Water	1.00	1.00	1.00	100	-	24
Air	0.0011	0.0018	0.61	-	-	-
Toluene	0.86	0.55	1.39	111	535	28
Benzene	0.88	0.60	1.32	80	1750	95
o-Xylene	0.88	0.81	1.11	144	175	7
TCB	1.46	0.55	2.39	87	1100	58
TCA	1.35	0.90	1.50	74	1500	123
PCE	1.61	0.84	1.73	121	200	17

Source: Mayer and Hassanizadeh (2005)

Li, Y (2005) has shown that an LNAPL in the subsurface exists in up to four different states. Some may exist as a pure liquid in the soil pores, which is called residual saturation; some may evaporate, which is called volatilization; some may be adsorbed to the surface of the soil particles, which is called sorption; and some may be dissolved in the groundwater, which is called dissolved plume.

Newell *et al.* (1995) show that the factors that affect NAPL migration in the subsurface are as follows: density (LNAPL or DNAPL), viscosity (governs mobilizes in subsurface), interfacial tension (pore scale effect), wettability (affinity of soil for fluids), capillary pressure (pressure across an interface), saturation (fraction of pore space containing fluid), and relative permeability (function of saturation).

2. Basic Fluid Mechanics in Porous Media

2.1 Porous Media

Corey (2003) mentioned that porous media could be applied to all matter because (1) the non-solid space within the solid matrix is interconnected; (2) the smallest dimension of non-solid space must be large enough to contain fluid particles, that is, it must be large compared to the mean-free path of fluid molecules; and (3) the dimensions of the non-solid space must be small enough such that when interfaces between two fluids occur within the non-solid space, the orientation of the interfaces is controlled primarily by interfacial forces.

Nield and Began (2006) described the porous media that consist of the materials in a solid matrix with an interconnected void. The solid matrix may be either rigid (the typical situation) or subject to small deformations. The interconnectedness of the voids (the pores) allows the flow of one or more fluids through the materials. In the simplest situation (single-phase flow), the void is saturated by a single fluid. In "two-phase flow," a liquid and gas share the void space. In the natural porous media, the distribution of pores with respect to shape and size is irregular, and the flow quantities (e.g., velocity and pressure) are clearly irregular. However, in typical experiments, the quantities of interest are measured over areas that cross many pores, and such space-averaged quantities change a regular manner with respect to space and time.

2.2 Porosity

The porosity (n) of a porous medium is defined as the fraction of the total volume of the medium that is occupied by void space. Then, 1-n is the fraction occupied by solids, as shown in Figure 2. For an isotropic medium, the surface porosity (that is, the ratio of void area to total area of a typical cross section) is normally equal to n.

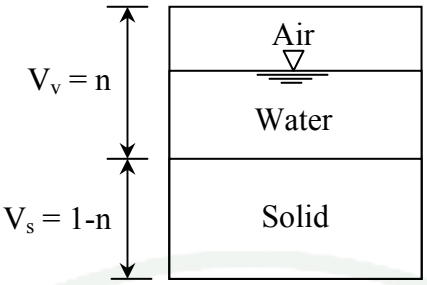

Figure 2 Porosity of a porous medium

The porosity (n) is assumed that all of the void space is connected. If some of the pore space in the medium is disconnected, then the porosity introduces an effective porosity, which is defined as the ratio of connected void to total volume.

For natural media, n does not normally exceed 0.6. Nonuniform grain sizes tend to lead to smaller porosity than uniform grain sizes because smaller grains fill the pores formed by larger grains. Table 2 shows a compilation of porosities and other properties of common porous materials.

Corey (2003) described the following factors that affect porosity:

2.2.1 Structure - Media with structure have larger porosity than media without structure.

2.2.2 Grain shape - A medium consisting of flat platelets can be packed such that the porosity is much smaller than that for a collection of spheres. However, it is also possible to stack the platelets so that the porosity is much greater than that for spheres.

2.2.3 Grain size distribution - A medium consisting of spheres of varying sizes normally has a smaller porosity than one consisting of more uniform spheres. The smaller spheres may fit into spaces between larger spheres, which reduce the porosity.

2.2.4 Mixing - A medium mixed with two different sizes of spheres has a low porosity. However, if the two different sizes are segregated into different regions, the porosity is same as that for a single-size medium.

2.2.5 Packing - The mechanical processes can affect the arrangement of soil particles: for example, particles settled out of water, deposited by wind or deposited by a geological process.

2.2.6 Cementation - The volume of cementing materials, which may have precipitated from the solution after the particles were deposited, reduces the porosity. Therefore, consolidated sandstones typically have smaller porosities than unconsolidated sand deposits.

Table 2 Properties of common porous materials

Materials	Porosity (n)	Permeability, K (cm^2)	Surface per unit volume (cm^{-1})
Agar-agar		$2x10^{-10}$-$4.4x10^{-9}$	
Black slate powder	0.57-0.66	$4.9x10^{-10}$-$1.2x10^{-9}$	$2x10^{3}$-$8.9x10^{3}$
Brick	0.12-0.34	$4.8x10^{-10}$-$2.2x10^{-9}$	
Catalyst (Fischer-Tropsch, granules only)	0.45		$25.6x10^{5}$
Cigarette		$1.1x10^{-5}$	
Cigarette filters	0.17-0.49		
Coal	0.02-0.12		
Concrete (ordinary mixes)	~ 0.1		
Concrete (bituminous)		$1x10^{-9}$-$2.3x10^{-7}$	
Copper powder (hot-compacted)	0.09-0.34	$3.3x10^{-6}$-$1.5x10^{-5}$	
Cork board		$2.4x10^{-7}$-$5.2x10^{-7}$	560-770
Fiberglass	0.88-0.93		
Granular crushed rock	0.45		
Hair (on mammals)	0.95-0.99		
Hair left		$8.3x10^{-6}$-$1.2x10^{-5}$	

Table 2 (Continued)

Materials	Porosity (n)	Permeability, K (cm^2)	Surface per unit volume (cm^{-1})
Leather	0.56-0.59	$9.5x10^{-10}$-$1.2x10^{-9}$	$1.2x10^{4}$-$1.6x10^{4}$
Limestone (dolomite)	0.04-0.10	$2x10^{-11}$-$4.5x10^{-10}$	
Sand	0.37-0.50	$2x10^{-7}$-$1.8x10^{-6}$	150-220
Sandstone ("oil sand")	0.08-0.38	$5x10^{-12}$-$3x10^{-8}$	
Silica grains	0.65		
Silica powder	0.37-0.49	$1.3x10^{-10}$-$5.1x10^{-10}$	$6.8x10^{3}$-$8.9x10^{3}$
Soil	0.43-0.54	$2.9x10^{-9}$-$1.4x10^{-7}$	
Spherical pickings (well shaken)	0.36-0.43		
Wire crimps	0.68-0.76	$3.8x10^{-5}$-$1x10^{-4}$	29-40

Source: Nield and Began (2006)

2.3 General Equation for Groundwater Flowing through Soil

2.3.1 Basic Relationship

For the one-dimensional flow of water in both saturated and unsaturated soil, Darcy's law, which can be written as follows, is applied:

$$q = kiA \quad (1)$$

The hydraulic conductivity (k) has the units of velocity, such as cm/s or mm/s, and is a measure of the resistance of the soil to water flow. When the properties of water affecting the flow are included, k may be written as

$$k\,(cm/s) = \frac{K\rho g}{\mu} \quad (2)$$

From Figure 3, Laplace's Equation for three dimensions can be derived as follows.

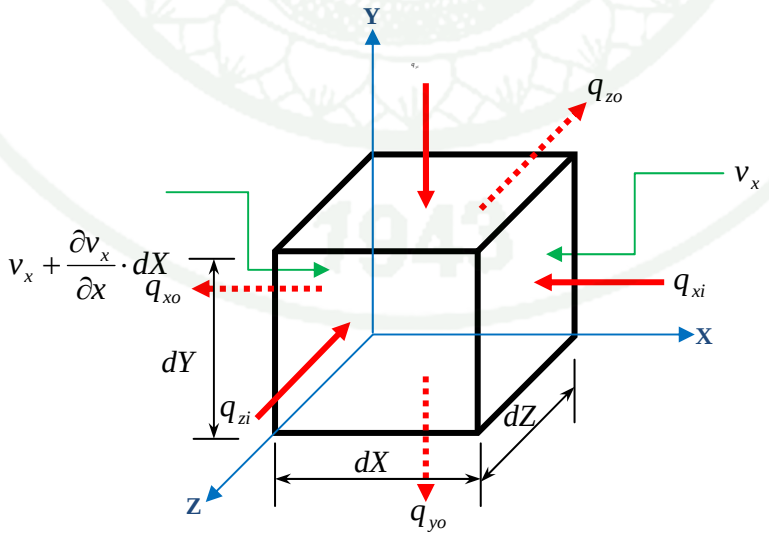

Figure 3 An elementary soil prism

In a typical mass balance analysis, the net flow of mass through the boundary of the fixed control volume element is equated to the (time) rate of change of mass within the element:

Mass flow in – Mass flow out = Rate of change of mass (3)

Darcy's law can be expressed as follows:

Flow in (X, Y and Z directions):

$$\left.\begin{aligned} q_{xi} &= v_x \cdot A = v_x \cdot dY \cdot dZ \\ q_{yi} &= v_y \cdot A = v_y \cdot dX \cdot dZ \\ q_{zi} &= v_z \cdot A = v_z \cdot dX \cdot dY \end{aligned}\right\} \quad (4)$$

Flow out (X, Y and Z directions):

$$\left.\begin{aligned} q_{xo} &= \left(v_x + \frac{\partial v_x}{\partial x} dX\right) dY \cdot dZ \\ q_{yo} &= \left(v_y + \frac{\partial v_y}{\partial y} dY\right) dX \cdot dZ \\ q_{zo} &= \left(v_z + \frac{\partial v_z}{\partial z} dZ\right) dX \cdot dY \end{aligned}\right\} \quad (5)$$

Determine net flow in each direction as follows:

$$\left.\begin{aligned} Net\ q_x &= q_{xi} - q_{xo} = -\frac{\partial v_x}{\partial x} dX \cdot dY \cdot dZ \\ Net\ q_y &= q_{yi} - q_{yo} = -\frac{\partial v_y}{\partial y} dX \cdot dY \cdot dZ \\ Net\ q_z &= q_{zi} - q_{zo} = -\frac{\partial v_z}{\partial z} dX \cdot dY \cdot dZ \end{aligned}\right\} \quad (6)$$

Determine total net flow as follows:

$$\begin{aligned} Total\ Net\ q &= \sum\left(Net\ q_x + Net\ q_y + Net\ q_z\right) \\ &= \frac{\partial\theta}{\partial t} dX \cdot dY \cdot dZ \end{aligned} \tag{7}$$

From Darcy's law $(v = ki)$,

$$\left.\begin{aligned} v_x &= k_x \frac{\partial h}{\partial x} \\ v_y &= k_y \frac{\partial h}{\partial y} \\ v_z &= k_z \frac{\partial h}{\partial z} \end{aligned}\right\} \tag{8}$$

Substituting equation (6) and equation (8) into equation (7), the general Laplace's Flow Equation is obtained;

$$-\left(\frac{\partial v_x}{\partial x} + \frac{\partial v_y}{\partial y} + \frac{\partial v_z}{\partial z}\right) dX \cdot dY \cdot dZ = \frac{\partial\theta}{\partial t} dX \cdot dY \cdot dZ$$

$$k_x \frac{\partial^2 h}{\partial x^2} + k_y \frac{\partial^2 h}{\partial y^2} + k_z \frac{\partial^2 h}{\partial z^2} = -\frac{\partial\theta}{\partial t} \tag{9}$$

2.3.2 Equation for Steady State Flows (Flow in = Flow out)

For saturated flow, the water content does not change with time (ignoring the compressibility of water and soil); thus,

$$\frac{\partial\theta}{\partial t} = 0$$

Therefore, equation (9) becomes

$$k_x \frac{\partial^2 h}{\partial x^2} + k_y \frac{\partial^2 h}{\partial y^2} + k_z \frac{\partial^2 h}{\partial z^2} = 0 \quad (10)$$

2.3.3 Equation for Unsteady State Flows

For transient (i.e., unsteady) flow, the water content would change with time (flow in ≠ flow out); thus,

$$\frac{\partial \theta}{\partial t} \neq 0$$

where θ = Volumetric water content

The phase relationship can be expressed as

$$\theta = \frac{S \cdot e}{1 + e_o} \quad (11)$$

Therefore,

$$\frac{\partial \theta}{\partial t} = \frac{\partial}{\partial t}\left(\frac{S \cdot e}{1 + e_o}\right) \quad (12)$$

Substituting equation (12) into equation (9), Laplace's Flow Equation for unsteady state flows is obtained:

$$k_x \frac{\partial^2 h}{\partial x^2} + k_y \frac{\partial^2 h}{\partial y^2} + k_z \frac{\partial^2 h}{\partial z^2} = \frac{1}{1 + e_o}\left(e \cdot \frac{\partial S}{\partial t} + S \cdot \frac{\partial e}{\partial t}\right) \quad (13)$$

This equation shows that the soil water characteristics and the hydraulic conductivity relationship affect water flowing in unsaturated soil.

3. Soil Water Characteristic Curve (SWCC)

SWCC explains the water holding capacity in the soil under different matrix suction levels. The water content can be defined as the amount of the water contained within the pores of the soil. In geotechnical engineering, the gravimetric water content is commonly used; it is a ratio of the mass of water to the mass of solids and pore air pressure and is defined as equal to zero. However, in soil science, the volumetric water content is commonly used; it is the ratio of the volume of water to the total volume of soil, and the soil pore pressure of unsaturated soil is always negative (less than atmospheric pressure). The negative pressure is called suction, and it can be expressed as in equation (14).

$$\text{Matrix suction} = u_a - u_w \quad (14)$$

SWCC can be used to derive the unsaturated soil property functions for the coefficient of permeability, shear strength and volume change. (Barbour, 1998; Fledlund *et al.*, 2000)

3.1 Features of SWCC

The typical SWCC of unsaturated soil can be divided into three stages, which are related to the process of desaturation, as shown in Figure 4 (Vanapalli *et al.*, 1996; Sillers *et al.*, 2001). The desaturation process can be described as follows:

3.1.1 Capillary saturation zone: the pore-water is in tension in this zone; however, the soil remains essentially saturated due to capillary forces. The capillary saturation zone continues up to the air entry value or bubbling pressure, $(u_a - u_w)_b$, of the soil where air starts to enter the largest size pores.

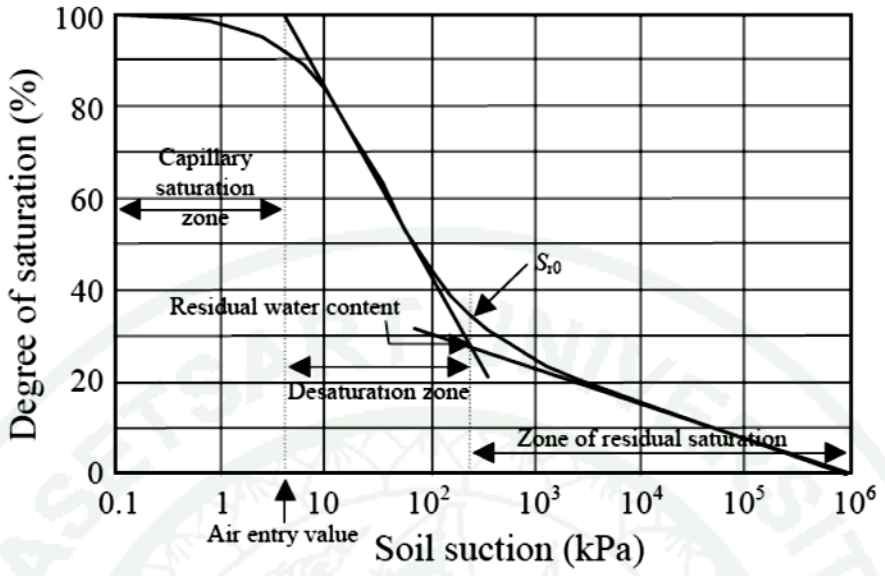

Figure 4 SWCC illustrating the regions of desaturation

Source: Sillers *et al.* (2001)

3.1.2 Desaturation or funicular zone: the liquid water within the pores is increasingly displaced by air in the desaturation zone. The desaturation zone ends when only residual water content, yr, is present, which is, pore water becomes essentially immobile within the soil matrix. Increases in soil suction do not result in significant changes in water content.

3.1.3 Residual saturation zone: the liquid water is tightly held to the soil, and moisture movement occurs mainly as vapor flow. There is little hydraulic flow of water through the pores; however, there may be some water movement in the form of film flow (Huang *et al.*, 1994). In the residual zone, the soil suction loses its physical significance and can then be better regarded as an equivalent term for the energy required to withdraw water from a unit mass of soil. The residual saturation zone is terminated when oven dry conditions exist (i.e., water content equals zero), which corresponds to a soil suction of approximately 1,000,000 kPa (Croney and Coleman, 1961). Water not driven off under these conditions is chemically bonded to the soil

and should not have a significant effect on the engineering behavior of the soil (Mitchell, 1976).

Tuller and Or (2004) described the SWCC as an important hydraulic property that has a significant effect on soil texture and soil structure as well as other constituents, including organic matter. The solute and contaminant transport in the environment must be predicted to determine the SWCC. They show typical SWCCs for soils with different textures to demonstrate the effect of porosity (saturated water content) and the varied slopes of the relationships resulting from variable pore-size distributions, as shown in Figure 5. In addition, Zhou and Yu (2005) found that water content and stress state have a greater influence on the SWCC than other effects, but their influence tends to decrease when suction increases.

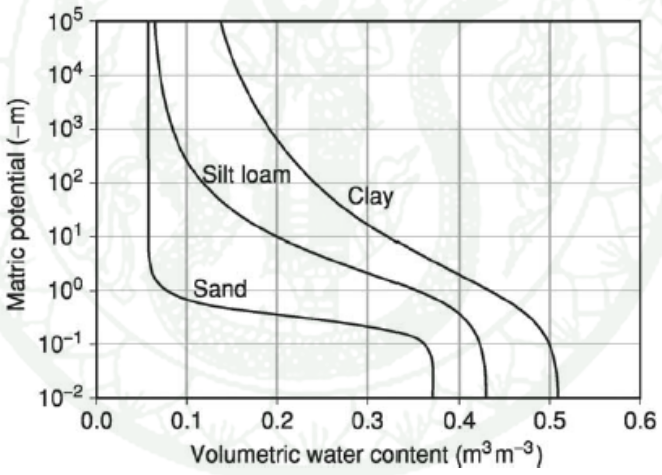

Figure 5 Typical soil-water characteristic curves for soils of different texture

Source: Tuller and Or (2004)

Under hysteresis conditions, the SWCC consists of two curves: the drying curve, or desorption process, and the wetting curve, or adsorption process, as shown in Figure 6. The desorption process shows that when the water is drained out or evaporated from the soil, the water content decreases and suction increases. The adsorption process shows that when the water infiltrates the soil, the water content

increases, and the suction decreases. The hysteresis loop indicates that the SWCC is not unique and should be taken into account in several steps when it is applied to geotechnical engineering problems. The initial wetting and drying curves form the boundaries of the SWCC. In addition, there are numerous immediate (drying and wetting) scanning curves that are asymptotic to the boundary curve (Fredlund, 2002).

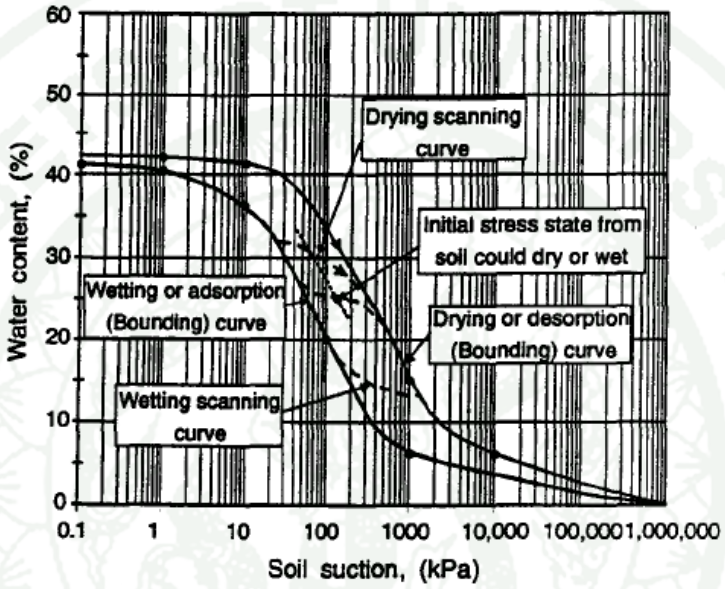

Figure 6 Description of hysteresis loop of SWCC

Source: Fredlund (2002)

3.2 Methods for measuring soil suction

Total suction comprises two components: matric suction and osmotic suction. The measurement of suction can be divided into two methods: the direct method and indirect method. The direct method is used to determine matric suction, and the indirect method is used to determine matric suction, including osmotic suction. Because this study only used a tensiometer to measure suction, consequently, suction will only be described based on the information provided by the tensiometer.

Pan *et al.* (2010) described a tensiometer as an instrument that is normally used to measure directly the negative pore-water pressure of soil. The basic concept is that the pressure of the water contained in a high air entry material will come to equilibrium with the soil water pressure to make it possible to measure negative soil water pressures. This instrument cannot measure osmotic suction because a true semi-permeable membrane for soluble salts does not exist in a tensiometer. Thus, the measurement only provides the value of the matric suction in the soil. A small ceramic cup is attached to a tube filled with de-aired water, which is connected to a pressure measuring device. Before a measurement can be collected, the ceramic cup and tube must be saturated by filling them with water and applying a vacuum to the tubing. Allowing the ceramic tip to dry reduces the water pressure in the sensor and removes any air bubbles that appear. Due to the cavitation problem, a ceramic cup with a higher air entry value is used to improve the tensiometer technique by increasing the matric suction above 100 kPa. However, the air in the sensor will result in poor or less negative measurements of the pore water pressure for the following reasons: (a) water vaporizes as the soil water pressure approaches the vapor pressure of water at the ambient temperature; (b) air in soil can diffuse through the ceramic material; and (c) air comes out of solution as the water pressure decreases. In addition, Pan *et al.* (2010) summarize the suction measurement methods as shown in Table 3.

Ridley and Burland (1993) developed tensiometers, called suction probes, as shown in Figure 7. They used the tensiometers to perform a triaxial compression test. The device was introduced to overcome the problem of cavitation associated with conventional tensiometers when the measured suction exceeds 100 kPa. They suggested that tensiometer should have the following characteristics: (a) an air-entry of the ceramic cup of 15 bars, (b) a small probe made of stainless steel or glass, and (c) calibration should be completed before use by injecting water through the ceramic cup into the probe at 20 bars for 2 days. The suction probe can measure suction up to approximately 1500 kPa for relatively long periods of time (i.e., more than 1 month).

Jotisankasa *et al.* (2007) developed miniature tensiometers at Kasetsart University. They propose two types of tensiometers: one that measures suction below 1 bar and one that measures suction up to 3 bars, as shown in Figure 8. These devices have been used to measure in-situ suction and to determine soil water retention curves. In addition, miniature tensiometers can be applied to measure suction during an unconfined compression test to determine the effective strength parameters of soft Bangkok clay. From the results, miniature tensiometers can be used to investigate the behavior of both fully saturated and unsaturated soil.

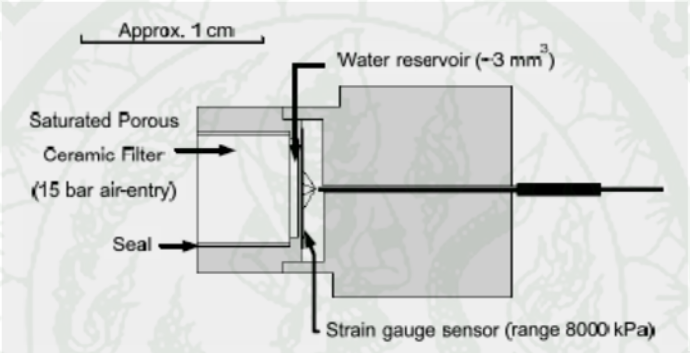

Figure 7 An Imperial College tensiometer or suction probe

Source: Ridley and Burland (1993)

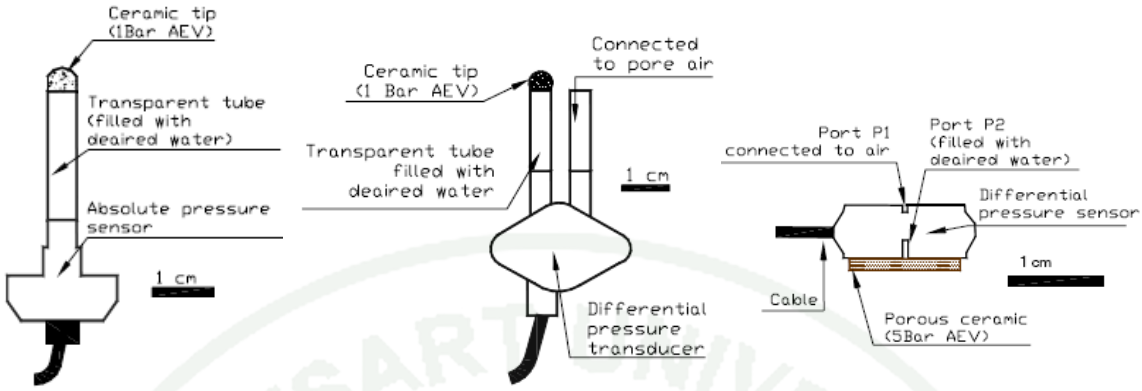

(a) (b) (c)

Figure 8 KU-tensiometer (a) low-suction absolute, (b) low-suction differential, and (c) high-suction differential

Source: Jotisankasa *et al.* (2007)

Table 3 Summary of suction measurement methods

		Technique (Method)	Suction range (kPa)	Equilibrium time
Direct suction measurement	Matric suction	axis-transition technique	0-1500	hours
		tensiometer		hours
		suction probe		minutes
Indirect suction measurement	Matric suction	time domain reflectometry	0-1500	hours
		electrical conductivity sensor	50-1500	6-50 hours
		thermal conductivity sensor	0-1500	hours-days
		in-contact filter paper	all	7-14 days
	Osmotic suction	squeezing technique	0-1500	Days
	Total suction	psychrometer technique	100-10000	1 hour
		relative humidity sensor	100-8000	hours-days
		chilled-mirror hygrometer	150-30000	10 minutes
		non-contact filter paper	all	7-14 days

Source: Pan *et al.* (2010)

3.3 Models of SWCC

Numerous equations have been proposed to simulate the SWCC. Most SWCC equations or models are empirical in nature and are based on the shape of the SWCC. However, even though most SWCCs are sigmoidal in nature, the equations do not produce sigmoidal curves (Leong and Rahardjo, 1997). In this study, two models of curve fitting, which are described as follows, are used.

3.3.1 Brook and Corey (1964)

Brooks and Corey are the first to propose equation for SWCC, and the curve is assumed to be an exponentially decreasing function of water content at soil suctions greater than the air-entry value and to remain the same for suction less than the air-entry value. In addition, the model is not suitable for a degree of saturation less than the residual value (Brooks and Corey, 1964). Based on the above observations, the model is more suitable for coarse-grained soils than fine-grained soils (Fredlund and Xing, 1994). The equation is given as follows:

$$\Theta = \frac{\theta - \theta_r}{\theta_s - \theta_r} = \left(\frac{\psi_b}{\psi}\right)^{\lambda} \quad (15)$$

The degree of saturation (S) has also been used as a substitute for normalized water content, which has been verified through several studies (Campbell, 1974; Clapp and Hornberger, 1978; Gardner *et al*., 1970a, 1970b; Rogowski, 1971; Williams *et al*., 1983; McCuen *et al*., 1981)

3.3.2 van Genuchten (1980)

The van Genuchten model is widely used to understand unsaturated soil behavior. The model is continuous and fits the SWCC over the entire range of soil suction with fitting parameters (α, n, and m). The model is given as follows:

$$\Theta = \left[\frac{1}{1+(\alpha h)^n}\right]^m \quad (16)$$

This form of the equation provides more flexibility than the previous equation described. To obtain a closed-form expression for hydraulic conductivity, van Genuchten (1980) related m and n through the equation m = (1-1/n). The α parameter is related to the air entry value; the n parameter is related to the pore size distribution of soil; and the m parameter is related to asymmetry of the model. If n is small, the slope of the SWCC is steep; otherwise, if n is high, the slope of the SWCC is shallow.

From equations (15) and (16), the van Genuchten model can be written in another form as follows:

$$\theta = \left[\frac{1}{1+(\alpha h)^n}\right]^m (\theta_s - \theta_r) + \theta_r \quad (17)$$

Stankovich and Lockington (1995) compare the plot of the SWCC used by the Brooks and Corey model (1964) and that of the van Genuchten model (1980). They suggested that both the Brooks and Corey model (1964) and van Genuchten model (1980) are more accurate for non-clayey soils (with a relatively narrow pore-size distribution) than for clayey soils.

Fredlund and Xing (1994); Zapata *et al.* (2000) and Sillers *et al.* (2001) summarized the SWCC equation used to fit the experimental data as shown in Table 4.

Table 4 Soil water characteristic curve used to fit experimental data

References	Equation	Parameter description
Fredlund and Xing (1994) (F & X)	$\theta_w = C(h)\left[\frac{\theta_s}{\left[ln\left[\exp(1)+\left(\frac{h}{a}\right)^b\right]\right]^c}\right]$ $C(h) = \left[1 - \frac{ln\left(1+\frac{h}{h_r}\right)}{ln\left(1+\frac{10^6}{h_r}\right)}\right]$	θ_w = volumetric water content a = a soil parameter that is primarily a function of the air entry value of the soil in kPa. b = a soil parameter that is primarily a function of the rate of water extraction from the soil, once the air entry value has been exceeded. c = a soil parameter that is primarily a function of the residual water content. h_r= a soil parameter in kPa that is primarily a function of the suction at which residual water content occurs.
van Genuchten (1980) (van G.)	$\theta_w = \theta_r + \frac{\theta_s - \theta_r}{\left[1+\left(\frac{h}{a}\right)^b\right]^c}$	θ_r = residual volumetric water content a = a soil parameter in kPa that is primarily a function of the air entry value of the soil. b = a soil parameter that is primarily a function of the rate of water extraction from the soil, once the air entry value has been exceeded.

Table 4 (Continued)

References	Equation	Parameter description
		c = a soil parameter that is primarily a function of the residual water content.
McKee and Bumb (1987)	$\theta_w = \theta_r + \frac{\theta_s - \theta_r}{1+\exp(1)^{\left[\frac{(h-a)}{b}\right]}}$	θ_r = residual volumetric water content a = curve fitting parameter b = curve fitting parameter
van Genuchten and Mualem (1980) (van G. & M)	$\theta_w = \theta_r + \frac{\theta_s - \theta_r}{\left[1+\left(\frac{h}{a}\right)^{bm}\right]^{\left(1-\frac{1}{bm}\right)}}$	θ_r = residual volumetric water content a = a soil parameter in kPa that is primarily a function of the air entry value of the soil. b_m= a soil parameter that controls the slope at the inflection point in the soil-water characteristic curve.
van Genuchten and Burdine (1980) (van G. & B)	$\theta_w = \theta_r + \frac{\theta_s - \theta_r}{\left[1+\left(\frac{h}{a}\right)^{b}\right]^{\left(1-\frac{2}{b}\right)}}$	θ_r = residual volumetric water content a = a soil parameter in kPa that is primarily a function of the air entry value of the soil b = a soil parameter that is primarily a function of the rate of water extraction from the soil, once the air entry value has been exceeded.

Table 4 (Continued)

References	Equation	Parameter description
Gardner (1958)	$\theta_w = \theta_r + \frac{\theta_s - \theta_r}{1+\left(\frac{h}{a}\right)^b}$	θ_r = residual volumetric water content a = a soil parameter in kPa that is primarily a function of the air entry value of the soil b = a soil parameter that is primarily a function of the rate of water extraction from the soil, once the air entry value has been exceeded.
Brooks and Corey (1964) (B & C)	$\theta_w = \theta_r + (\theta_s - \theta_r)\left(\frac{a_b}{h}\right)^{b_b}$	θ_r = residual volumetric water content a_b = bubbling pressure in kPa. b_b = pore size index
Williams *et al*. (1983)	$\ln \Theta_e = A + B \ln h$	a = fitting parameter b = fitting parameter
Farrel and Larson (1972)	$h = (u_a - u_w)_b \exp[\alpha(\theta_s - \theta_w)]$	α= empirical constant $(u_a\text{-}u_w)_b$ = air-entry value

Table 4 (Continued)

References	Equation	Parameter description
Assouline *et al*. (1998)	$\theta_w = \theta_L + (\theta_s - \theta_L)\left[1 - exp\left[-\xi\left(\frac{1}{\psi} - \frac{1}{\psi_L}\right)^{\eta}\right]\right]$	ψ = capillary head ψ_L = capillary head that corresponds to a very low water content at which the hydraulic conductivity is negligible θ_L = volumetric water content at capillary head ψ_L η = fitting parameter ξ = fitting parameter

Source: Fredlund and Xing (1994); Zapata *et al.* (2000) and Sillers *et al.* (2001)

3.4 Models of Permeability

The hydraulic conductivity (k) of an unsaturated soil is not constant. Lu and Likos (2004) described it as a function of material variables that depend on the pore structure (e.g., void ratio and porosity), the pore fluid properties (e.g., density and viscosity), and the amount of pore fluid in the system (e.g., water content and degree of saturation). The hydraulic permeability function is typically shown in terms of matric suction head, degree of saturation or volumetric water content.

The hydraulic conductivity function can be described using a conceptual model, as shown in Figure 9, which illustrates a series of cross section areas for a rigid mass of relatively coarse grained soil (e.g., sand). The soil is fully saturated in

Figure 9(a) and allowed to drain under increasing suction, as shown in Figure 9(b) and Figure 9(c). Finally, a residual condition in Figure 9(d) is reached. The SWCC and hydraulic conductivity function corresponding to these four saturation conditions are illustrated in Figures 10(a) and 10(b) (Lu and Likos, 2004).

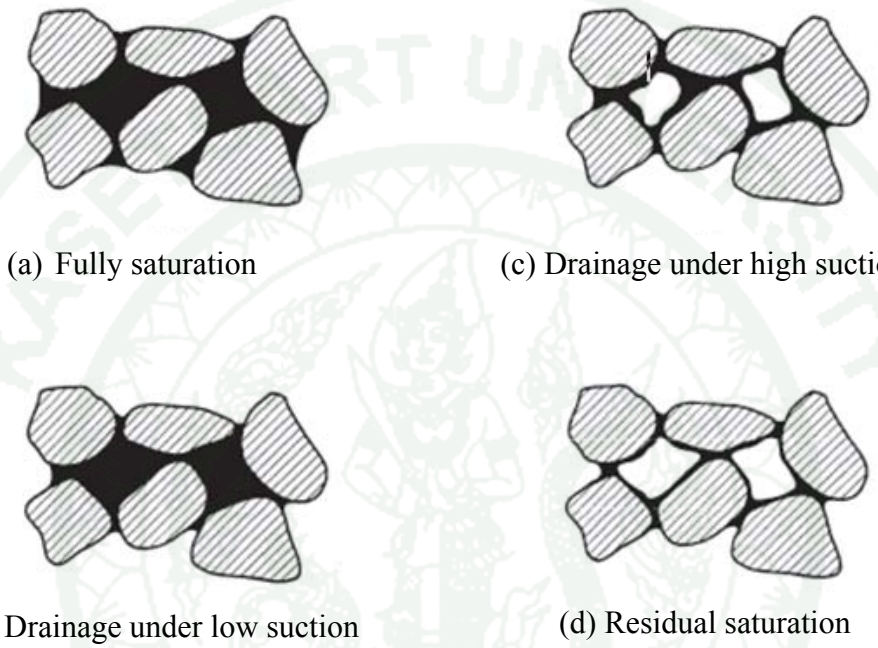

(a) Fully saturation

(c) Drainage under high suction

(b) Drainage under low suction

(d) Residual saturation

Figure 9 Conceptual distributions of pore water and pore air in a cross-sectional area of a rigid soil matrix during the drainage process

Source: Lu and Likos (2004)

In the current study, Jackson (1972) formalism was used to predict the unsaturated hydraulic conductivity function from the SWCC. He proposed methods for calculating the hydraulic conductivity of unsaturated soil from SWCC that have been used by several researchers, but the Marshall (1985), and Millington and Quirk (1959) methods are the easiest to employ because they use conductivity values. Both methods proposed equations based on the following equation:

$$k_i = \frac{30\gamma^2}{\rho g \eta} \frac{\in_i^p}{n^2} \sum_{j=i}^{m} [(2j+1-2i)h_j^{-2}] \quad (18)$$

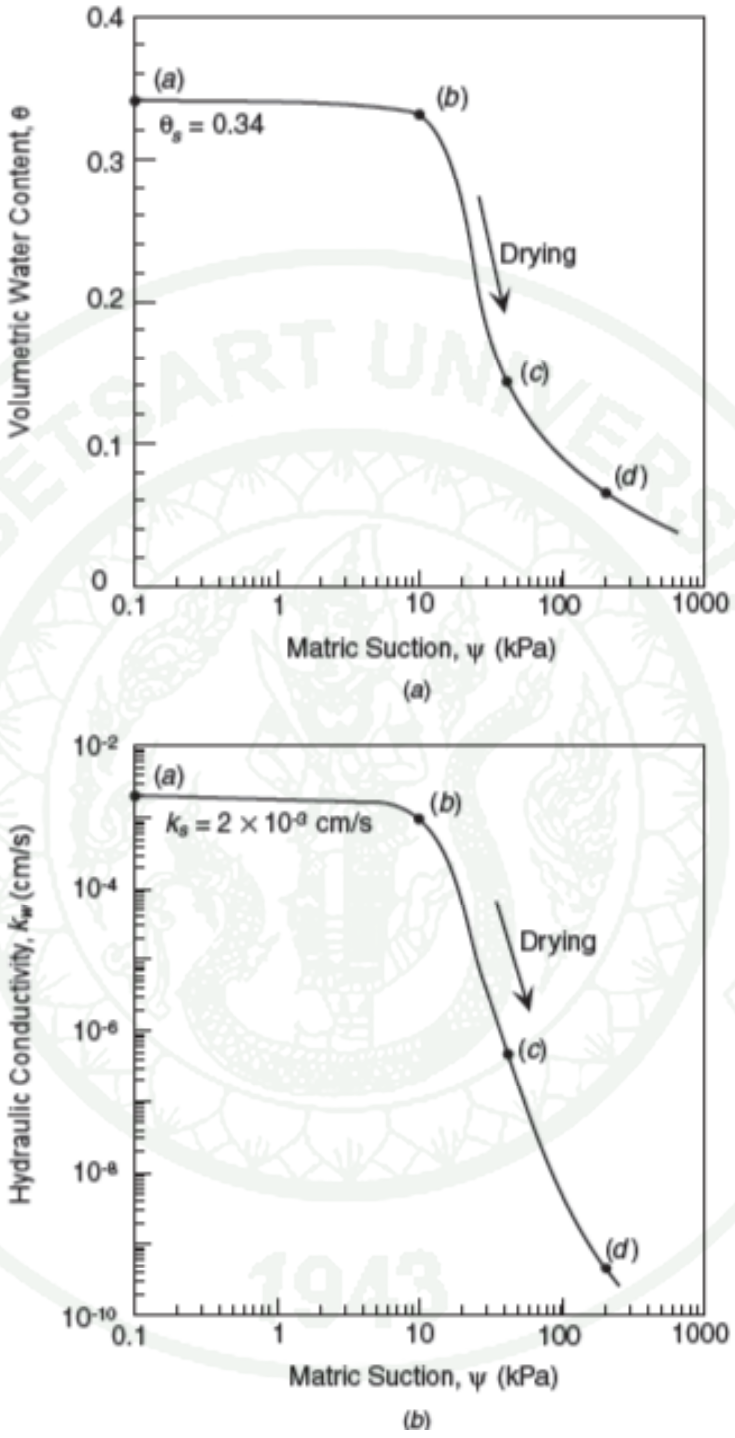

Figure 10 (a) Conceptual soil-water characteristic curve and (b) hydraulic conductivity function corresponding to saturation conditions for the rigid soil matrix shown in Figure 9

Source: Lu and Likos (2004)

where k_i is the hydraulic conductivity (cm/min) corresponding to the i^{th} water content increment, γ is the surface tension of water, ρ is the density of water, g is the gravitational constant, and η is the viscosity. The number 30 is a composite of the constant 1/8 from Poiseuille's equation, 4 from the square of $r = 2\gamma/h$, where r is the pore radius, and 60, which converts the units from seconds to minutes. The term $\in$ represents the water-filled porosity, which is usually taken as the volumetric water content, and n equal water content increases. The exponent of $\in$, p, is a constant, and its value depends on the method of computation. The summation indices are j and i, and m is the number of increases for which the calculation is to be made.

From equation (18), both the M and MQ methods require a matching factor to adequately represent experimental data. Using the ratio of the measured to the calculated saturated conductivity k_s/k_i as the matching factor, the equation can be rewritten as follows:

$$k_i = k_s(\in_i / \in_1)^p \frac{\sum_{j=i}^{m}[(2j+1-2i)h_j^{-2}]}{\sum_{j=1}^{m}[(2j-1)h_j^{-2}]} \qquad (19)$$

where p = 0 for the Marshall formulation and p = 4/3 for Millington and Quirk. Jackson used the data from the literature to fit the curve, which is shown in Figure 11 and 12. He found that the best fit values average to approximately 1, which corresponds to the suggestion made by Kunze *et al*. (1968).

Moreover,van Genuchten (1980) suggested the relative permeability function, which is based on Mualem (1976), using the soil water characteristic curve as follows:

$$k_r = \Theta^{1/2}\left[\int_o^{\Theta}\frac{1}{h(x)}dx \Big/ \int_o^{1}\frac{1}{h(x)}dx\right]^2 \qquad (20)$$

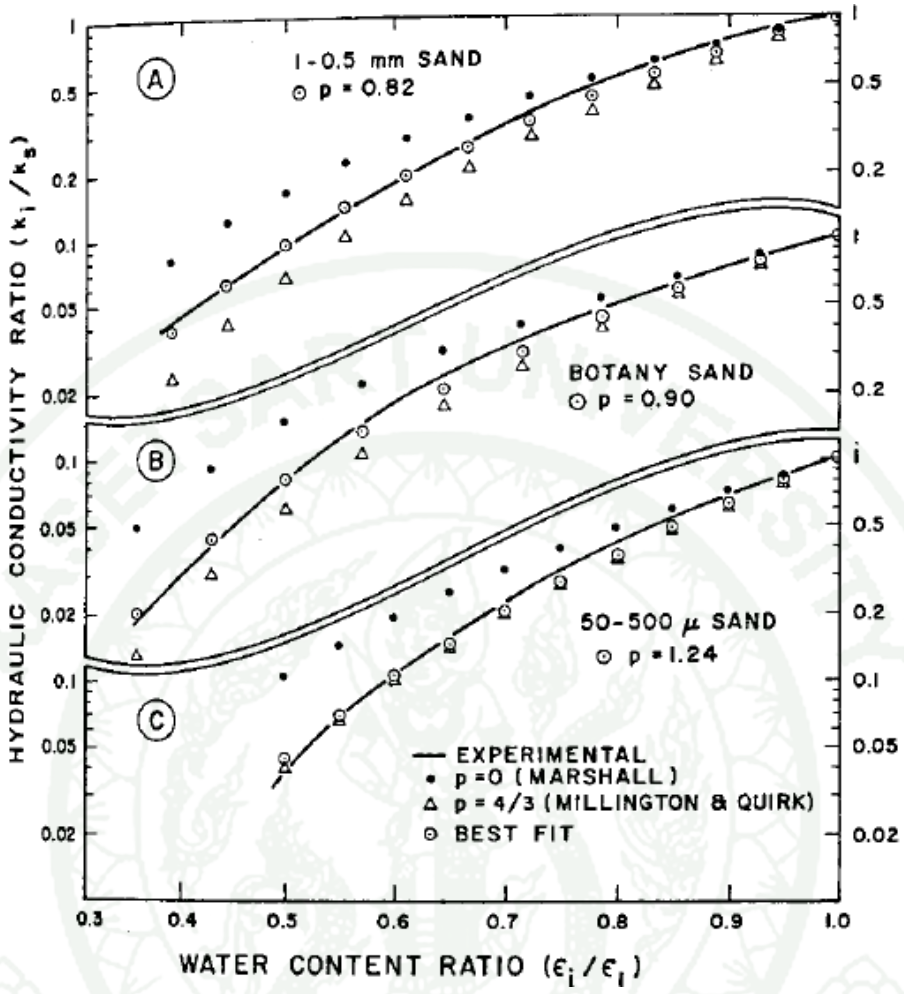

Figure 11 Hydraulic conductivity ratios vs. water content ratio for three porous materials

Source: Jackson (1972)

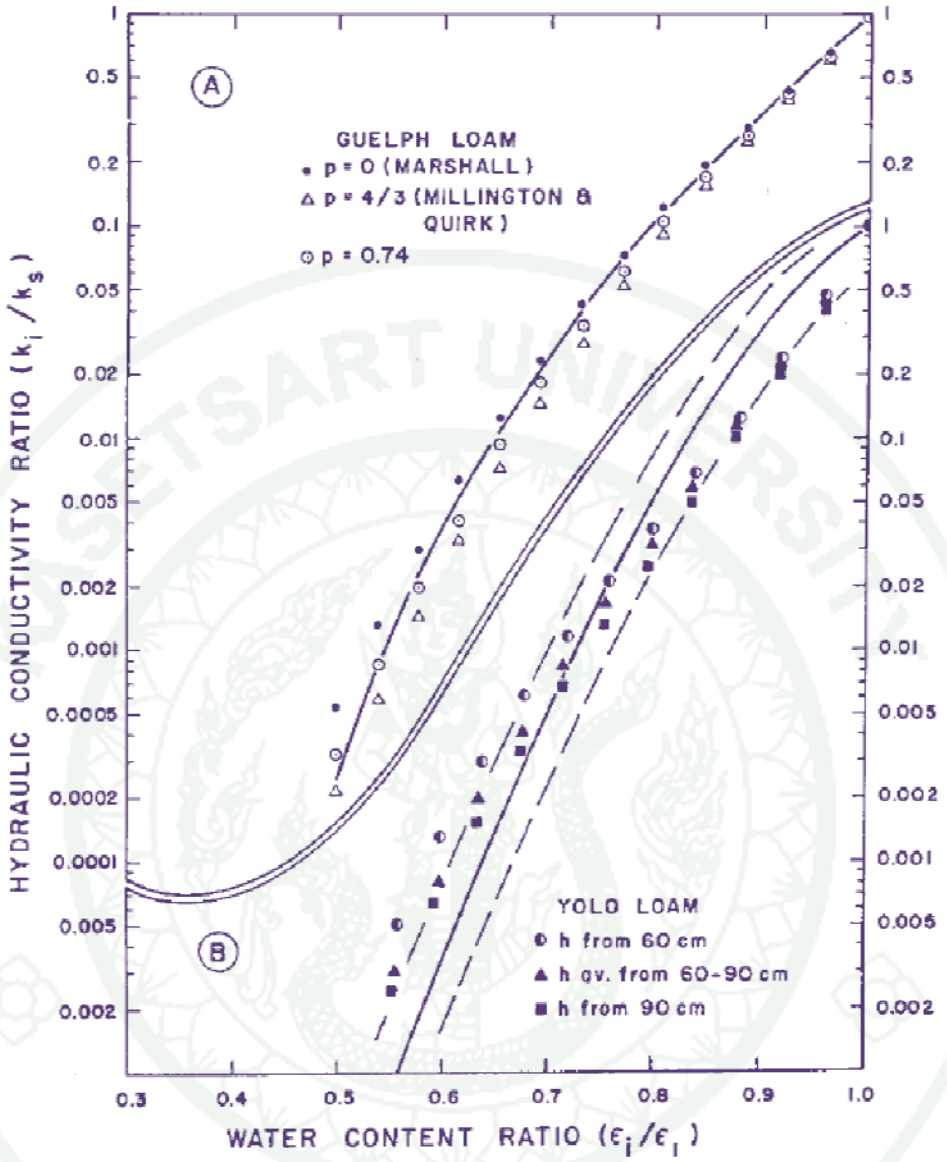

Figure 12 Hydraulic conductivity ratios vs. water content ratio for two soils

Source: Jackson (1972)

where h is the pressure head, and Θ is the effective volumetric water content found in equation (16). Equation (20) can be simplified when certain restrictions are imposed on the values of m and n in equation (16). Solving this equation for h = h(Θ) and substituting the resulting expression into equation (20) gives

$$k_r(\Theta) = \Theta^{1/2}\left[\frac{f(\Theta)}{f1)}\right]^2 \quad (21)$$

where

$$f(\Theta) = \int_0^{\Theta}\left[\frac{x^{1/m}}{1-x^{1/m}}\right]^{1/n} dx \quad (22)$$

Substituting x = y^m into equation (22) leads to

$$f(\Theta) = m\int_0^{\Theta^{1/m}} y^{m=1+1/n}(1-y)^{-1/n}\,dy \quad (23)$$

Equation (23) represents a particular form of the Incomplete Beta-function, and in the most general case, no closed-form expression can be derived. However, it is easily shown that for all integer values of k =m-1+1/n, integration can be performed without difficulties. For the particular case when k= 0 (i.e., m=1-1/n) integrating equation (23) yields

$$f(\Theta) = 1-(1-\Theta^{1/m})^m, \qquad (m=1-1/n) \quad (24)$$

and because f(1) = 1, equation (21) becomes

$$k_r(\Theta) = \Theta^{1/2}\left[1-(1-\Theta^{1/m})^m\right]^2, \ (m=1-1/n;\ 0<m<1) \quad (25)$$

The relative permeability can also be expressed in the term of the pressure head by substituting equation (16) into equation (25), i.e.,

$$k_r(h) = \frac{\left\{1-(\alpha h)^{n=1}\left[1+(\alpha h)^n\right]\right\}^2}{\left[1+(\alpha h)^n\right]^{m/2}}, (m=1-1/n) \quad (26)$$

Fredlund *et al.* (1994) show the curve fit from several equations, and they conclude that it is possible to use the normalized water content (volumetric or gravimetric) or degree of saturation data versus suction to predict the permeability function. In addition, Leong and Rahardjo (1997) studied the three categories of permeability function for unsaturated soil, including empirical, macroscopic and statistical models, to compare the results with experimental data. They show that it is possible to transform regenerate statistical models to macroscopic models and to empirical models. He concluded that the statistical model demonstrates good performance and can be readily applied. They also summarized the empirical equations for the unsaturated coefficient of permeability, as listed in Tables 5 and 6.

Table 5 Empirical equations for the unsaturated coefficient of permeability k(θ)

Function	Reference
$k_r = \Theta^n, where\ \Theta = (\theta - \theta_r)/(\theta_s - \theta_r), and\ \mathrm{n} = 3.5$	Averjanov (1950)
$k = k_s \left(\frac{\theta}{\theta_s} \right)^n$	Campbell (1973) Ahuja (1973, 1974) Gillham *et al*. (1976) Zachmann *et al*. (1981)
$k = k_s \exp[\alpha(\theta - \theta_s)]$	Davidson *et al*. (1969) Dane and Klute (1977)

Source: Fredlund *et al.* (1994)

Table 6 Empirical equations for the unsaturated coefficient of permeability k(ψ)

Function	Reference
$k = k_s$, for $\psi \le \psi_{aev}$	Brooks and Corey (1964)
$k_r = (\psi / \psi_{aev})^{-n}$ for $\psi \ge \psi_{aev}$	
$k_r = \exp(-\alpha\psi)$	Gardner (1958)
$k = k_s /(a\psi^n + 1)$	
$k = a\psi + b$	Richards (1931)
$k = k_s$ for $\psi \le \psi_{aev}$	Rijtema (1965)
$k_r = \exp[-\alpha(\psi - \psi_{aev})]$ for $\psi_{aev} \le \psi \le \psi_1$	
$k = k_1\left(\frac{\psi}{\psi_1}\right)$ for $\psi > \psi_1$	
$k = \alpha\psi^{-n}$	Wind (1955) Weeks and Richards (1967)
$k = a \exp(b\psi)$	Christensen (1943)
$k = k_s \exp[b(\psi - \psi_b)]$ for $\psi > \psi_b$	Phillip (1986)

Note ψ_1 is the residual soil suction (i.e., ψ_1), and k_1 is the coefficient of permeability at $\psi = \psi_1$

Source: Leong and Rahardjo (1997)

3.5 Scaling Factor Method

Parker *et al.* (1987) proposed that for a given porous medium, the effective-saturation/capillary-head function could be written in a generalized form. The saturation-capillary relationships for two of the three two-phase systems (i.e., air-water, air-oil and oil-water) are as follows:

$$S^*(h^*) = \overline{S}_w(\beta_{aw}h_{aw}) \quad (27a)$$

$$S^*(h^*) = \overline{S}_w(\beta_{ow}h_{ow}) \quad (27b)$$

$$S^*(h^*) = \overline{S}_o(\beta_{ao}h_{ao}) \quad (27c)$$

where $S^*(h^*)$ is the generalized function or a scaled saturation-capillary head function; a, o and w refer to air, oil and water, respectively; β_{ij} is a fluid pair-dependent scaling factor; and $\overline{S}_j$ is the wetting phase effective saturation.

Lendhard and Parker (1987) show that the values of β depend on the interfacial tensions (σ_{ij}). They also focus on the effective saturation ($\overline{S}$), which is calculated according to the following:

$$\beta_{aw}h_{aw} = \beta_{ao}h_{ao} = \beta_{ow}h_{ow} \quad (28)$$

They then note that it is convenient to choose β_{aw}=1 and apply Laplace's equation of capillarity to obtain:

$$\frac{\sigma_{aw}}{R_{aw}} = \frac{\beta_{ao}\sigma_{ao}}{R_{ao}} = \frac{\beta_{ow}\sigma_{ow}}{R_{ow}} \quad (29)$$

where R is the radius of curvature of the fluid interfaces.

For idealized monotonic drainage paths in a soil, they show that the fluid interfaces have the same geometry for any two-phase system if the solid surfaces are completely wet due to wetting fluid and the contact angle with the surface is zero. Consequently, assuming that $R_{aw} = R_{ao} = R_{ow}$ at a fixed-wetting phase, saturation yields

$$\sigma_{aw} = \beta_{ao}\sigma_{ao} = \beta_{ow}\sigma_{ow} \quad (30)$$

Thus,

$$\beta_{ao} = \frac{\sigma_{aw}}{\sigma_{ao}} \quad (31a)$$

$$\beta_{ow} = \frac{\sigma_{aw}}{\sigma_{ow}} \quad (31b)$$

Moreover, Lenhard (1994) and Fagerlund *et al.* (2006b) suggested that the scaling factor for a rigid porous medium can be determined with the following equation:

$$\frac{1}{\beta_{ow}} + \frac{1}{\beta_{ao}} = \frac{1}{\beta_{aw}} \quad (32a)$$

Thus,

$$\beta_{ow} = \frac{1}{1 - \frac{1}{\beta_{ao}}} \quad (32b)$$

Murphy *et al.* (1987) introduced the effect of scaling factors α_{gw} and α_{ag} for gasoline-water and air-water systems, respectively, as shown in Figure 13. Their study converted to equivalent NAPL-water curves using the scaling function proposed by Laverett (1941).

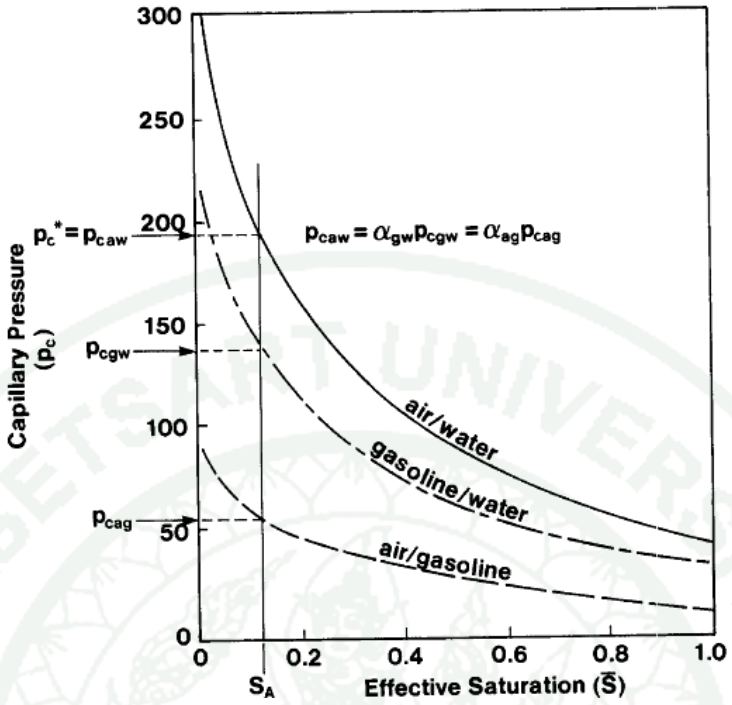

Figure 13 Scaling of the scaled saturation-capillary head (S-P) functions

Source: Murphy *et al.* (1987)

Moreover, Murphy *et al.* (1987), Wipfler *et al.* (2004), Lenhard (1994), Kechavarzi *et al.* (2005) and Fagerlund *et al.* (2006b) described the relationships between two-phase S-P functions and three phase systems after determining the scaling factor. For an air-water system, the van Genuchten (1980) equation states that

$$\bar{S}_w = \left[1+\left(\frac{\alpha P_{caw}}{\rho_w g}\right)^n\right]^{-m} \quad (33a)$$

Air-NAPL-water S-P relationships can be predicted via equation (33a), by extending the two-phase S-P relationships and assuming that the water saturation in a three-phase system is a function of the NAPL-water capillary-pressure head and that the total-liquid saturation is a function of the air-NAPL capillary-pressure head. This assumption is equivalent to assuming that no air-water interface occurs in the three-

phase system as long as the NAPL is continuous. Consequently, three-phase S-P relationships can be predicted from

$$\overline{S}_w = \left[1+\left(\frac{\alpha\beta_{ow}P_{cow}}{\rho_w g}\right)^n\right]^{-m} \quad (33b)$$

$$\overline{S}_l = \left[1+\left(\frac{\alpha\beta_{ao}P_{cao}}{\rho_w g}\right)^n\right]^{-m} \quad (33c)$$

where $\overline{S}_w$ and $\overline{S}_l$ are effective water and total-liquid saturations that are defined analogously to those in equation (33a). The NAPL-water and air-NAPL scaling factors (i.e., β_{ow} and β_{ao}, respectively) are the same as those defined for two-phase systems. Additionally, α, n and m are the curve fitting parameters for the air-water reference system.

4. Soil Cement Barrier

4.1 Introduction

Soil-cement walls are structures that are often used to improve the geotechnical properties of soft soil. They can be constructed by two methods: (1) the rotary mixed method (Figure 14), which is the technique preferred for cohesive soil and is commonly used in Japan, and (2) the jet grouting method (Figure 15), which is a technique for both cohesive soil and cohesionless soil. The latter method is particularly useful for sandy soil in which the injection of cement slurry is more effective than an injection into clay. This approach offers the advantage of building wall columns in both vertical and inclined directions through the cement-based grout. For these reasons, this study focuses on using soil cement walls to prevent LNAPL migration.

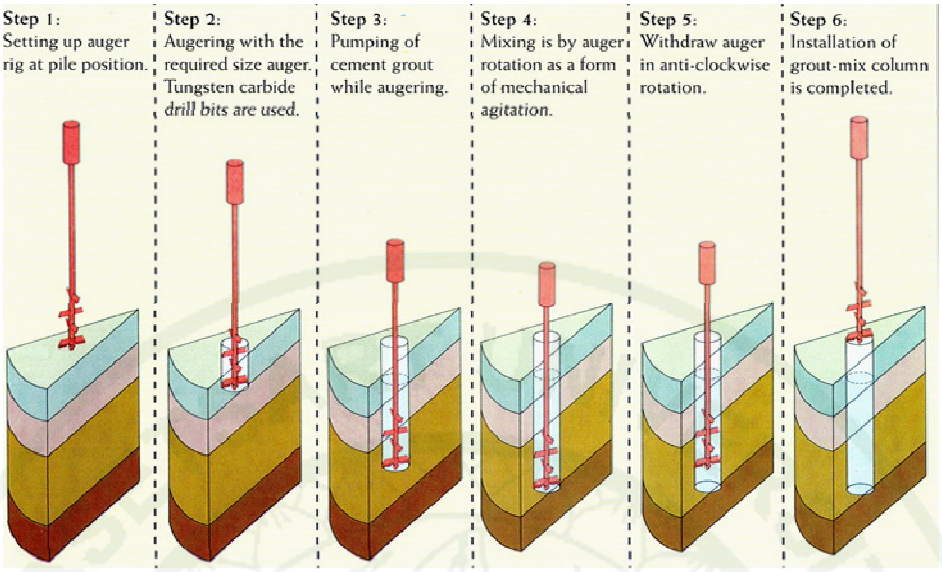

Figure 14 Soil cement column procedure using the deep mixing method

Source: Johnny (2005)

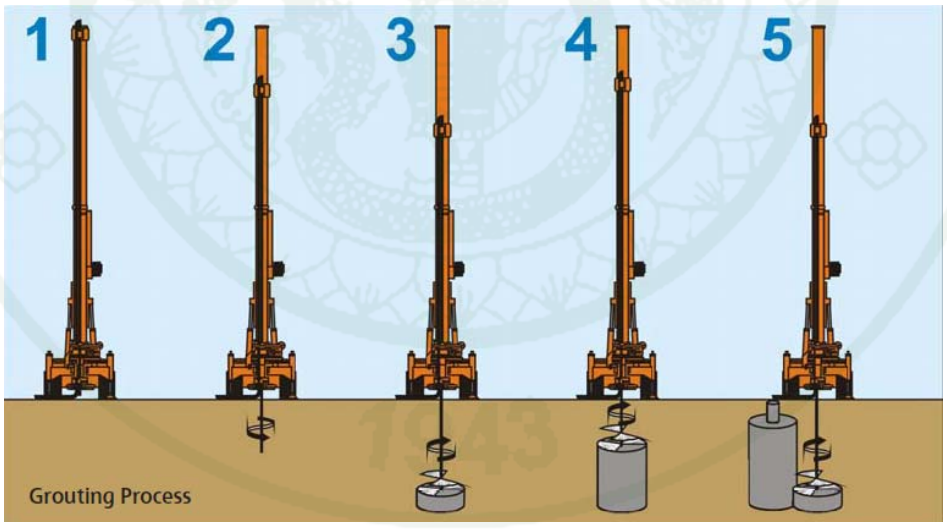

Figure 15 Soil cement column procedure using the jet grouting method

Source: Colli Drill (2006)

Nicholson *et al*. (1997) found that sands and coarse-grained soils are the easiest to mix, but even very stiff clays can be treated, albeit with slower penetration rates and increased slurry usage. They summarized a range of typical values for strength and permeability of treated soils that is based on over twenty-five projects performed in the United States using DSM, SSM, and jet grouting, as shown in Table 7. Moreover, they concluded that soil mixing can be used for barriers and containment in most soils for the following reasons:

a) Its high strength and homogeneity ensure a permanent barrier;

b) Low permeabilities make it ideal for water and contaminant barriers;

c) Spoil production is reduced compared to trenching methods;

d) A high degree of confidence in quality can be ensured;

e) Jet grouting and SSM can be used to supplement or solidify; and

f) New techniques combining jet and mechanical mixing reduce costs.

Yu *et al.* (1999) studied the permeability of a soil-cement mixture. Sixteen samples with three mix properties were used to test the coefficient of permeability. These samples were made in the laboratory and obtained from different positions at the project site. The hollow cylinder seepage test was used to determine the coefficient of permeability. The results show that the coefficient of permeability of soil-cement mixture was generally on the order of 10^{-8} cm/s. Moreover, the confining pressure and seepage pressure have little effect on the coefficient of permeability in the specified range.

Table 7 A range of typical values for strength and permeability of treated soils

Soil Type	Cement Usage	UCS	Permeability
Sludge	240 to 400 kg/m^3 (400 to 700 lbs/cy)	70 to 30 kPa (10 to 50 psi)	1x10^{-6} cm/sec
Organics silts and clays	150 to 260 kg/m^3 (260 to 450 lbs/cy)	350 to 1400 kPa (50 to 200 psi)	5x10^{-7} cm/sec
Cohesive silts and clay	120 to 240 kg/m^3 (200 to 400 lbs/cy)	700 to 2100 kPa (100 to 300 psi)	5x10^{-7} cm/sec
Silty sands and sands	120 to 240 kg/m^3 (200 to 400 lbs/cy)	1400 to 3500 kPa (200 to 500 psi)	5x10^{-6} cm/sec
Sands and gravels	120 to 240 kg/m^3 (200 to 400 lbs/cy)	3000 to 7000 kPa (400 to 1000 psi)	1x10^{-5} cm/sec

Note Strengths can generally be increased with additional cement. Permeability can be lowered with the use of bentonite or proprietary reagents.

Source: Nicholson *et al*. (1997)

Consoli *et al.* (2010) study the effect of the water cement ratio and cement content on the hydraulic behavior of soil cement bentonite (SCB) and soil bentonite (SB) mixtures permeated with water and diesel oil to assist with the design of vertical cutoff wall construction. They used water and bentonite of 100% and 12%, respectively, to mix with SM soil. The results of the hydraulic conductivity determination are shown in Table 8. They found that the hydraulic conductivity of SB increased with the permeation of diesel oil. The results from X-ray diffraction tests suggest that the maximum double layer thickness of SB specimen may be reduced by diesel oil permeation, which potentially increases the seepage pore space and hydraulic conductivity of the SB mixture. Adding Portland cement to the SB mixtures increased their hydraulic permeability when permeated with water. Conversely, adding Portland cement to the SB mixture decreased the hydraulic conductivity when diesel oil permeated the specimens. This result might be a result of diesel oil

permeation, which has a relatively smaller impact on the double layer characteristics of the SCB specimens.

Table 8 Hydraulic conductivity test results for the SB and SCB specimens

Properties	SB	SCB (w/c = 2)	SCB (w/c = 4)	SCB (w/c = 6)
Water content (%)	102	98	99	98
Bulk unit weight (kN/m^3)	14.2	13.7	13.5	13.7
Dry unit weight (kN/m^3)	7.0	6.9	6.8	6.9
Void ratio	2.9	3.3	3.2	3.1
Hydraulic conductivity (water) (m/s)	$1.6x10^{-9}$	$4.3x10^{-8}$	$1.6x10^{-7}$	$5.9x10^{-7}$
Hydraulic conductivity (diesel oil) (m/s)	$1.1x10^{-6}$	$8.0x10^{-9}$	$5.2x10^{-10}$	$1.4x10^{-8}$

Source: Consoli *et al.* (2010)

4.2 Application for containment

Heiser and Dwyer (1995) proposed a close-couple barrier for the containment of subsurface waste or contaminant migration, as shown in Figure 16. A close-coupled barrier is produced by first installing a conventional cement grout curtain followed by a thin lining of a polymer grout. Drilling will be completed at a 45° angle to the ground to form an ice cream cone shaped barrier. One row of cement columns will be grouted in a circular pattern followed by a second row of columns behind and touching the first row in a honey comb fashion. The final barrier will be 41 feet in diameter at the top and will extend approximately 23 to 24 feet below grade. After successful installation and integrity verification, they concluded that this technology is applicable to any buried or surface waste form that has the potential to release mobile contaminants. Unlike many other subsurface barrier technologies, close-coupled barriers are applicable to a wide range of waste materials and geohydrologic conditions. This characteristic is extremely advantageous because nearly every subsurface barrier has site-specific conditions that require the flexibility

offered by this technology; more specifically, this technology can place barrier materials that are compatible with virtually any waste form in almost any geologic setting.

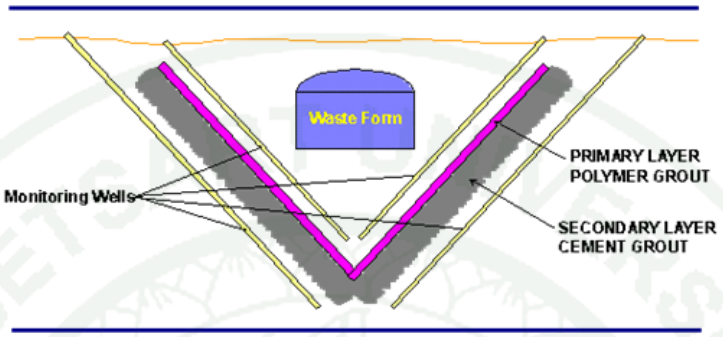

Figure 16 Schematic of closed-coupled barrier demonstration

Source: Heiser and Dwyer (1995)

Gurney (2001) mention that soil mixing can be used to form a number of containment and remediation systems, as shown in Figure 17.

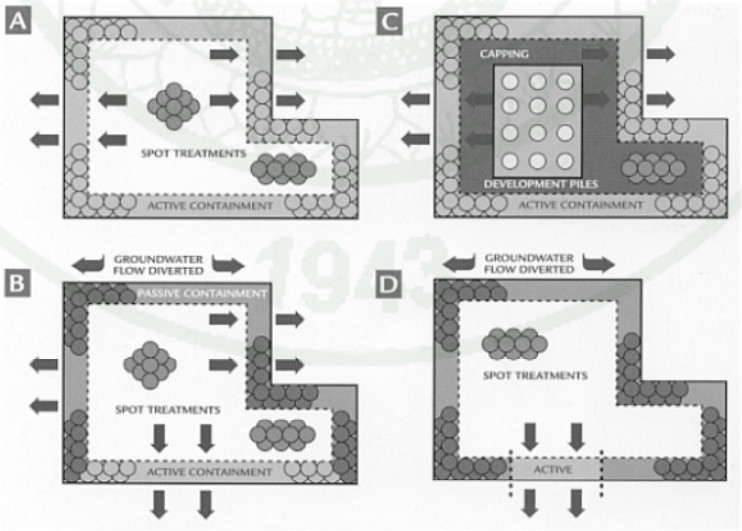

Figure 17 Geoenvironmental applications of soil cement

Source: Gurney (2001)

a) Active containment. An active containment barrier consisting of a double wall of overlapping soil columns constructed around the periphery of the site is used in combination with hot spot treatment of severely contaminated areas.

b) Passive and active containment. A combination of active and passive containment is used to manage on-site and off-site groundwater flows. This method is particularly useful when the site being treated forms part of a wider contaminated area.

c) Development piles and capping. An active containment solution incorporates development piles constructed using the same basic equipment with just a change of auger. Ground improvement is also possible using the in situ mixing process.

d) Funnel and gate. A funnel and gate containment system can be used to carefully control the flow of groundwater from the site.

5. Studies of Contaminant Migration

5.1 Introduction

Several experimental studies have been reported in the literature. Qualitative experiments (Schwille, 1988; Kueper *et al.*, 1989; Schroth *et al.*, 1998; Wipfler *et al.*, 2004) have proved useful in extending the physical understanding of some multiphase flow processes under varied hydrogeological conditions. Other more quantitative experiments have focused on developing and improving the constitutive relationships commonly used to model multiphase flow (Lenhard and Parker, 1988; Lenhard *et al.*, 1988; Lenhard, 1992; Busby *et al.*, 1995). A few one-dimensional (Eckberg and Sunada, 1984; Reible *et al.*, 1990; Thomson *et al.*, 1992; Lenhard *et al.*, 1993) and two-dimensional quantitative experiments have been conducted to study the behavior of NAPL in the unsaturated zone (Schiegg, 1990; Host-Madsen and Jensen, 1992; Pantazidou and Sitar, 1993; Van Geel and Sykes, 1994; Illangasekare *et*

al., 1995; Oostrom *et al.*, 2003). These experiments provide mostly complete data sets that are important for up-scaling processes from the laboratory to the field and for conceptual modeling of relevant mechanisms as well as for testing some of the capabilities of current numerical models. In addition, the number of investigators using the centrifuge to study the problem of subsurface contamination has increased significantly. In a centrifuge model, similar stress levels to those experienced by the actual site (prototype) can be reproduced, and transport processes can be simulated in a relatively short time. Self-weight effects, which must be considered for contaminant transport problems in porous media, can be consistently modeled by use of a centrifuge, whereas these effects are difficult to model mathematically or with other physical modeling using the earth's gravity.

5.2 Numerical Modeling

A numerical program utilized in this study is TMVOC, which is used to simulate LNAPL migration. The TMVOC simulator is used within the PetraSim, which is an integrated program for TOUGH2 (Transport Of Unsaturated Groundwater and Heat) model creation, analysis, and results display. The TMVOC simulator is a numerical simulator for three-phase non-isothermal flow of water, soil, and gas and a multicomponent mixture of volatile organic chemicals (VOCs) in multidimensional heterogeneous porous media. It is an extension of the TOUGH2 developed at the Lawrence Berkeley National Laboratory. This simulator is designed for application to contamination problems that involve hydrocarbon fuel or organic solvent spills in saturated and unsaturated zones. It can model contaminant behavior under “natural” environmental conditions, as well as in engineered systems, such as soil vapor extraction, groundwater pumping, or steam-assisted source remediation (Pruess and Battistelli, 2002; 2003). In the past, modeling of multiphase organic contaminant migration was performed by several authors, including Abriola and Pinder (1985), Kaluarachchi and Parker (1989), Pruess and Battistelli (2002), Soga *et al.* (2003), Dunn (2005), Fagerlund *et al.* (2006), Battistelli (2008), Rasmusson (2009).

5.2.1 Governing Equation

To develop the flow equations used in the TMVOC simulations, a mass balance equation is used for each of the components. The description is largely based on the TMVOC User's Guide (Pruess and Battistelli, 2002). The model considers gas, water and NAPL as separate phases. These phases consist of three components: air, water and chemical. For example, a gas phase may be a mixture of air, water and chemicals, or in the case of pure steam, it would be only water. Note the difference between water as a component and water as a phase. In a non-isothermal mode, heat is considered a fourth component. For each of the components, a balance equation is formulated:

$$\frac{d}{dt}\int_{V_n} M^{\kappa} dV_n = \int_{\Gamma_n} F^{\kappa} \bullet n \, d\Gamma_n + \int_{V_n} q^{\kappa} dV_n \qquad (34)$$

a) The mass accumulation term (M^{κ})

The total mass of component κ is obtained by summing over the fluid phases β (i.e., liquid, gas, NAPL) as follows:

$$M^{\kappa} = \phi \sum_{\beta} S_{\beta} \rho_{\beta} X_{\beta}^{\kappa} \qquad (35)$$

In TMVOC, all mass densities are expressed in molar units (gram-moles per m^3); the composition of fluid phases is then expressed in terms of mole fractions of the different components. For the VOCs, a more general form of the mass accumulation term is used that includes equilibrium sorption on the solid grains as follows:

$$M^{\kappa} = \phi \sum_{\beta} S_{\beta} \rho_{\beta} X_{\beta}^{\kappa} + (1-\phi)\rho_R \rho_w x_w^{\kappa} K_d \qquad (36)$$

Similarly, the heat accumulation term in a multiphase system is

$$M^{\kappa} = \phi \sum_{\beta} S_{\beta}\, \rho_{\beta}\, u_{\beta} + (1-\phi)\rho_{R}\, C_{R}\, T \qquad (37)$$

b) The flux term (F^{κ})

The flux term is calculated as the sum of advection/convection and diffusion/conduction, where the former is calculated by a multiphase extension of Darcy's law as follows:

$$F^{\kappa}_{advection/convection} = \sum_{\beta} - X^{\kappa}_{\beta}\, k\, \frac{k_{r\beta}\rho_{\beta}}{\mu_{\beta}} \left(\nabla P_{\beta} - \nabla P_{\beta}\, g\right) \qquad (38)$$

In the case of heat flux, the mass fraction is once again replaced by the specific internal energy. Mass flux by diffusion is included in the gas and water phase through Fick's law as follows:

$$F^{\kappa}_{diffusion} = \sum_{\beta} - \phi\, S_{\beta}\, D^{\kappa}_{\beta}\, \rho_{\beta}\, \nabla X^{\kappa}_{\beta} \qquad (39)$$

Diffusion in the water phase is not described in the TMVOC User's manual and has not been included in the presented simulations. Heat flux by conduction is calculated from Fourier's law as follows:

$$F_{conduction} = -\mathrm{K_t} \nabla \mathrm{T} \qquad (40)$$

c) The mass/ heat generation term (q^{κ})

The last term addresses sinks and sources, and different types exist. The types used may represent various forms of sinks and sources, such as deliverability wells (pumps), heat injection or production (temperature changes) and fluid injection or withdrawal (pollution spill).

5.2.2 Spatial Discretization

The continuum equations (equation 34) are discretized in space using the integral finite difference (IFD) method (Edwards, 1972; Narasimhan and Witherspoon, 1976). The appropriate volume averages are introduced as follows:

$$\int_{V_n} M_V \, dV = V_n M_n \tag{41}$$

Surface integrals are approximated as a discrete sum of averages over surface segments Anm as follows:

$$\int_{\Gamma_n} F^{\kappa} \bullet n \, d\Gamma = \sum_m A_{nm} F_{nm} \tag{42}$$

The discretization approach used in the integral finite difference method and the definition of the geometric parameters are illustrated in Figure 18.

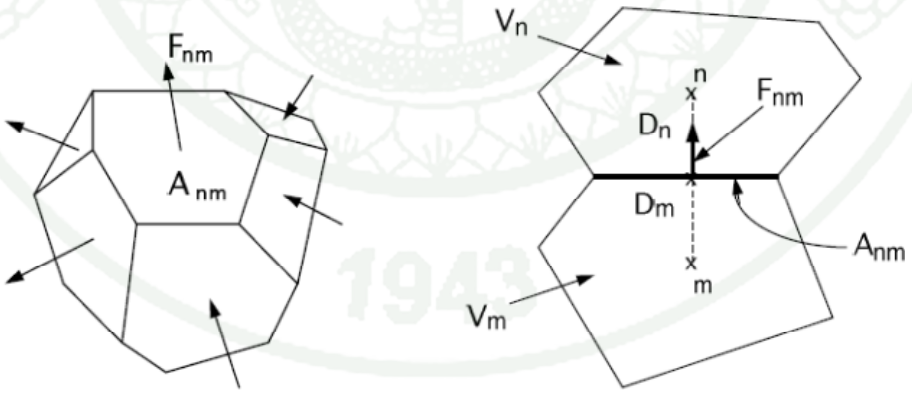

Figure 18 Space discretization and geometry data in the integral finite difference method

Source: Pruess and Battistelli (2002)

The discretized flux corresponding to the basic Darcy flux term is pressed in terms of parameters for volume elements V_n and V_m as follows:

$$F_{\beta,nm} = -k_{nm}\left[\frac{k_{r\beta}\,\rho_\beta}{\mu_\beta}\right]_{nm}\left[\frac{P_{\beta,n}-P_{\beta,m}}{D_{nm}}-\rho_{\beta,nm}\,g_{nm}\right] \quad (43)$$

TMVOC requires input data on space discretization (MESH/GRID), soil (ROCKS) and chemical (CHEMP) properties, the solvent to be used and the initial and boundary conditions. If sinks or sources (GENER) exist, they must be specified.

5.3 Centrifuge Modeling

Centrifuge modeling is regarded as a valuable means of testing that enhances the understanding of the physical behavior of soil under complex static or dynamic stress fields (e.g., Schofield, 1980). Examples vary widely and include (classical) problems such as the stability of slope, retaining structures, embankments, foundation and tunnel, heat transfer (through conduction and convection), diffusion (i.e., consolidation), seepage, earthquakes, wave loading, contaminant transport, freeze/thaw and the effects of deep mining (Azizi, 2000). Mitchell (1998) and Charles,W.W. Ng and Bruce, L.K. (2001) list large centrifuge modeling facilities known to be in operation, as shown in Table 9.

Table 9 Known large centrifuge modeling facilities through 2001

Country	Location	Maximum		Year of Commission
		a/g	kg	
Australia	University of Western Australia	200	200	1990
Canada	Queen's University, Ont.	300	100	1984
	University of New Brunswick	200	100	1992
	Memorial University, Newfoundland	200	700	1993
China	Nanjing Hydraulic Research Institute	200	100	1982
	IWHR, Beijing	300	1500	1991
	Tsinghua University, Beijing	250	200	1993
Hong Kong	HKUST, Kowloon	150	4000	2000
Denmark	Danish Engineering Academy, Lyngby	N/A	N/A	N/A
France	CESTA, Bordeaux	100	200	N/A
	Laboratoire Central des Ponts et Chausses	200	500	1985
Germany	Institute of SMFE, Bochum	250	2000	1987
Israel	Institute of Technology, Haifa	100	5000	N/A
Italy	ISMES Laboratory, Bergamo	600	400	1988
Japan	Chuo University, Tokyo	180	1000	N/A
	Osaka City University	200	N/A	N/A
	Port and Harbour Research Institute	115	2700	N/A
	University of Utsunormiya	300	150	1987
	Kyoto University, Kyoto	200	N/A	1988
Netherlands	Delft Geotechnic Institute	300	5500	1989
Switzerland	ETH Zurich Geotechnical Drum Centrifuge	440	2000	1999
Russia	Hydroproject Institute, Moscow	N/A	N/A	N/A
Singapore	National University	200	200	1988
U.K.	Cambridge University	200	100	1975
	UMIST, Manchester	1000	750	1969
	University of Liverpool	100	200	1974
	City University, London	200	400	1989

Table 9 (Continued)

Country	Location	Maximum		Year of Commission
		a/g	kg	
U.S.A.	USC-Caltech Centrifuge, Los Angeles	175	100	1974
	University of California, Davis	100	3600	1989
	Rensselaer Polytechnics Institute, N.Y.	200	450	1989
	Boeing Corporation, Seattle	600	180	N/A
	University of Maryland	200	70	1989
	M.I.T., Massachusetts	200	70	N/A
	University of Florida	120	60	N/A
	University of Colorado	200	2000	1990
	Case Western Reserve University, Ohio	200	180	1997
	University of California, San Diego	130	500	2001

Source: Mitchell (1998); Charles,W.W. Ng and Bruce, L.K. (2001)

5.3.1 Principle of centrifuge modeling

The main features of the centrifuge equipment are depicted in Figure 19. Centrifuge modeling aims to reproduce identical stresses in a model and to replicate the corresponding prototype with a small-scale accelerated modeling time. If a centrifuge model in which the geometry is linearly reduced by a factor of N from the corresponding prototype dimensions experiences a centrifugal force of Ng, the product of depth and acceleration becomes the same in the model and the prototype. Thus, as shown in Figure 20, the stress distributions in the model will be identical to those in the prototype. As a result, the self-weight effects in the prototype can be simulated in the centrifuge model but not the 1-g model.

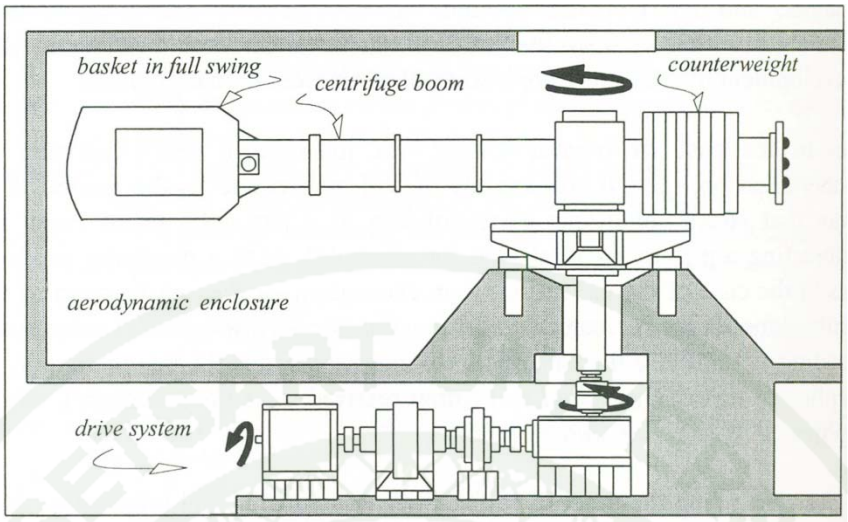

Figure 19 The main features of the centrifuge equipment

Source: Azizi (2000)

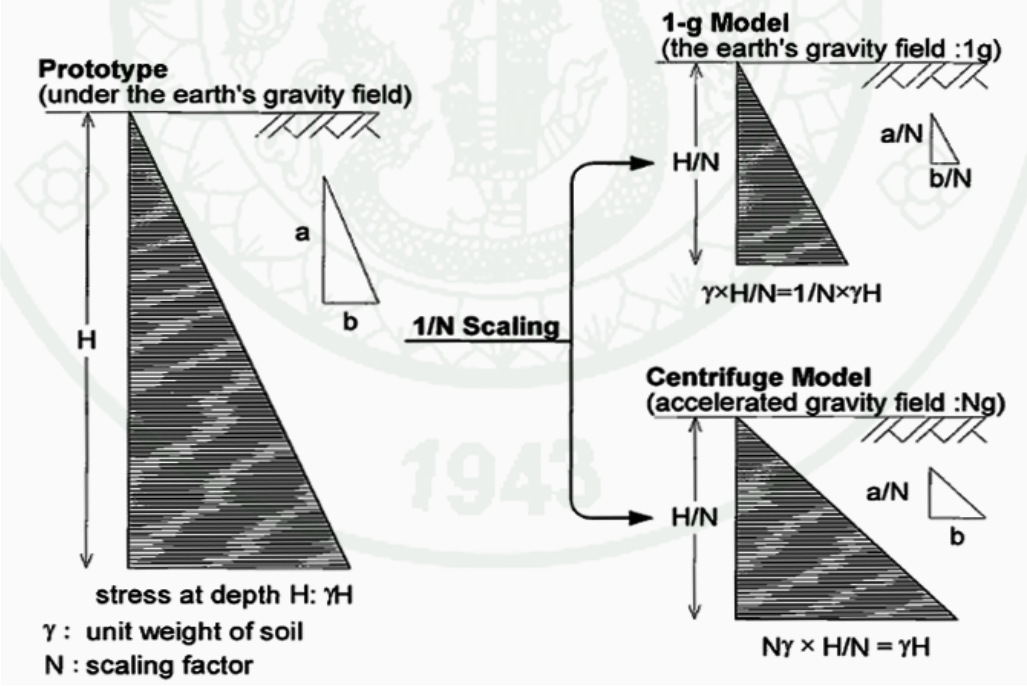

Figure 20 Stress distribution of prototype and model

Source: Nakajima *et al*. (1998)

From past studies that have used the centrifuge technique, the advantage of the geotechnical centrifuge can be summarized as follows:

a) The centrifuge modeling tests provide good data because soil and pore water at homologous points in the model and in the prototype are at identical stress (Schofield, 1995).

b) The centrifuge model provides a visual representation of reality because it simply constructs a model of the real situation to find out what happens (Mitchell, 1991).

c) The centrifuge model can generally accommodate the three-dimensional aspects of a problem (Mitchell, 1991).

d) The centrifuge model is a suitable tool for developing design criteria and study behavior mechanisms for geotechnical engineering (Chandrasekaran, 1998).

e) The centrifuge model can be used to analyze a complex real situation in which several interacting influences exist (Chandrasekaran, 1998).

f) The centrifuge model can model specific prototype conditions to obtain qualitative indications of prototype behavior (Frydman, 1998).

5.3.2 Scaling laws for contaminant transport

Centrifuge scaling laws for contaminant transportation in porous media were presented by Arulanandan *et al.* (1988) utilized dimensional analysis. Azizi (2000) expresses scaling laws for basic properties describing flow as follows:

a) Length

According to Figure 35 and Figure 36, the stress similarities between a model subjected to an acceleration of N g and a prototype subjected to the acceleration due to gravity g imply that the model dimensions are N times smaller than those of prototype. Thus, using the (same) subscript m for model and p for prototype, it follows that

$$L_m = L_p N^{-1} \quad (44)$$

b) Unit weight

As densities of the model and the prototype are identical, the corresponding unit weights are as follows:

$$\gamma_p = \rho g$$

and

$$\gamma_m = \rho N g = N\gamma_p \quad (45)$$

Therefore, the unit weight of model is N times larger than that of prototype.

c) Hydraulic gradient

According to Darcy's law, the hydraulic gradient can be thought of as a pressure gradient because it is defined as the ratio of the total head loss Δh to the length of flow path along which Δh is lost through friction; thus, at the limit:

$$i = \frac{dh}{dl} \quad (46)$$

However, the pore water pressure is identical in both the model and the prototype, and therefore,

$$i_p = \frac{dh}{(dl)_p}$$

$$i_m = \frac{dh}{(dl)_m}$$

Thus, making use of equation (44), it follows that:

$$i_m = \frac{dh}{(dl)_p(1/N)}$$

$$= Ni_p \quad (47)$$

As a result, the hydraulic gradient in the centrifuge model is N times larger than the one in the prototype.

d) Seepage velocity

Darcy's law, expressed in terms of seepage velocity in the centrifuge model, is as follows:

$$v_m = ki_m \quad (48)$$

Knowing that the model and prototype have identical permeability and substituting for the hydraulic gradient from equation (47) into equation (48), it follows that

$$v_m = kNi_p$$

$$= Nv_p \quad (49)$$

Thus, as in the case of the hydraulic gradient, the seepage velocity is N times larger in the centrifuge model than in the prototype.

e) Seepage time

The seepage time can be expressed as the ratio of the length of the flow path to the seepage velocity; thus, for the model,

$$t_m = \frac{L_m}{v_m} \tag{50}$$

A straight substitution for L_m and v_m from equations (44) and (49), respectively, into the above equation yields

$$t_m = \left(\frac{L_p}{N}\right)\left(\frac{1}{Nv_p}\right)$$

$$= \frac{1}{N^2}t_p \tag{51}$$

Accordingly, water seeps N^2 times faster in the centrifuge model than in the prototype.

f) Seepage flow

Using Darcy's law, the flow quantity flow per unit length in the centrifuge model can be expressed as follows:

$$q_m = L_m v_m t_m \tag{52}$$

where L_m = the length of flow path

Now, making use of equations (44), (49) and (51), it is easy to establish that

$$q_m = \frac{1}{N^2} q_p \quad (53)$$

The above equation shows that the flow quantity per unit length in the centrifuge model is N^2 times smaller than the one in the prototype. Note that if the scale law between total flow quantities in the centrifuge model and in the prototype was the target, then one must remember that

$$Q_m = A_m v_m t_m \quad (54)$$

An approach similar to that the used previously leads to the following:

$$Q_m = \frac{1}{N^3} Q_p \quad (55)$$

Thus, the total flow quantity (in L^3T^{-1}) in the model is N^3 times smaller than that occurring in the prototype.

Furthermore, Garnier *et al.* (1998), Cooke and Mitchell (1991), Mitchell and Stratton (1994) and Knight and Mitchell (1996) indicate that the dissolved contaminant movement through unsaturated soil may be accurately represented by centrifuge modeling and confirm the theoretical work of Arulanandan *et al.* (1988) by experimentation. Rezzoug *et al.* (2004) also confirm the relationship ($h_c^p = Nh_c^m$) between capillary rise in the prototype and the model by the test results, and their experimental results also support the scaling law of seepage time ($t_c^p = N^2 t_c^m$). Irane and Hu (2004) and Hu *et al.* (2006) show the listing of scaling factors for pollutant transport problems, as shown in Table 10.

Table 10 Scaling Factors for pollutant Transport Problems

Parameter	Symbol	Dimension	Prototype	Model
Linear dimension	L	L	1	$1/N$
Volume	V	L^3	1	$1/N^3$
Mass	m	M	1	$1/N^3$
Density	ρ	ML^{-3}	1	1
Gravity	g	LT^{-2}	1	N
Pressure	P	MLT^{-2}	1	1
Surface tension		MLT^{-2}	1	1
Temperature	T	K	1	1
Flow velocity	V	LT^{-1}	1	N
Time	t	T	1	$1/N^2$
Viscosity	μ	$ML^{-1}T^{-1}$	1	1
Permeability	k	LT^{-1}	1	N
Intrinsic permeability	K	L^2	1	1
Concentration	C	ML^{-3}	1	1
Porosity	ϕ	1	1	1
Dispersion coefficient	D	L^2T^{-1}	1	1
Decay coefficient	k	T^{-1}	1	1

Source: Irane and Hu (2004); Hu *et al.* (2006)

5.4 Previous Studies on LNAPL Migration

Simpson *et al.* (1997) used two dimensional multiphase flow experiments to investigate LNAPL transport in the vadose zone and to support work on Vesion2.0 development of Hydrocarbon Spill Screening Model (HSSM). In their investigation, they found that when medium sand overlaid coarse sand, the LNAPL was spread over a wide area in the medium sand due to lateral flow, but when it reached the coarse sand, it moved through a narrow channel because of the higher conductivity of the coarse sand. In the case of the coarse sand overlaying medium sand, the anticipated

result was LNAPL spreading at the interface, but they found no change at the interface because the contrast in hydraulic conductivity of the two sands was relatively small. The effect of the increase and decrease of water level affected the LNAPL lens that travels with the water level. When the water level decreases, some residual LNAPL can be trapped in the vadose zone.

Chevalier (1998) simulated the thickness of a gasoline lens resulting from a spill in the subsurface using experimental and numerical investigations. The experiments were conducted in a glass tank (1 m x 1 m x 5 cm), and Ottawa sand was packed in the tank. The gasoline was dyed with an oil red biological stain to follow fluid movement in the soil matrix. The results indicated that the gasoline formed a lens above the region of water-saturation pores, and a thin film of gasoline migrated beyond the boundaries of lens as pollution and reduced the height of the capillary fringe. The mathematical equations developed by Pantazidou and Sitar (1993) and Schroth (1995), as well as a capillary tube model, were used to predict the thickness of the lens. The result of the numerical prediction is a reasonable estimate based on the observed vertical thickness of NAPL.

Esposito *et al.* (1999) examined the mechanics of LNAPL movement in a partially saturated porous granular medium using an experimental centrifuge technique. Granular media with two different levels of porosity were tested using the centrifuge test at 20 g and 30 g. The duration of the tests corresponded to a prototype equivalent of 110 days. They summarized the results as follows: (1) the LNAPL could displace the capillary fringe and displace the water table; (2) the plume experienced more lateral spread in dense sand than in loose sand; and (3) the porosity influences both the residual LNAPL content and the contaminated volume.

Mohammadi *et al.* (2003) investigated the mechanism of an immiscible organics spill in a variably saturated soil. The experimental investigation contained two main sets of laboratory tests: determining the physical characteristics of the soil, such as saturated hydraulic conductivity, soil-moisture retention curves, and the dry density, and investigating the NAPL flow using n-heptane. The results of the

experiment proved that the NAPL moving downward from a coarse-grained material encounters a higher entry pressure when it comes into contact with a finer-grained layer. Initially, the contaminant descends and spreads out fairly symmetrically. Upon encountering the layer of fine-grained sand, however, a higher entry pressure is required, which causes lateral spreading and accumulation of heptane on the fine-grained layer. In addition, the results from numerical simulation correspond with the results of the physical experiment.

Soga *et al.* (2003) performed four geotechnical centrifuge tests with different soil layer systems to investigate the movement and entrapment of water and LNAPLs in unsaturated layer soil deposits. They clearly observed the effect of the textural interface in the layered system cases; the LNAPL downward movement stopped when it reached the interface of the finer sand overlying a coarser sand layer and when the plume could penetrate the coarser sand layer after the LNAPL pressure exceeded a certain value. These centrifuge test data coupled with the numerical analyses show that the NAPL properties, the subsurface soil structure, the initial water saturation, and the NAPL infiltration rate affect the entrapment conditions in heterogeneous unsaturated soil deposits.

Irene and Hu (2003) used centrifuge modeling to simulate long-term LNAPL migration in unsaturated soils at a gravitational acceleration of 75 g. Gasoline, which was used as LNAPLs, was released into the unsaturated soil according to prototype times of 1, 5 and 10 years. The test results show that the gasoline infiltrated the vadose zone and moved downwards to form a high concentration zone above the water table and then spread out laterally. The concentration of benzene, toluene, ethylbenzene and xylenes (BTEX), which represent the main components of gasoline, decreased with time and gradually moved further. The water solubility of BTEX affected their individual migration pattern and concentration distributions in unsaturated soil. Moreover, soil properties influence gasoline transport behavior.

Hamza and Elansary (2000) developed a mathematical and numerical model to simulate the transport and fate of NAPLs in near-surface granular soil. The movement of NAPLs through a porous medium can be described by a coupled set of non-linear partial differential equations that are generated by combining balance equations with constitutive relationships. Two-phase couple flow, including hysteresis and mass transfer effect, was considered. The developed model was used to investigate pollution behavior through a saturated zone to determine proper remediation. Plume migration was presented for two different cases: first, when a continuous slow rate of NAPL reaches the water table; and second, when a large volume of NAPL suddenly reaches the water table in a relatively short time. They found that when a large volume of fluid reaches the capillary fringe over the relatively short time, it can cause the fringe to collapse and depress the water table.

Wipfler *et al.* (2004) studied LNAPL infiltration in a sand-filled chamber in the case of inclined layers of an unsaturated zone using two laboratory 2-D experiments. The first experiment contained a fine sand matrix and a coarse sand layer, and the second experiment contained a coarse sand matrix and a fine sand layer. In addition, the simulation results of a numerical model were compared with the experiment results. The first experiment demonstrated that after the LNAPL was released, it spread above the coarse sand layer and moved along the interface downward to the side. At a certain distance above the water table, it infiltrated the coarse sand and became trapped between the fully saturated finer sand borders. The second experiment showed that after the LNAPL was released, it experienced almost no resistance at the coarse to fine sand interface and infiltrated the fine sand. The liquid moved downward inside the fine sand layer and infiltrated the coarse sand below a certain distance above the water table, where it again became trapped between the fine sand borders. The main effect of the LNAPL movement behavior was the water saturation that acted as a capillary barrier. Furthermore, the LNAPL contours obtained from numerical three-phase flow simulations agree well with the experimentally obtained contours.

Hayashi and Allersma (2004) performed a centrifuge model test to observe LNAPL transportation by ground water flow in a sand deposit. A floating impermeable sheet was inserted into the soil layer to stop the migration of LNAPL. They concluded that the LNAPL filtered downward to the water table and spread along the surface of the ground water. The LNAPL was transported underneath the impermeable wall by ground water flow. However, the sheet wall created a space in which the accumulated LNAPL could be extracted from the sand deposit. In addition, they suggested that the transportation mechanism depended on many parameters, such as the density of the sand deposit, the velocity of the water, the quantity and type of contaminant, and the depth of the barrier.

Dunn (2005) investigated air and LNAPL entrapment in the partially saturated fringe (PSF) in a heterogeneous system in the presence of a rising water table using laboratory experiments and numerical simulation. He demonstrated that both air and LNAPLs can be hydraulically entrapped below the water table during imbibition in the presence of hydraulic heterogeneities. According to the results, his work shows that air and LNAPL entrapment is significantly influenced by the degree of connectivity of heterogeneities, the rate of imbibition, as well as the capillary rise, permeability, and air entry characteristics of the sediments.

Hu *et al.* (2006) used the centrifuge modeling technique to investigate the migration process of LNAPLs and soil vapor extraction (SVE). Two series of centrifuge experiments were conducted to simulate a gasoline spill from a leaking underground storage tank (UST) and the subsequent subsurface migration of the gasoline along with a soil remediation technique. The gasoline was released into the unsaturated soil for the equivalent of 1 year of prototype time; then, compressed air was injected into the soil mass for periods of 2 and 4 months to extract LNAPLs. According to the results of LNAPL migration, LNAPLs moved downward and spread laterally from the leakage point; then, they formed a high concentration zone on top of the capillary fringe. After SVE was performed for 2 months and 4 months, 47% of BTEX and nearly 68% were removed from the unsaturated soil, respectively. They

mention that centrifuge modeling is a useful technique for investigating LNAPL movement in soils and the SVE remediation technique.

Kamon *et al.* (2006) studied migration of LNAPLs in the subsurface under the influence of a fluctuating water table using experimental and numerical simulators. They used a column test experiment to measure the S-p relationship under fluctuating water table conditions and verified the results with a numerical simulator. Liquid paraffin was used as the LNAPL in the column test. Then, they took the fitted parameters of the S-p model from the column test as the input parameters for the numerical simulator. This simulation was used to determine the behavior of benzene migration under water fluctuation conditions and was compared to the actual in-situ investigation results. From the simulation, they found that the benzene first infiltrated the soil and migrated vertically and laterally under the influence of gravitational and capillary forces; next, it dissolved and experienced advection in the downward-flowing water-phase or the upward-flowing water-phase, depending on the seasonal variation of the water table; and finally, it was transported as a vapor benzene constituent in the soil gas, where the increased gas-phase density induced downward movement. In addition, their study proved that LNAPL could be effectively trapped below the water table.

Kechavarzi *et al.* (2008) conducted two, two-dimensional multiphase flow experiments to investigate the effect of textural interfaces on water and LNAPL pressure and saturation distribution during infiltration and drainage. According to the experiments, they reported that LNAPL entrapment, which contributed to long-term soil and water contamination, depended strongly on the initial water saturation and water pressure at the layer interfaces. Additionally, the texture contrasts between soil layers, which led to permeability and capillary barriers, affected the LNAPL entrapment.

Battistelli (2008) demonstrated the multiphase organic spills in coastal areas with a numerical simulator, i.e., TMVOC. His simulation focused on the effects of seawater intrusion on the distribution of contaminants within the aquifer and the effects of the construction of an impervious wall on the NAPL plume migration. He concluded that seawater intrusion concentrated the VOC flux in the upper aquifer section. However, the contaminant was present at lower depths, and the impervious wall reduced the overall contaminant flux to the sea due to the containment of free NAPL in smaller volumes, which limited the contact between the free NAPL and the ground water.

Kererat and Soralump (2009a; 2009b) simulated benzene migration in the subsurface as a consequence of a constant rate spill in the unsaturated zone. The four conceptual models used in this study were as follows: (1) without ground water flow, (2) ground water flow, (3) without ground water flow with containment and (4) ground water flow with containment. This simulation focused on the effect of permeability, including three different soil permeabilities and three barrier permeabilities. Results show that gasoline migration without flow only occurs due to gravity driven NAPL plume flow and diffusion of dissolved benzene in the groundwater. In the presence of aquifer flow, dissolved benzene may be transported over long distances by advective flow. Without the groundwater flow, the contaminant migration is contained by a barrier in the vadose zone; the dissolved benzene plume reaches less than 2 m below the water table. Consequently, the depth of the wall should be more than 2 m below the groundwater level. With groundwater flow, the concentration of contamination depends on the hydraulic gradient that enhances the transport processes. The hydraulic gradient affects the depth of contaminant migration outside the wall. From the simulated scenarios, it can be concluded that the barriers can be used to limit the spread of benzene spilled in the unsaturated zone.

Kamaruddin *et al.* (2011) reviewed laboratory and numerical simulations of qualitative and quantitative experiments of hydrocarbon migration in subsurface environments in the ground. The flow behavior of LNAPL was observed in a qualitative experiment without data acquisition for saturation mapping, and no data were presented from numerical simulation. In a quantitative experiment, data acquisition was essential for numerical simulators to verify and validate numerical models. This review only considers LNAPL flow behavior experiments in the unsaturated zone with and without numerical modeling, as shown in Table 11, and they also reviewed the numerical simulators that were used to simulate LNAPL migration, as shown in Table 12.

According to previous centrifuge experiments, the summaries of centrifuge modeling details for LNAPL migration in a subsurface are shown in Table 13.

Table 11 Qualitative and quantitative infiltration and redistribution of LNAPL experiments in the unsaturated zone with and without numerical modeling

Size of sand tank (HxLxW)[a] in cm	Wall materials	Porous media	LNAPL	Amount of LNAPL	Saturation imaging[d]	References
Qualitative infiltration and redistribution of LNAPL experiments						
80x260x20 105x105x15	Glass	Heterogeneous	Heating oil, kerosene	-	-	Schwille (1967)
120x69x1.27	Glass	Homogeneous, Heterogeneous	Soltrol 110	1.248 L	-	Catalan and Dullien (1995)
60x50x0.95	Glass	Homogeneous	Soltrol 220	0.010 – 0.022 L	LTM	Schroth *et al.* (1998a)
68x112x3	Glass[b]; stainless steel[c]	Homogeneous	Gasoline	0.035 L min^{-1}	-	McDowell and Powers (2003)
Quantitative infiltration and redistribution of LNAPL experiments without numerical modeling						
61x71x5	Glass, Lucite[b]; stainless steel[c]	Homogeneous, Heterogeneous	Kerosene	0.350 L	-	Pantazidou and Sitar (1998)
120x150x6	Glass[b]; aluminum[c]	Homogeneous	n-heptane	20.000 L	LRM	Van Geel and Sykes (1994b)
122-183x975 x5.08	Plexiglas[b]; stainless steel[c]	Homogeneous, Heterogeneous	Soltrol 220	Varies	GMR	Illagasekare *et al.* (1995)

Table 11 (Continued)

Size of sand tank (HxLxW)[a] in cm	Wall materials	Porous media	LNAPL	Amount of LNAPL	Saturation imaging[d]	References
100x100x5	Glass	Homogeneous	Gasoline	0.03 L min^{-1}	-	Chevalier (1998)
180x120x8	Glass[b]; perspex[c]	Homogeneous, Heterogeneous	Soltrol 220	3.0 L	MIAM	Kechavarzi *et al.* (2000)
180x120x8	Glass[b]; perspex[c]	Homogeneous	Soltrol 220	3.0 L	MIAM	Kechavarzi *et al.* (2005)
180x120x8	Glass[b]; perspex[c]	Homogeneous	Soltrol 220	4.0 L	MIAM	Kechavarzi *et al.* (2008)
Quantitative infiltration and redistribution of LNAPL experiments with numerical modeling						
40x90x5	Plexiglas	Homogeneous	Soltrol C, transmission oil	-	-	Hochmuth and Sunada (1985)
100x100x8	Plexiglas	Homogeneous	Bayoil 82	4.0 L	GRM	Host-Madsen and Jensen (1992)
24x24x24	Acrylic	Homogeneous	Soltrol 220, mineral oil	0.5 L	-	Simmons *et al.* (1992)
100x167x5	Glass[b]; kynar[c]	Homogeneous	Soltrol 220	0.825 L	GRM	Oostrom *et al.* (1997)
120x150x6	Glass[b]; Aluminum[c]	Homogeneous	n-heptane	2.0 L	LRM	Van Geel and Sykes (1997)

Table 11 (Continued)

Size of sand tank (HxLxW)[a] in cm	Wall materials	Porous media	LNAPL	Amount of LNAPL	Saturation imaging[d]	References
108x152x8.2	Ultem plastic	Homogeneous	Soltrol 130	15 L	GRM	Waddill and Parker (1997)
60x50x1	Glass	Heterogeneous	Soltrol 220	0.01 – 0.02 L	LTM	Schroth *et al.* (1998b)
40x40x2.5	Plexiglas	Heterogeneous	Jet fuel A-1	0.015 L	-	Wipler *et al.* (2004)
75x102x5.5	Glass	Homogeneous	Lard oil	0.4 L	GRM	Oostrom *et al.* (2006b)
35.6x87.6x37	Plexiglas[b]; Aluminum[c]	Homogeneous	Paraffin liquid	0.8 L	-	Kererat *et al.* (2013)

Note [a]HxLxW: height x length x width. [b]Front wall. [c]Back wall. [d]LTM: light transmission method with no saturation mapping; LRM: light reflection method; GRM: gamma radiation method; MIAM: multispectral image analysis method

Source: Kamaruddin *et al.* (2011)

Table 12 Existing two-dimensional numerical models designed primarily for NAPL simulations

Numerical model	Description of model	Numerical formulation	GUI Support[a]	Provider[b]	Reference
ARMOS	Areal multiphase organic simulator program.	Finite element	Yes	Environmental Systems Technologies, Inc.	Kaluarachchi *et al.* (1990)
MAGNAS	A multidimensional finite element transport of water, NAPL and air through porous media.	Finite element	Yes	HydroGeoLogic Inc.	Huyakorn *et al.* (1992)
MOFAT	A two-dimensional finite element program for multiphase flow and multicomponent transport.	Finite element	Yes	USEPA	Katyal *et al.* (1991)
NAPL simulator	A subsurface flow and transport mathematical model for movement and fate of NAPL contaminants in near surface granular soils.	Finite element	No	USEPA	Guarnaccia *et al.* (1997)
STOMP	Subsurface transport over a multi-phase model.	Finite difference	Yes	Pacific Northwest National Laboratory	Oostrom *et al.* (2007)

Table 12 (Continued)

Numerical model	Description of model	Numerical formulation	GUI Support[a]	Provider[b]	Reference
TOUGH2v2	A numerical simulator for no isothermal flows of multicomponent, multiphase fluids in one, two and three-dimensions.	Finite difference	Yes	Lawrence Berkeley National Laboratory	Pruess *et al.* (1999)
UTCHEM	A three-dimensional chemical flood simulator	Finite difference	Yes	Center of Petroleum and Geosystems Engineering (University of Texas, Austin); USEPA	Center of Petroleum and Geosystems Engineering (2000)
VENT2D	A multi-compound vapor transport and phase distribution model	Finite difference	No	Benson	Benson (1994)

Source: Kamaruddin *et al.* (2011)

Table 13 Previous centrifuge modeling of LNAPL migration in partially saturated soil

G level	Time (min)	Porous media	LNAPL	Amount of LNAPL (ml)	Flow rate (ml s^{-1})	Measure instrument	References
104	N/A	Homogeneous	Gasoline	22.22	N/A	Nothing	Chang *et al.* (1995)
15	384	Homogeneous	Silicon oil	296.3	0.25	Nothing	Knite and Mitchell
30	96,288	Homogeneous	Silicon oil	37	0.13, 0.055		(1996)
20	396	Homogeneous	N/A	207.5	N/A	Nothing	Esposito *et al.* (1999)
30	176	Homogeneous		61.48			
20	210	Homogeneous	Soltrol 220	140	N/A	Resistivity probe	Kechavarz and Soga
						NAPL tensiometer	(2002)
						Water tensiometer	
20	60	Homogeneous	Soltrol 220	226.42	N/A	Resistivity probe	Soga *et al.* (2003)
20	60	Heterogeneous	Soltrol 220	194.96		NAPL tensiometer	
20	70	Heterogeneous	Soltrol 220	283.02		Water tensiometer	
20	320	Heterogeneous	Silicon oil	182.29			
50	210	Homogeneous	Gasoline	20	N/A	Nothing	Irene *et al.* (2004)

Table 13 (Continued)

G level	Time (min)	Porous media	LNAPL	Amount of LNAPL (ml)	Flow rate (ml s^{-1})	Measure instrument	References
75	95	Homogeneous	Gasoline	6	N/A	Nothing	Irene *et al.* (2004)
75	474	Homogeneous	Gasoline	6			
75	950	Homogeneous	Gasoline	6			
30	360	Homogeneous	Motor oil	N/A	N/A	Nothing	Hayashi and Allersma (2004)
75	95	Homogeneous	Gasoline	6	N/A	Nothing	Hu *et al.* (2006)
30	128	Homogeneous	Paraffin liquid	800	0.015	Pore water pressure sensors	Kererat *et al.*(2013)

MATERAIALS AND METHODS

In this chapter, the materials and equipment as well as the methodology that were used to study LNAPL migration are explained. This study was divided into four parts as follows: (1) SWCC determination of soil and soil cement samples, (2) LNAPL migration experiments with and without containment using a physical small tank model, (3) a LNAPL migration experiment with containment considered with and without flow conditions using a centrifuge model and (4) numerical simulation of LNAPL migration to compare the results with those from the physical tank model experiment and centrifuge experiment. Experiments to determine SWCC and LNAPL migration using a small tank model were performed at Rajamangala University of Technology Rattanakosin Wangklaikangwon. The selected porous medium was sandy soil to allow the contaminant to flow easily through soil layers. Gasoline and paraffin liquid were used to represent LNAPL in the physical small tank experiment and centrifuge model experiment, respectively. Sandy soil was mixed with Portland cement to create a soil cement barrier to contain contaminant migration. A KU (Kasetsart University) tensiometer was used as a device to measure the suction of all specimens based on water content. Water-suction data from tensiometric measurements were used to construct SWCC. A TMVOC simulator, which was a module of Petrasim 4.2, was used to simulate LNAPL migration. A centrifuge model experiment was conducted at Rensselaer Polytechnic Institute (RPI), Troy, New York. The gravitational acceleration (g level) selected in the centrifuge test was 30 g. During centrifuge spinning, data acquisition and video recording were used to record the behavior of LNAPL migration throughout testing.

Facilities

1. Soil suction determination

1.1 Experimental materials

Two types of soil were used to represent samples of sandy soils in Thailand and were collected from the provinces of Chonburi and Huahin. Chonburi soil is artificial foundry sand, i.e., AFS35. AFS (American Foundrymen's Society Average Fineness Number) was used to denote the relative grading of sand, and it was calculated using the old BS mesh numbering system for sieves. Huahin soil was a natural sandy soil from Rajamangala University of Technology Rattanakosin Wangklaikangwon. The grain size distributions of both sandy soils are shown in Figure 21. The characteristics and basic properties of both soils, including soil cement, are shown in Table 14. Soil cement walls made from a mixture of Chonburi and Huahin soil mixed with Portland cement type I and water had cement content and water cement ratios of 220 kg/m^3 and 2, respectively (Nicholson *et al*., 1997).

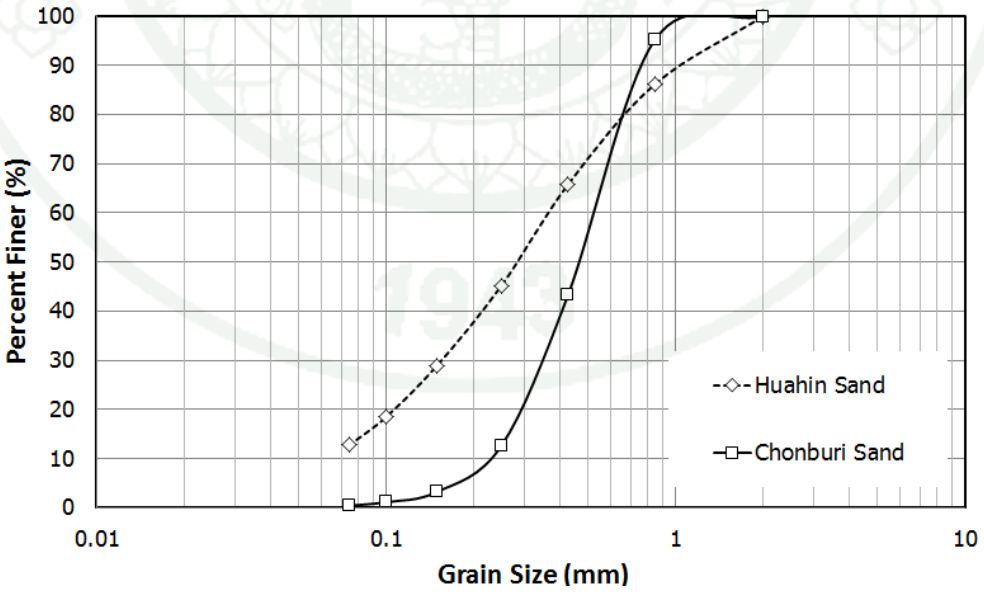

Figure 21 Grain size distribution curve of Chonburi and Huahin soil

Table 14 The characteristics and basic properties of the experiment materials

Properties	Sandy soil		Soil cement	
	Chonburi	Huahin	Chonburi	Huahin
D_{10}, mm	0.222	0.063	-	-
D_{60}, mm	0.562	0.376	-	-
C_u	2.53	5.29	-	-
USCS	SP	SM	-	-
Specific gravity	2.69	2.62	2.68	2.68
Porosity	0.41	0.40	0.35	0.35
Dry density, g/cm^3	1.60	1.64	1.73	1.74
Permeability, cm/s	2.564×10^{-2}	7.837×10^{-4}	1.399×10^{-7}	3.794×10^{-8}

1.2 Instruments

In this study, a miniature KU tensiometer was used to measure the suction of soil and soil cement samples. It comprises a MEMs (Micro-Electro-Mechanical Systems) pressure sensor, 1-BAR High-Air-Entry porous ceramic and a transparent acrylic tube that can measure suction values from 0 to 100 kPa, as shown in Figure 22 (Jotisankasa, 2009). The tensiometer needs to be saturated and de-aired before use. Therefore, the vacuum chamber and electrical vacuum pump shown in Figure 23 are used to saturate the tensiometer. The suction measurement setup can be described as follows: the signal cable from the tensiometer is connected to a read out box that can support four signal cables of the tensiometer; then, the signal from the readout box can be measured by a digital multimeter, as shown in Figure 24.

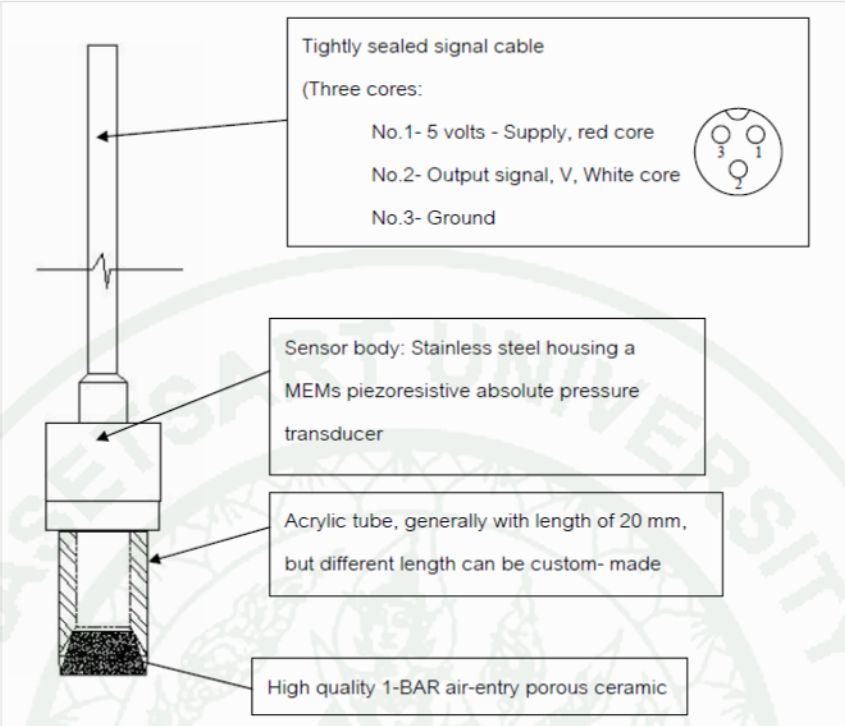

Figure 22 Basic components of a KU tensiometer

Source: Jotisankasa (2009)

Figure 23 The vacuum chamber and vacuum pump used to saturate the tensiometer

Figure 24 Experimental set up for suction monitoring

The soil and soil cement samples were prepared in the PVC ring to prevent water evaporation from the samples as shown in Figure 25. A spray bottle and a dryer (Figure 26) were used to increase and decrease water in the soil and soil cement samples to change the degree of saturation during experiment. In addition, a digital balance and a digital vernier caliper, as shown in Figure 27, were used to measure changes in the height and water content of the samples.

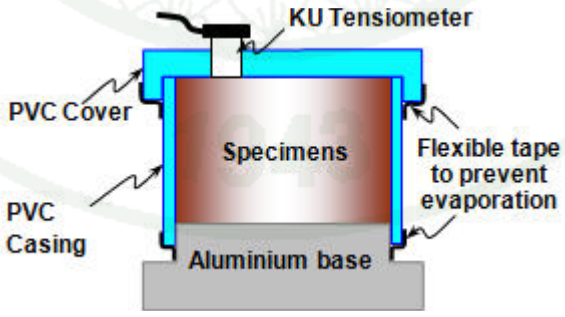

Figure 25 Sample preparation

Source: After Sutthinun (2009)

Figure 26 Devices used to increase and decrease water in the samples

Figure 27 Devices to measure the changes in the dimensions and water content of the samples

2. LNAPL migration experiment using a 1g model

2.1 Model configuration

Plexiglas with a thickness of 10 mm was used to construct the two-dimensional tank model because gasoline does not affect Plexiglas. The geometry of the Plexiglas model for each test is shown in Figure 28 and is a modification of that proposed by Sripongphichit (2006). The overall dimensions of the physical small tank model used for experiment were 79.2 cm long x 9.7 cm thick x 38 cm high, and the inner dimensions were 64 cm long x 7.7 cm thick x 36 cm high. It was composed of two water tanks on the left and right sides, which had a faucet at the bottom. A perforated wall with holes with a diameter of 0.9 cm that was dovetailed with a nylon net was installed between the water tank and soil layer. A gasoline storage container that was 9.15 cm long x 8.52 cm wide x 8.63 cm high (Figure 29) was placed on top of the model and on the cover.

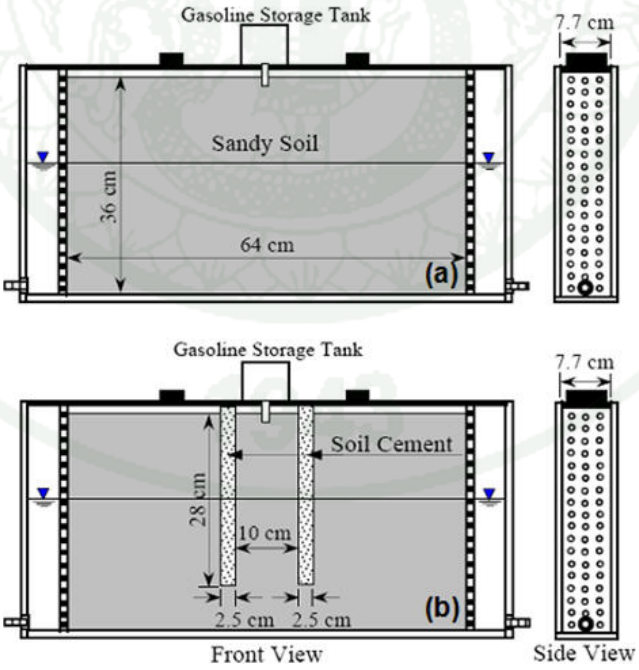

Figure 28 Test geometries (a) without containment and (b) with containment

Source: Kererat and Chaikaew (2009a)

Figure 29 A gasoline storage container

2.2 Experimental materials

The sandy soil and soil cement samples used in this experiment were same materials used for SWCC determination. Two sandy soils were used as porous media, while the soil cement samples were used as barriers and had the following dimensions: 2.5 cm thick, 7.7 cm wide and 29 cm deep. The LNAPL used in the experiment was 91 octane gasoline with a density of 0.72 g/ml, a dynamic viscosity of 0.45 cp, a surface tension of 35 dyne/cm, an aquifer residual saturation of 0.15 and a vadose zone residual saturation of 0.05 (Weaver and Charbeneau, 2000). The LNAPL was dyed red with Sudan IV to enhance the intensity of red color for visual observation with a weight ratio of 0.1% (Sripongphichit, 2006) because Sudan IV was inert, which does not affect the properties of LNAPL. Moreover, Sudan IV was not soluble in water (Smith and Zhang, 2001), and the water used in the experiments was de-aired water, which represents the ground water in the model.

3. LNAPL migration experiment using centrifuge modeling

3.1 The RPI geotechnical centrifuge machine

Centrifuge modeling was performed at Rensselaer Polytechnic Institute (RPI), Troy, New York. The RPI centrifuge was a modified RPI Model 655-1 with a

capacity of 150 g-tons, as shown in Figure 30. The centrifuge machine comprises (a) a swinging basket; (b) a centrifuge boom; (c) a balancing counterweight; (d) a hydraulic rotary joint and electrical slip-rings assembly; (e) a drive system; (f) an aerodynamic enclosure; and (g) in-flight imbalance measurement and automatic balancing systems, including automatic shutdown if excessive imbalance is detected. It has a nominal radius of 2.7 m and a platform radius of 3.0 m. The space available for the payload was 1 m in depth, 1 m in width, and 0.8 m in height with a maximum height of 1.2 m. These specifications do not exceed the limits of the RPI centrifuge, which were 160 g, 1.5 ton, and 150 g-tons, which is the product of payload weight and g's. The centrifuge was equipped with a fiber optic rotary joint, 28 rings and a wireless network, which were available to the user for data transmission. A hydraulic rotary joint was also installed with a total of six joint passages available to the user, two of which were rated for 3,000 psi hydraulic oil. In addition, a forced-air ventilation system provided cooling within the enclosure, and a system of security interlocks prevented machine startup if the enclosure access doors were not securely locked.

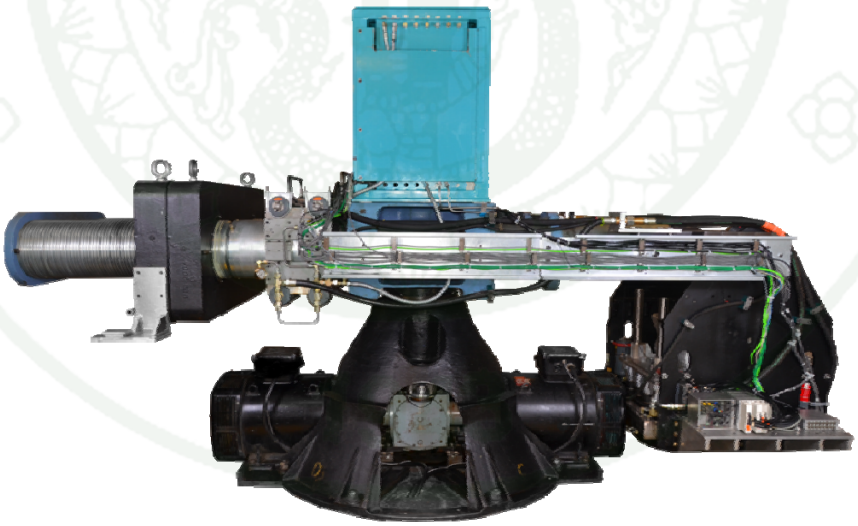

Figure 30 The RPI geotechnical centrifuge machine

Source: The Center for Earthquake Engineering Simulation (1989)

3.2 Model configuration

A strongbox that is 37.0 cm wide, 87.6 cm long and 35.6 cm high, equivalent to the prototype dimensions of 11.10 m x 26.28 m x 10.68 m at 30 g, was used for the experimental programs. The box consists of a 5 cm thick front Plexiglas wall and a 2.5 cm thick aluminum plate for the remaining sides. The geometry of the models with model units at 1 g is shown in Figure 31. Two soil cement walls used for containment were constructed in both conditions and were located 5 cm (1.50 m in the prototype) from the spill point in left and right directions. Each wall was 2 cm wide, 37 cm long and 20 cm high, equivalent to the prototype dimensions of 0.60 m x 11.10 m x 6.00 m at 30 g, and the wall embedded in the sand layer was 13.5 cm below the ground surface. The height of the wall above the ground surface was used to prevent LNAPL flow across the wall. The total height of the sand deposit was 26.7 cm (8.01 m in the prototype).

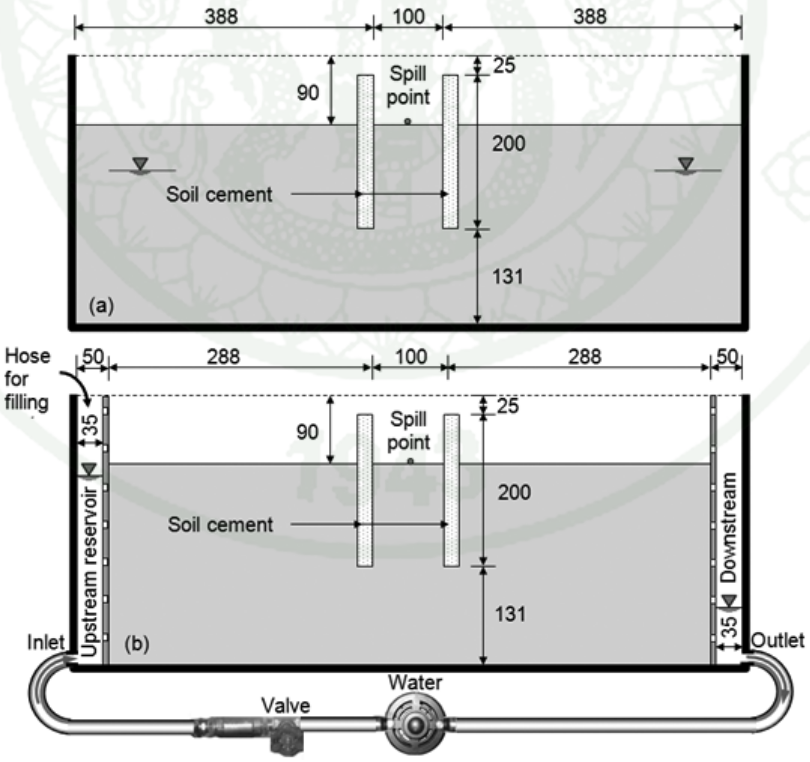

Figure 31 Schematic diagram of strongbox for (a) no groundwater flow and (b) ground water flow (model unit: mm)

3.3 Experimental materials

The sandy soil used in this study was Nevada sand which is silica sand with a particle density of 2,650 kg/m^3, a maximum dry density of 1,709.14 kg/m^3, a minimum dry density of 1,513.74 kg/m^3 and a hydraulic conductivity range of 4.75 m/day to 1.99 m/day, depending on its relative density. The grain size analysis determined as shown in Figure 32 that the Nevada sand was a uniformly graded soil with a D_{10} of 0.090 mm, a D_{30} of 0.122 mm, a D_{60} of 0.185, a C_u of 2.056, and a C_c of 0.894. In this experiment, the desired dry density of the soil was 1,600 kg/m^3, which corresponds to a relative density of 50% and a porosity of approximately 40%. The saturated hydraulic conductivity used for this sand was 5.6×10^{-3} cm/s. Moreover, the grain size distribution curve of Nevada sand is similar to Chonburi sand.

The soil cement walls used in this study were 2 cm thick, 37 cm wide and 20 cm deep. The desired thickness and dry density of the soil cement wall in the prototype scale were 60 cm and 1,740 kg/m^3, respectively. The mix proportions were calculated using a water cement ratio (w/c) of 2 and a cement content of 220 kg/m^3 (Nicholson *et al*. 1997). This cement content used in this study is a parametric study to achieve the hydraulic conductivity not more than the order of 10^{-6} cm/s (recommended by LaGrega et al. 2001) including the thickness of wall is small, therefore, the strength of soil cement walls have to be high strength. The pressurized constant head test was used to measure the hydraulic conductivity of soil cement materials which is 1.4×10^{-7} cm/s (Kererat and Chaikeaw 2009a).Two soil cement walls were constructed by cast in place. Both ends of soil cement wall were adhered to a rubber sheet and fixed to the side walls of the strongbox.

The LNAPL used in this experiment was paraffin liquid (Sigma-Aldrich, USA), selected for its very low volatility at room temperature, its negligible solubility in water and low hazard to health ratio (Kamon *et al*. 2006). To enhance the intensity of paraffin's red color, Sudan IV (Scholar Chemistry, USA**)** which is the dark-brown powder was used as a dye at a ratio of 0.1% by weight (Sripongphichit 2006). The properties of paraffin liquid, benzene and water are summarized in Table 15.

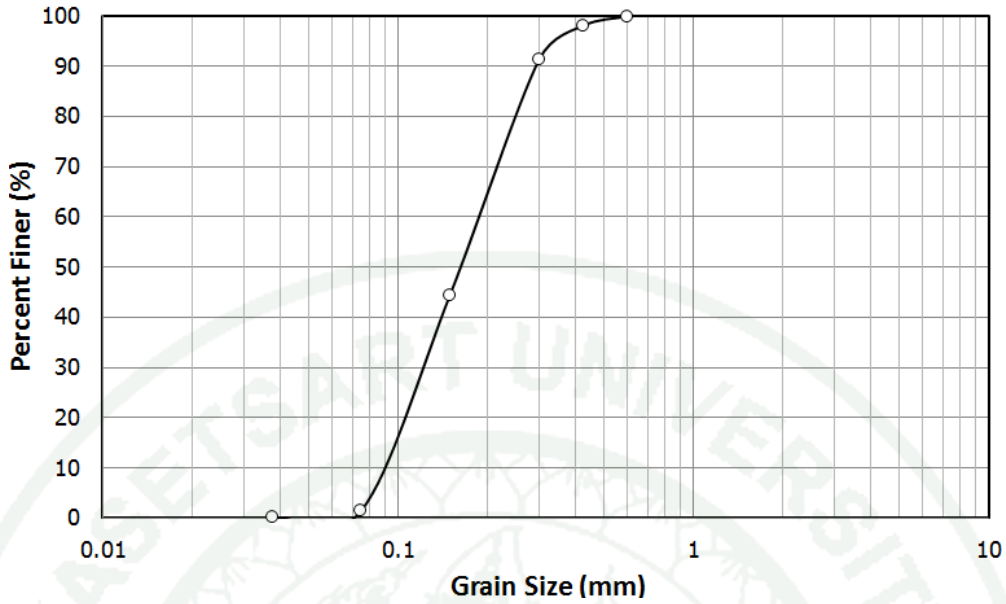

Figure 32 Grain size distribution curves of Nevada sand

Table 15 Properties of paraffin liquid, gasoline and water

	Liquid paraffin	Gasoline	Water
Formula	$C_{20}H_{42}$ (Above)	C_4 to H_{12}	H_2O
Appearance	Colorless, odorless	Red color	Colorless, odorless
Boiling point	> 300°C	20°C -200°C	100°C
Melting point	-18°C	5.5°C	0°C
Evaporation rate	Non volatile		
Solubility	Insoluble in water	100-200 mg/l*	
Viscosity	170 mPa.s	0.45 mPa.s	
Hazard nature	Non toxic	Toxic	
Surface tension	31.07 mN/m	35 mN/m	72.75 mN/m
Interfacial tension	62.06 mN/m	50 mN/m	
Specific gravity	0.88 g/cm^3	0.72-0.78 g/cm^{3*}	0.998 g/cm^3

Source: Kamon *et al.* (2006); * Zogorski *et al.* (1997)

3.4 Groundwater flow system

The groundwater flow system was designed and developed to investigate an effect of differential pressure head on the behavior of LNAPL migration. Figure 31(b) presents the test setup for the groundwater flow case. In these tests, the strongbox was divided into three sections using two 1.27 cm thick perforated walls made of aluminum covered with geotextile. The sand deposit was contained in the center section of the strongbox, and the two side sections were used as water reservoirs to control the water table at the boundaries of the soil sample. To maintain the groundwater flow along the length of the model, a differential pressure needed to be maintained. It was accomplished by creating water reservoirs at both ends of the model. The wall of the reservoir in contact with the soil was perforated with many small holes to allow the water to flow freely and evenly into the soil. A pump system was developed to collect water from the low pressure reservoir (downstream) and return it to the high pressure supply reservoir (upstream). The flow rate of the pump was adjustable to allow the desired pressure differential in the two reservoirs to be set, thereby controlling the groundwater flow within the model. A separate water supply hose was also installed in the high pressure reservoir. Furthermore, water can be added to the model through the centrifuge rotary joint to minimize any loss of water in the model caused by evaporation during the experiment.

3.5 LNAPL spill system

A special spill system developed for this study was composed of a container and a spill system. The container was 28 cm in diameter and 15 cm high. It was welded to U-shaped steel bars that could be mounted on the top of the strongbox by bolts, as shown in Figure 33. The spill system was developed to release the LNAPL to the soil surface at the center of the model container while the centrifuge was spinning at 30 g. At the beginning of the test, a normally closed solenoid valve held the LNAPL in the container. When the test was ready to run, the LNAPL was released through a very small interchangeable orifice. This system was tested extensively with various sizes and numbers of orifice holes to achieve the desired

flow rate. In addition, the container was designed to have a large diameter and a minimum height to minimize the change in the flow rate through the orifice as the head in the container diminished. The LNAPL was released in the atmosphere through the orifice with the constant rate. The constant flow rate was monitored using the pore pressure sensor installed at the bottom of the LNAPL container.

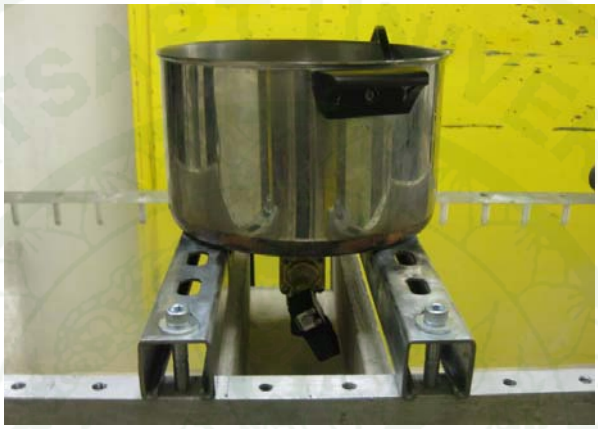

Figure 33 LNAPL release container

3.6 Instruments

The sand was placed into the box by pluviation (Figure 34), also known as sand raining. The pluviation was made of sheet metal formed into a triangular funnel with a row of 1.6 mm holes at the bottom of the instrument to release the sand. It is 15.25 cm wide and 15.9 cm high. To observe the behavior of LNAPL migration, on-board cameras and pore pressure sensors were used in this centrifuge experiment. The video from all cameras was recorded in mp4 format. The installations of the on-board cameras are shown in Figure 35. Pore pressure sensors were placed at various locations in the model to investigate the changes of pore pressure. The sensor locations under without and with groundwater flow conditions are shown in Figure 36 and Figure 37, respectively. Both video records and data from pore pressure sensors were stored in a network data acquisition system with Internet Teleobservation/Teleoperation. Without groundwater flow (tests 1 and 2), thirteen pore pressure sensors were installed within the sand deposit, and another one was

located at the bottom of the LNAPL container. With groundwater flow, twelve and fifteen pore pressure sensors were installed within the sand deposit for test 3 and test 4, respectively; two probes were located at the bottom of each reservoir, and another one was located at the bottom of the LNAPL container.

(a) Front (b) Side (c) Bottom

Figure 34 Pluviator from the front, side and bottom views

Figure 35 The location of on-board cameras

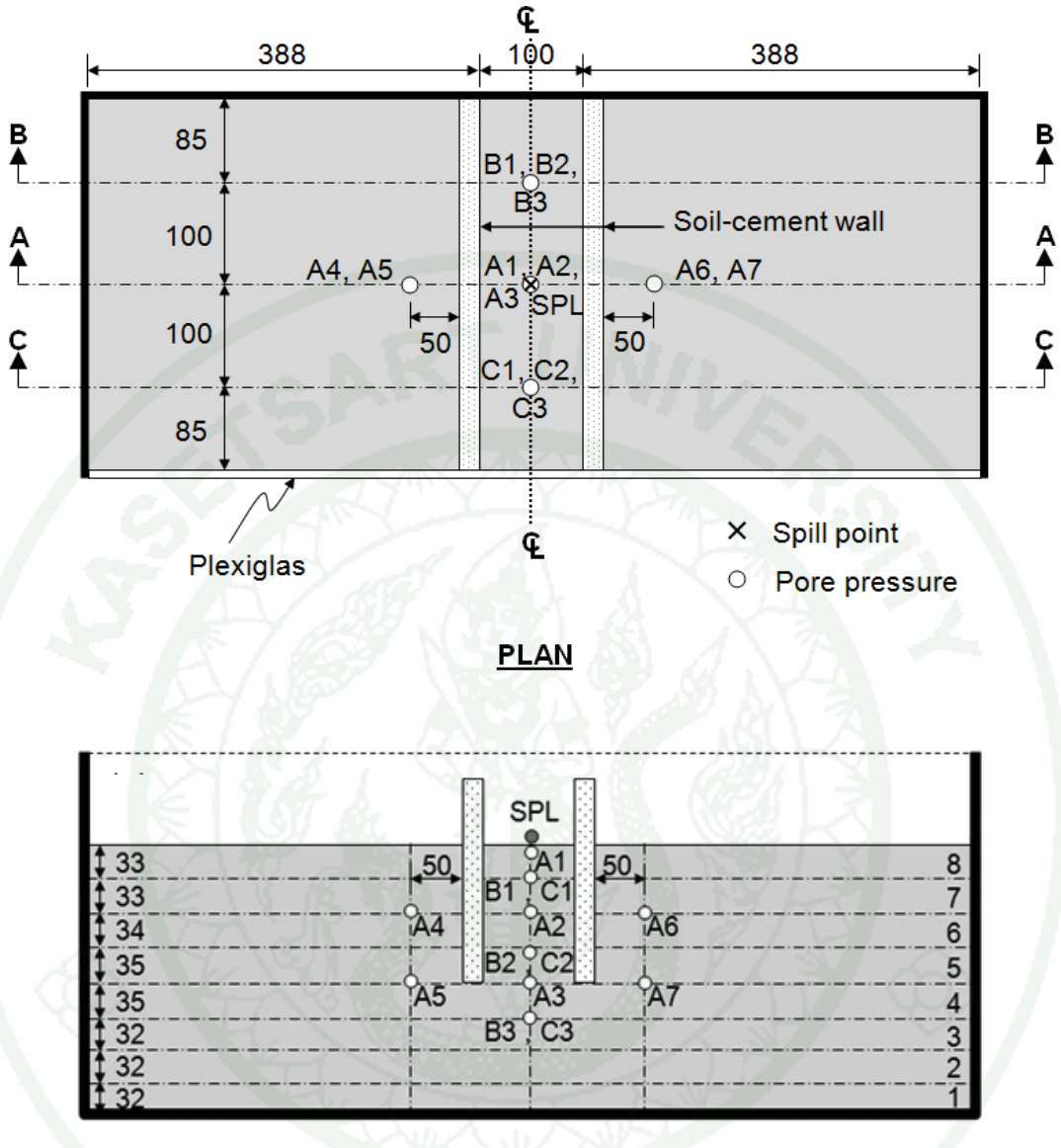

Figure 36 Sensor locations for the experiment without groundwater flow

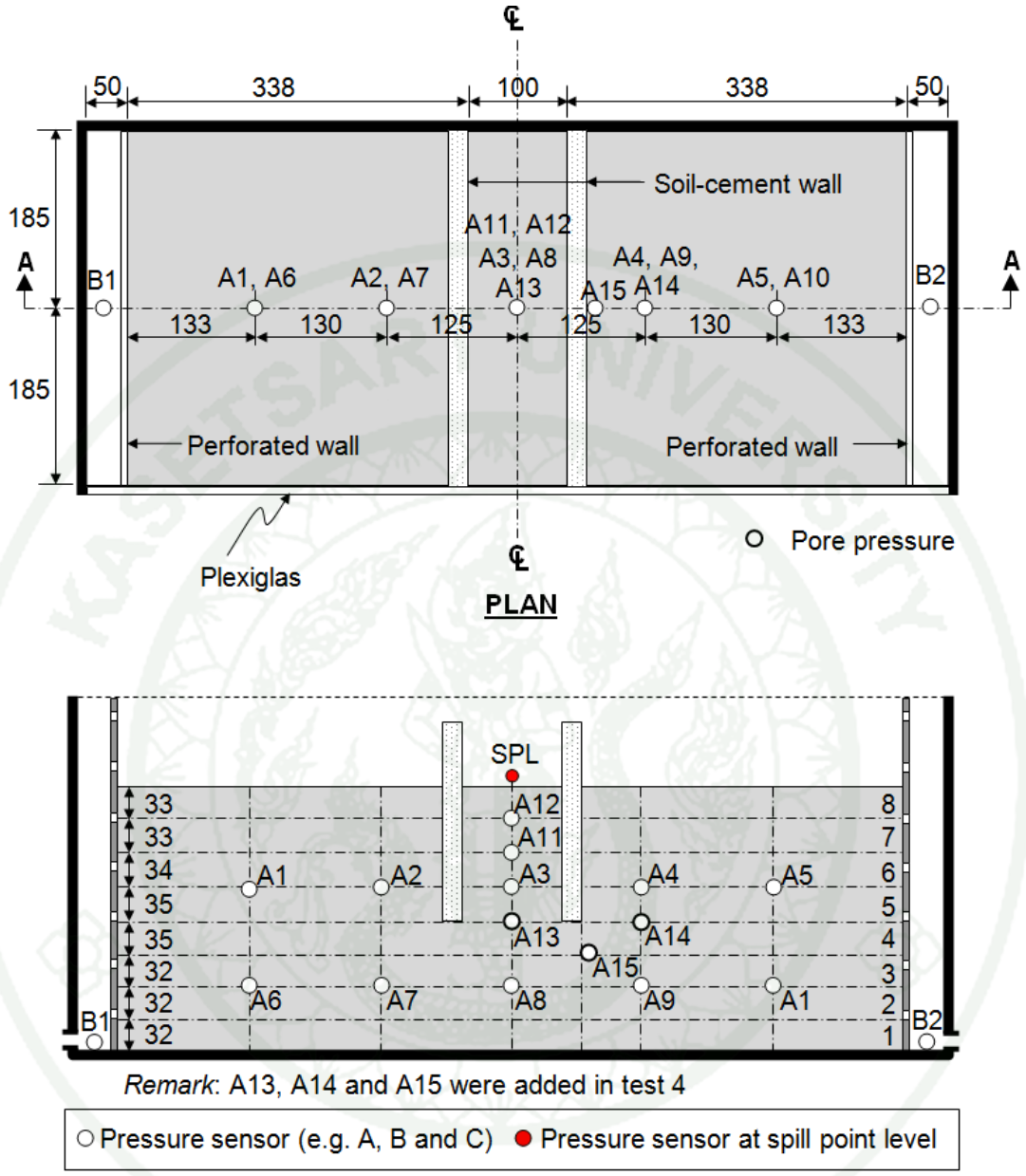

Figure 37 Sensor locations for the experiment with groundwater flow

4. Numerical simulator

The TMVOC simulator (Figure 38), which was a module within PetraSim 4.2 (TOUGH2), was used to simulate LNAPL migration. This simulator requires input data on space discretization (MESH/GRID), soil (ROCKS) and chemical (CHEMP) properties, the solvent to be used as well as initial and boundary conditions. If sinks or sources (GENER) exist, they must be specified. TMVOC discretizes space and time using an integral finite difference method (IFDM) and first-order backward finite difference, respectively. TMVOC provided some standard capillary pressure functions and relative permeability functions. PetraSim already provided a standard VOC (NAPL), and a new VOC could be created by the user with some modification. During creation, the user specifies an existing VOC on which to base the new VOC. All data from the existing VOC are copied to the new VOC, so that the user only needs to change the values that are different in the new VOC.

SEEP/W (Figure 39), which was a module within Geostudio, was a finite element software product for analyzing groundwater seepage and excess pore-water pressure dissipation problems within porous materials such as soil and rock. It could be used to draw flow nets and compute the pore water pressures and flow rates.

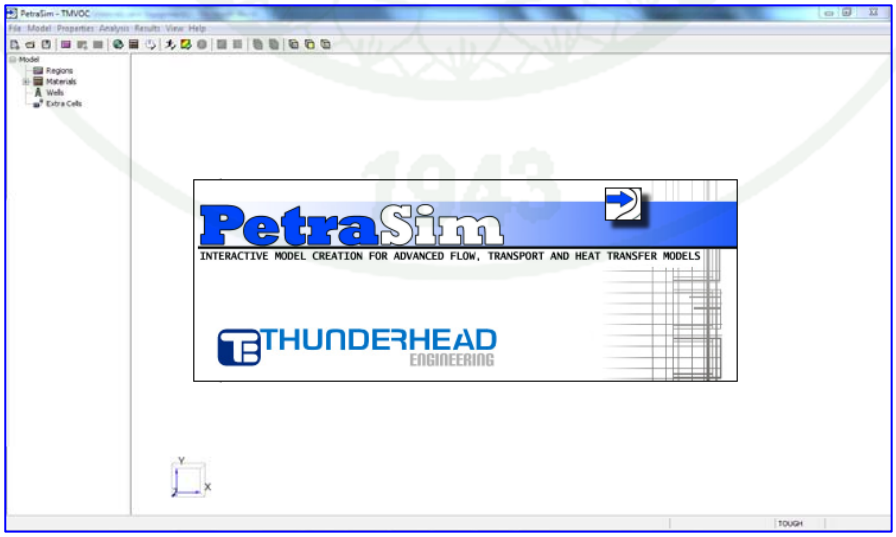

Figure 38 Graphic User Interface (GUI) of TMVOC simulator

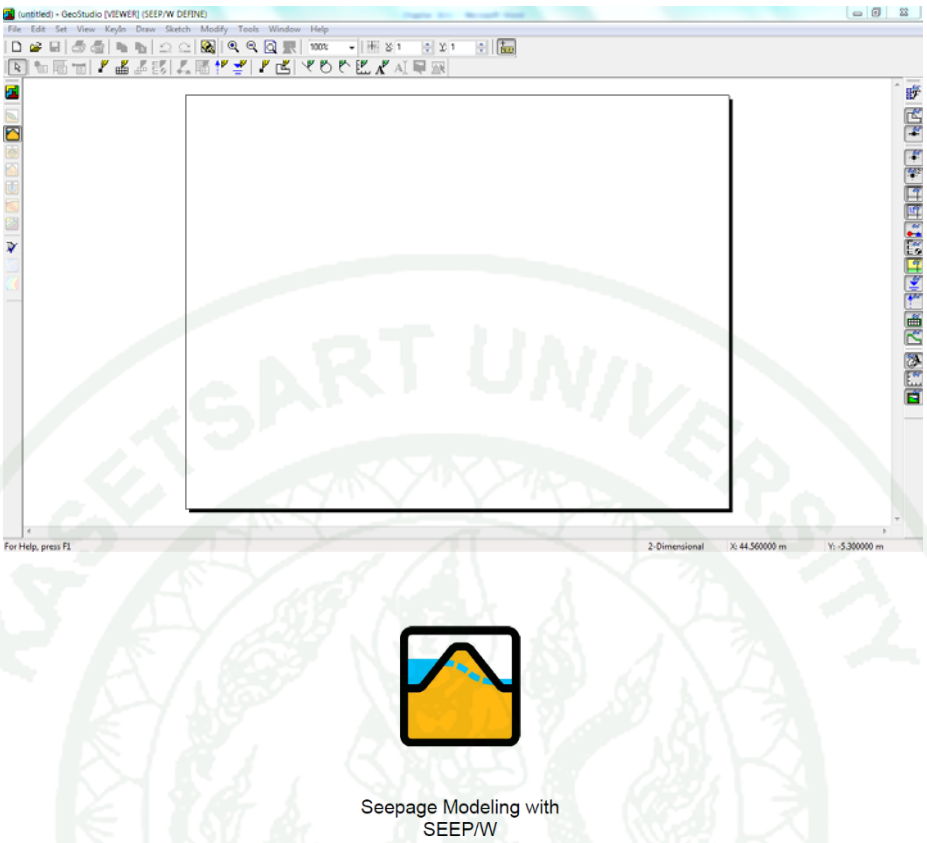

Figure 39 Graphic User Interface (GUI) of SEEP/W simulator

Research Methodology

According to the introduction of this chapter, this research is composed of four parts: laboratory experiment, physical tank model, centrifuge model and numerical model. The results from all studies will include the construction method for using soil cement column to contain contaminant migration. The flowchart of the methodology is shown in Figure 40.

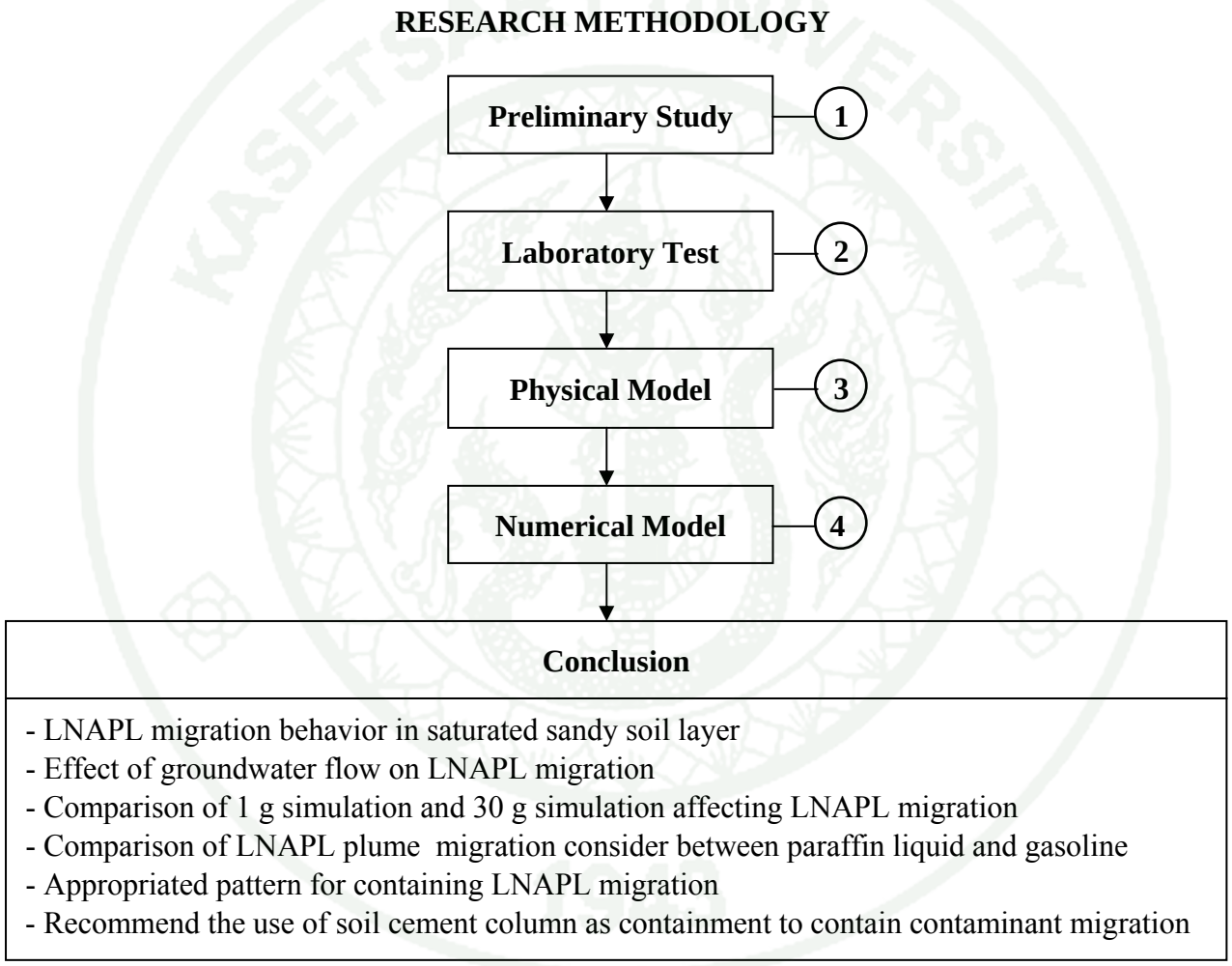

Figure 40 Flowchart of methodology

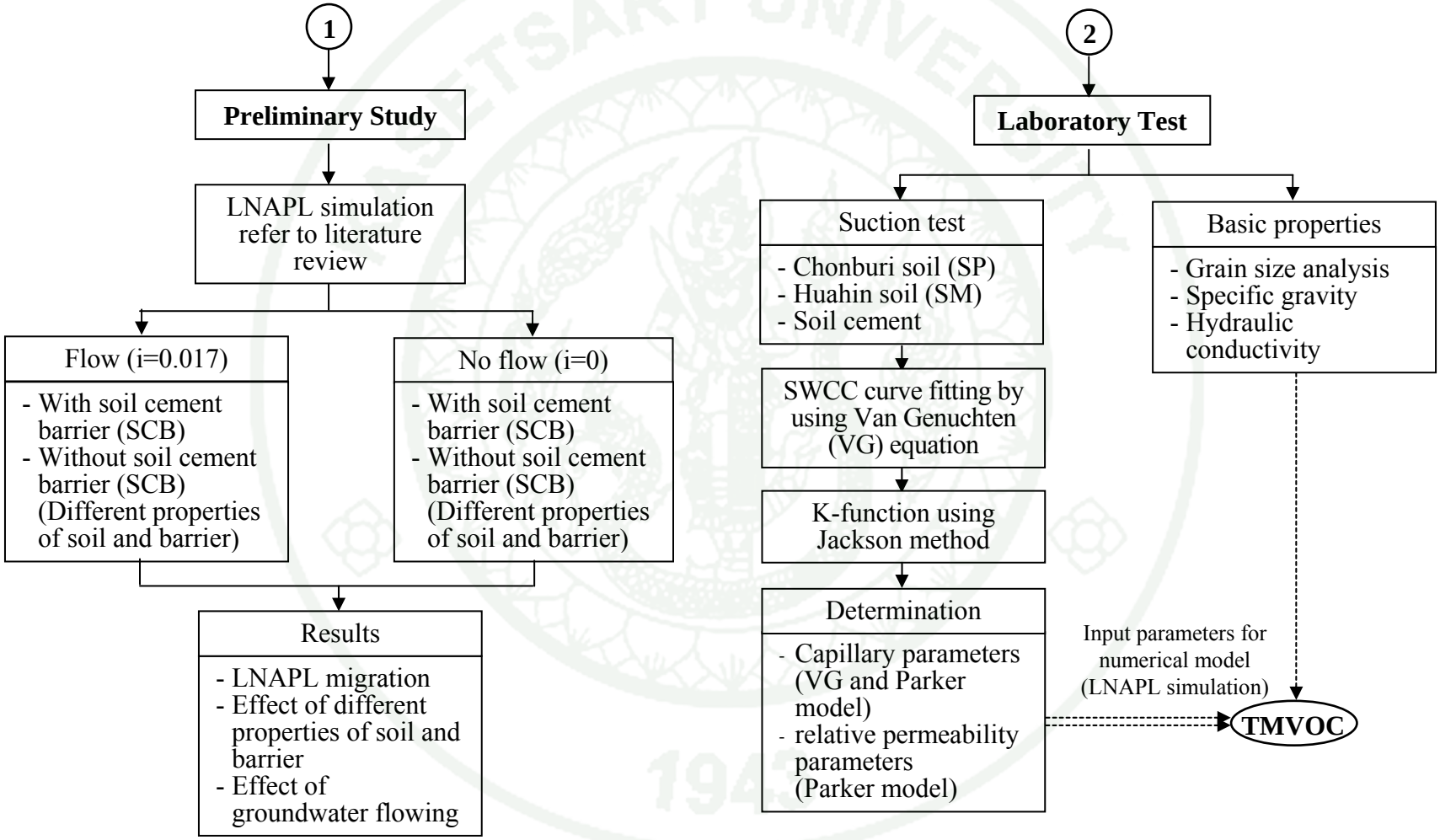

Figure 40 (Continued)

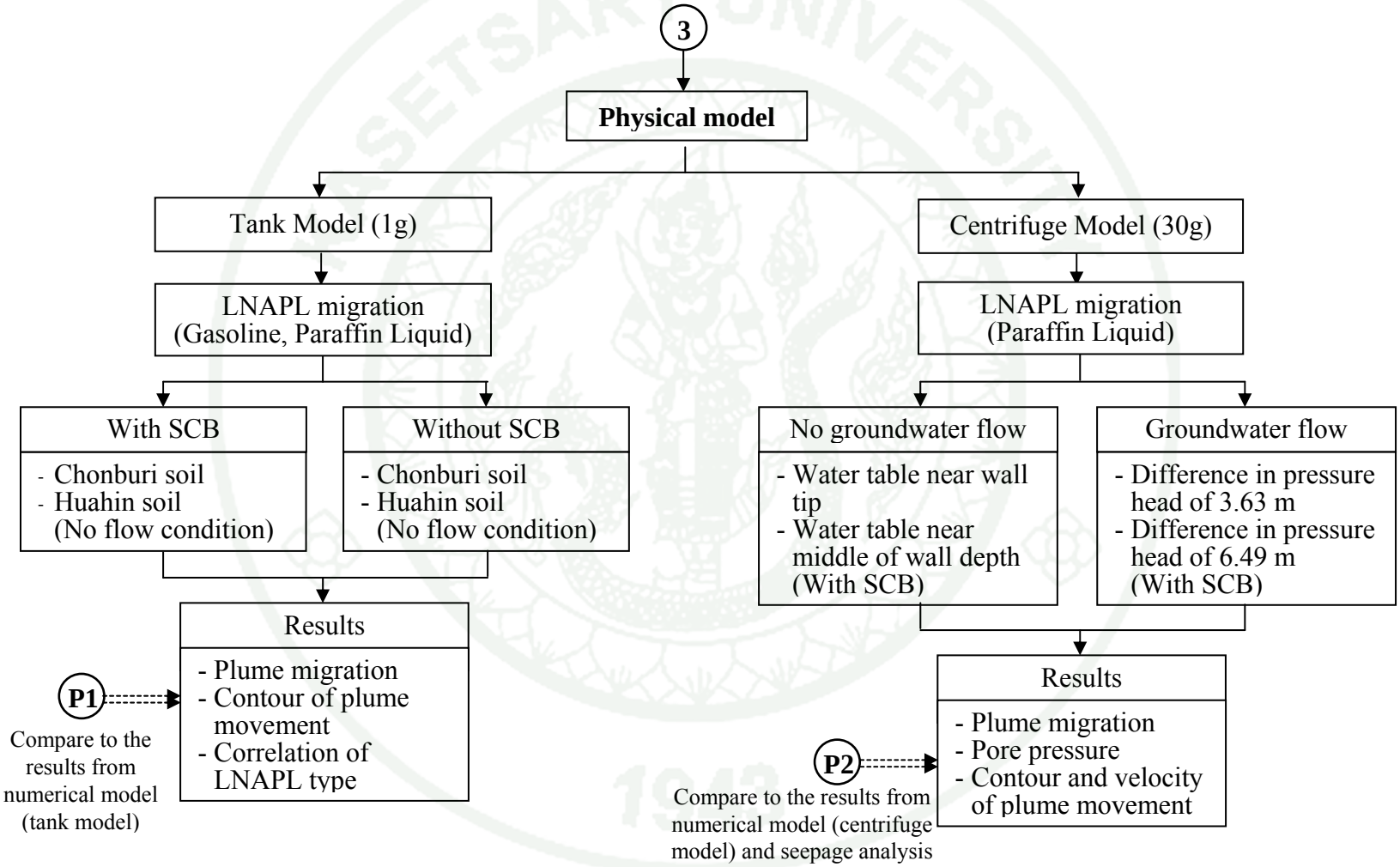

Figure 40 (Continued)

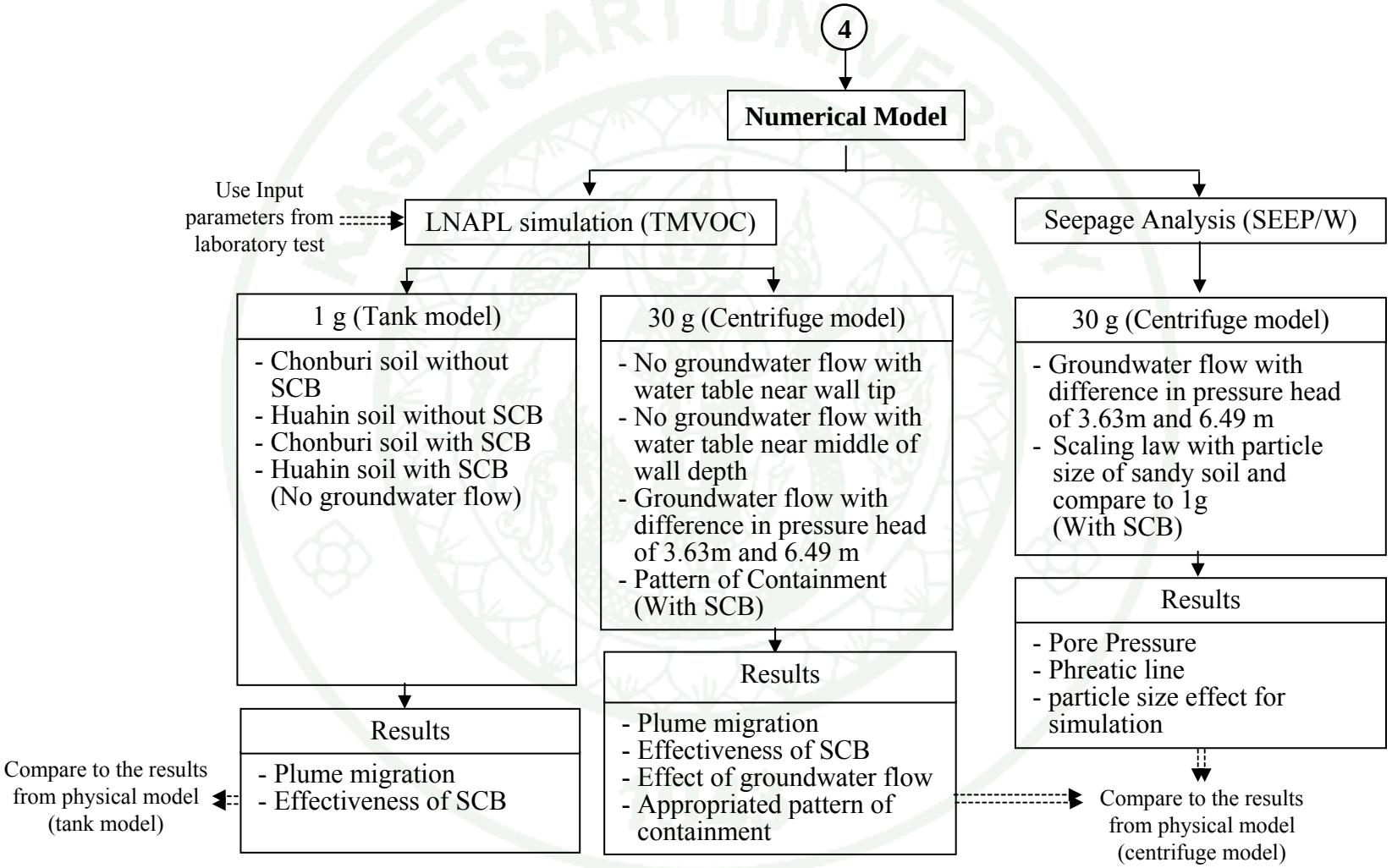

Figure 40 (Continued)

This research was based on a simulation study of LNAPL migration through containment with and without flow. The simulations took into account different barrier materials and different aquifer hydraulic gradients. This preliminary study addresses the processes controlling the migration of VOCs spilled in the vadose zone in the presence of vertical containment walls in sandy aquifers. The properties of the containment used in these simulations were derived from bibliographic sources. Consequently, experimental derived properties were determined as part of SWCC determination. The results from this experiment can be used to determine capillary parameters and relative permeability parameters, which are used as input model parameters. Both the physical small tank model experiment and centrifuge model experiment were performed to verify that the soil cement barrier could be used to contain LNAPL migration as well. To confirm the result of each experiment, numerical modeling was conducted for comparison. In addition, all experiments show the behavior of LNAPL migration under various conditions: (1) with containment, (2) without containment, (3) with flow and (4) without flow. Finally, the results obtained from the entire study will include suggestions for fieldwork. The descriptions of the methodology are shown as follows.

1. Preliminary study

TMVOC simulator was conducted to simulate LNAPL migration which refers to Batistelli (2008). The description of this study could be presented as shown follows.

1.1 Model characteristics and material properties

The conceptual models used in the study are shown in Figure 41. They are two dimensional sections 60.2 m long, 15.1 m thick and 1 m wide. The characteristics of the four models are: (1) no ground water flow (hydraulic gradient equal to zero), (2) ground water flow with a hydraulic gradient of 0.017 (water table difference of 1 m along a distance of 60 m (1/60), (3) no ground water flow with containment

(hydraulic gradient equal to zero), and (4) ground water flow with a hydraulic gradient of 0.017.

Effect of intrinsic permeability ($K_i=k_{darcy}\mu/\rho g$) was studied. Three intrinsic permeability values of soil were used which are 10^{-9} m^2, 10^{-10} m^2 and 10^{-11} m^2. The intrinsic permeability of barrier value was also indicated which are 10^{-13} m^2, 10^{-14} m^2 and 10^{-15} m^2. This study considers a total of 24 different cases. The relative permeability and capillary pressure curves for three-phase systems are described according to the Stone (1970) and Parker *et al*. (1987) models, respectively. The simulations are performed at a constant temperature of 20 °C. The atmospheric boundary conditions are fixed at the grid top and specified as constant absolute pressure of $1.01x10^5$ Pa.

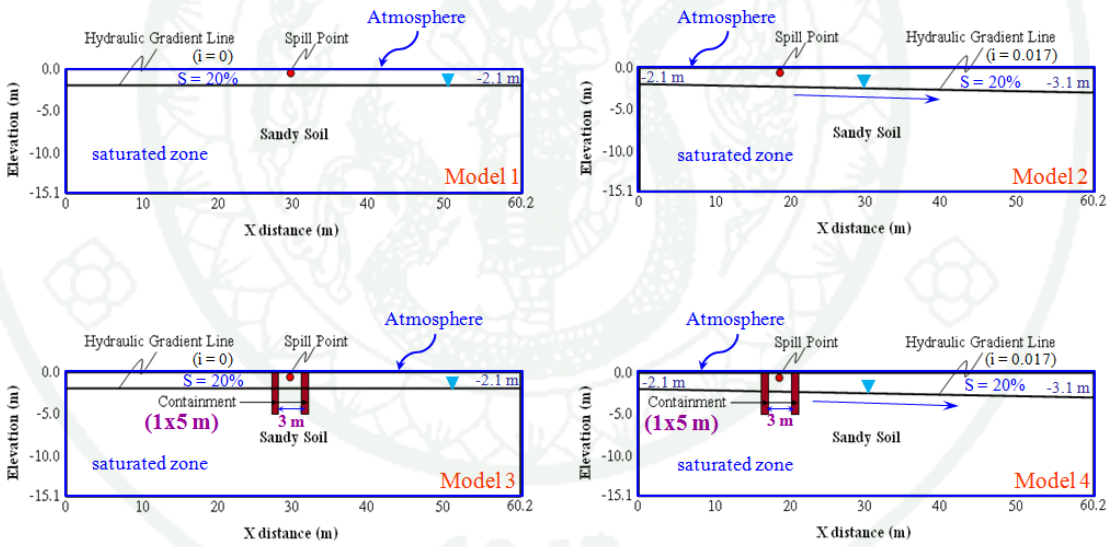

Figure 41 Conceptual model of preliminary simulation

1.2 Simulated scenarios

The modeling is discretized with 16 layers and 62 columns for a total of 992 elements. The vertical and horizontal spacing is 1x1 m, except the elements of top row which are 1x0.1 m; left and right boundary columns have the spacing of 0.1x1 m. The simulations are divided into several steps as follows: (1) setting up the initial

conditions at left and right boundary columns; (2) run to steady state controlled by gravity and capillary forces and subjected to the boundary conditions at lateral and top grid sides specified for each case; and (3) modeling of spill for 2 years starting from the steady state conditions obtained at step 2. The LNAPL spill has been modeled assuming a constant rate of 1.154×10^{-5} kg/s, equivalent to 1 kg/day. In this study, the effectiveness of barrier is analyzed looking at the effects of aquifer permeability and hydraulic gradient.

2. SWCC determination

The suction of soil and soil cement samples were measured by KU (Kasetsart University) tensiometer which can measure the values of suction from 0 to 100 kPa (Jotisankasa *et al*., 2007). Figure 42 shows the set up for suction-monitoring on soil and soil cement samples. The point-wise measurement was used to be the method in this study that Tapparnich (2010) proposes the process of testing as follows: (1) takes specimen into PVC ring and soak it for about four days (2) after that, measure dimension and weigh specimen (3) install tensiometer at the top of specimen for measuring the suction including measure and weigh it after finish measurement (4) reduce the weight of specimen about 2 or 3 grams and cover and cure it for 24 hours (5) perform stage 3 and 4 again until water content closed to zero or the suction is close to 100 kPa and (6) dry in oven to determine the final water content. After the experiment, the test data were used to construct soil water characteristic curve (SWCC) by using a Van Genuchten (1980) equation. The SWCC used to determine hydraulic conductivity function (k-function) using Jackson (1972) formula. The static two-phase capillary-saturation (P-S) relationships of the tested material (NAPL-water and air-water) were determined from SWCC (air-water) using a scaling factor method (Parker *et al*., 1986; Gudbjerg *et al*., 2004).

Figure 42 Experimental set up for suction-monitoring

3. 1g model experiment

The soil layer was prepared by pouring the sandy soil over distilled water. The water level in the tank was raised progressively and always maintained higher than the soil surface (2 cm above surface) during pouring to avoid excessive particle segregation in water. For the models with a barrier, when the sandy soil layer reached to 8 cm above the bottom, the soil cement barrier which has the dimension of 30 cm high x 77 cm wide x 2.5 cm thick was constructed from the center line of 5 cm in both left and right directions, and left for a day. Then the soil pouring continued until the height of the layer was 36 cm. After soil was poured completely, the water was drained to maintain the water level of 0.22 m and 0.10 m above the bottom for Conburi soil and Huahin soil, respectively and left for four days to steady state condition. Consequently, the storage tank contained 300 cm^3 of gasoline with octane 91% mixed with Sudan IV to enhance the intensity of red color was placed on the top and on the center line of the tank model. The criteria of the experiments were a no-flow condition for the water and LNAPL phases. The duration was kept constant for 210 minutes and 900 minutes for Chonburi soil and Huahin soil, respectively. Additional to investigate the effect of LNAPL types on LNAPL migration, the paraffin liquid was also used as LNAPL in experiment for Chonburi soil because it is

nontoxic substance (Kamon *et al*. 2006). During the experiment, images of the gasoline plume of each model were taken using a digital camera under constant light conditions. The concentration of the plume was measured by image analysis using an Adobe Photoshop program and the contour plots of contaminated plume using Surfer Program.

4. Centrifuge model experiment

4.1 Soil cement wall preparation

Before pouring the sand into the box, soil cement walls were constructed within the box. The dry density of the soil cement wall used in this test was the same as in small tank model experiment. The water cement ratio (W/C) was 2 and the quantity of cement was 220 kg/m^3. The mixture of each wall was shown in Table 16. The dimension of each wall was 2 cm thick by 37 cm long by 20 cm depth. Two walls were located at 5cm from the center in the left and right direction as shown in Figure 43.

Table 16 The mixture of each soil cement wall

Materials	Mass (g)
Nevada sand	2541.44
Cement	367.84
Water	735.68

4.2 Soil preparation and instrumentation

Dry sand was placed in the strongbox from a constant height using pluviation, also known as sand raining as shown in Figure 44. Sand was poured in the top opening of the funnel, and a device was moved in a smooth back and forth motion across the box to let the sand fall evenly into the box. Sand was pluviated lift by lift and pore pressure sensors were placed at each lift. Details of the thickness of the lift and the locations of the sensors are shown in Figures 36 and 37. The sand density in

each lift was verified to ensure a uniform sand density throughout the sand model. After the dry sand preparation was completed, a predetermined amount of water was gradually added to the sand until it reached the desired water level. This process is conducted by slowly dripping water into a sponge placed on the sand surface at a corner of the strongbox as shown in Figure 45. The water level was monitored using pore pressure sensors during the centrifuge spin up.

Figure 43 Installation of the soil cement wall into the box

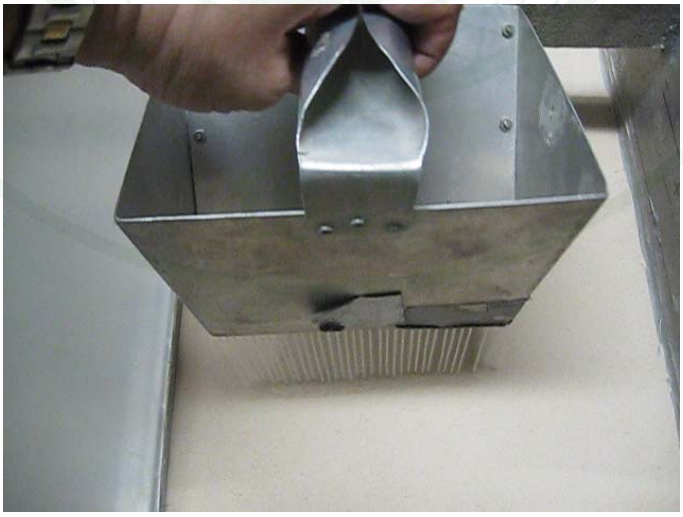

Figure 44 Sand raining using pluviator

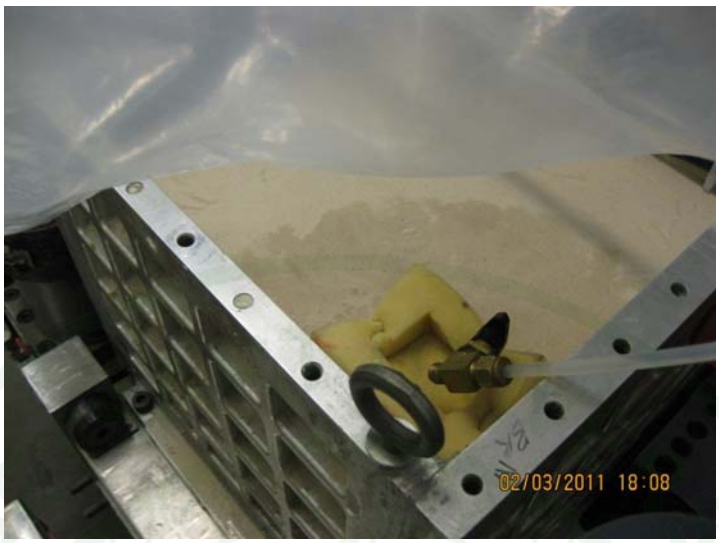

Figure 45 The water filling to sand

4.3 Experimental procedure

After finished sand layers preparation and instrument installation, water was filled by slowly injection into the sand deposit until water level reached to 4.3 cm below the sand surface. The process used to supply the LNAPL to the sand deposit was as follows. After placing the strong box on the swinging basket, the supply container was attached on top of the strong box and at the center. The 800 ml LNAPL was stored in container at 1g. The LNAPL will be released after centrifuge machine startup with flow rate of 0.015 ml/s under acceleration gravity of 30 g. The g-level of 30 was used in this testing because the desired thickness of soil cement wall was 60 cm in prototype. For ground water flow condition, when centrifuge machine startup, water would be filled into the upstream reservoir to create the ground water flow. At the downstream reservoir, water would be released and used the pump to circulate the water to the upstream reservoir. Water level in the upstream and downstream reservoir was controlled throughout testing. In the prototype scale, the volume of LNAPL was 21,600 liters and the duration of testing was 80 days.

5. Numerical simulation

5.1 LNAPL migration for Small tank and centrifuge modeling

The input parameters required for the numerical simulation are grouped into three sets as described below:

5.1.1 The properties of soil and soil cement which are the particle density, the porosity and the hydraulic conductivity were the same as the properties of experimental materials of centrifuge test described previously.

5.1.2 The k-S-P relation parameters are described below.

a) Capillary pressure parameters (S-P parameters): The air-water saturation-capillary head (S-P) curve was developed by Rungruang and Kerarat (2010). Experiments were performed using a sandy soil. These properties are specific gravity, dry density, porosity and grain size distribution.

b) Model parameters proposed by the van Genuchten (1980) was used to fit experimental data and the S-P curve. The static two-phase saturation-capillary head (S-P) relationships of the soil and soil-cement (NAPL-water and air-NAPL) were determined from SWCC (air-water) using a scaling factor method (Leverett, 1941; Parker *et al*., 1987). The scaling factors obtained from the interfacial tensions of the two liquids were used to construct the S-P curves for the two-phase air-NAPL and NAPL-water systems. The van Genuchten model (1980) and Parker model (1987) were fitted to the model parameters for the soil and soil cement. Relative permeability parameters (k-S parameters): The S-P curve used to determine hydraulic conductivity function (k-function) using Jackson (1972) formula. Parker model (1987) was fitted to the k-S parameters for the soil and the soil cement.

5.1.3 The chemical properties of LNAPL can also be found in Reid *et al*. (1987). These properties include fluid density and viscosity of LNAPL.

The two-dimensional sections of the numerical models are generated to replicate the cross sections of the physical models (1g models and centrifuge models). The groundwater levels measured from the physical models are used as the side boundary conditions. The grid spacing of the numerical models in the vertical and the horizontal directions is based on the groundwater levels and the thickness of the containment. The simulations were performed under isothermal conditions. In this condition, the heat transfer is not occurrence; therefore the enthalpy parameter is not defined as discussed by Pruess and Battistelli (2003). The atmospheric boundary conditions are fixed at the grid top and specified as the constant absolute pressure of 1.013×10^5 Pa. A soil grain specific heat of 50,000 J/kg °C and a porosity of 0.999 are assumed for the atmospheric grid blocks because effects of the inner domain on the atmospheric boundary are negligible due to the volume of the atmospheric boundary (Rasmusson 2009). The walls are modeled as low permeability material. The water head differences obtained from the centrifuge tests were used to setup the left side and right side boundary condition. The simulated pore pressure distributions referring to the water pressure measured from the physical model tests were calculated by equation (56) to set up the boundary condition and the model is run to reach the steady-state condition before introduction of the LNAPL. The pressure assigned to the nodal point of the groundwater table obtained from the locking grid block is calculated according to the following equation:

$$P = P_{atm} + \rho_w g h \quad (56)$$

where P_{atm} is the atmospheric pressure (101,300 Pa); ρ_w is the water density (9,789 N/m^3); g is the gravitational acceleration vector (9.81 m/s^2); and h is the distance from the groundwater table to the element node.

5.2 Stress levels effect

Many researchers have investigated contaminant transport in soil, and several researchers have used centrifuge modeling to study the behavior of the

migration. The purpose of centrifuge modeling is to reproduce identical stresses in a model and a corresponding prototype with a small scale, accelerated modeling time, as shown in Figure 46. Figure 46(a) shows the water pressure profile under hydrostatic conditions in a prototype soil deposit with a thickness of *H*. The equivalent *N* g centrifuge model has a soil deposit with a thickness of *H/N* (N times smaller than the prototype) and is shown in Figure 46(c). Considering the increase in the unit weight of water in the increased gravity field ($\gamma_w=\rho_w N$ g, where ρ_w is the water density), the same ‘‘scaled’’ pore water pressure profile can be achieved at a distance of H/N from the water level. Thus, the water pressure in the centrifuge model will be identical to those in the prototype. When the same model is at 1 g, the water pressure profiles are not the same as those of the prototype, as shown in Figure 46(b)

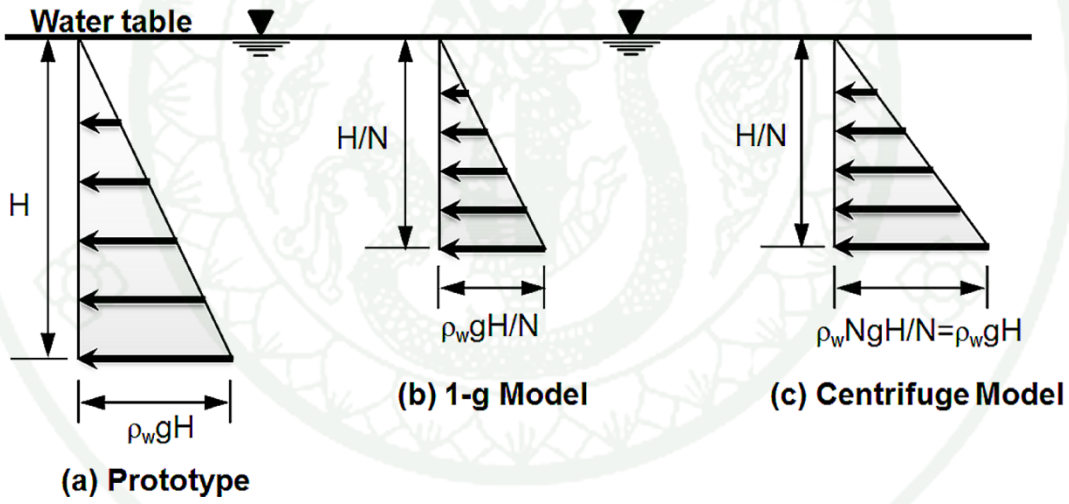

Figure 46 Pressure distribution for (a) prototype under the earth’s gravity field; (b) 1-g model under the earth’s gravity field:1g; and (c) centrifuge model under acceleration gravity field:Ng

For contaminant transport problems, the self-weight effect should be considered in relation to the three factors (Nakajima *et al*. 1991; Taylor 1995). First, the movement of liquid contaminant is greatly dependent on the porous medium’s hydraulic properties, which are strongly influenced by the pore size and the particle orientation of the soil. Reproducing identical stresses at corresponding points in the

model and the prototype can lead to a similar hydraulic conductivity distribution. Second, when contaminant transport has interactions between fluids with different specific gravities, density gradients must be scaled in the model. Third, potential gradients are important when contaminant migration problems involve flow in an unsaturated zone and an area adjacent to the water table. Furthermore, Taylor (1995), and Zhou and Yu (2005) mention that stress levels are greater influence on SWCC and permeability than other effects that result in the movement of LNAPL migration. The flow chart of stress levels affecting materials properties that result in the LNAPL migration is shown in Fig. 47.

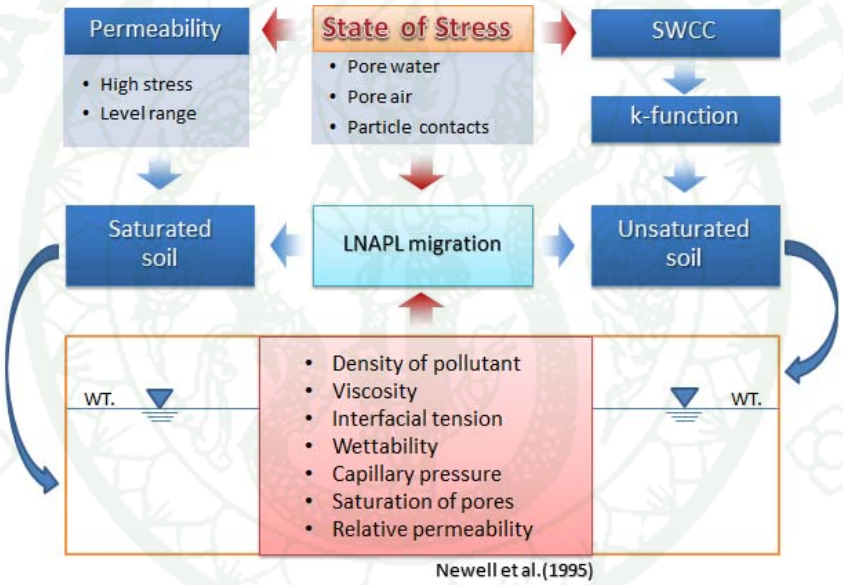

Figure 47 The stress levels affect materials properties that result in the LNAPL migration

To describe why this experiment use centrifuge modeling and how the scaling theories are developed. The numerical simulations are performed to examine the seepage behavior comparing between the models used and no used scaling law. The effect of groundwater flow is evaluated by seepage analysis. This analysis is based on the centrifuge model experiments. The major components in solving a seepage analysis are as follows:

5.2.1 Geometry of models is generated to replicate the cross section of centrifuge model in groundwater flow condition (prototype). These models are considered in with soil cement wall.

5.2.2 The properties of soil and soil cement are referred to the properties of the experimental materials and suction measurement. For 1 g simulation, the dimensions of the model are 35.6 cm high and 87.6 cm long. For 30 g simulation, the dimensions of the model which extend using scaling laws are 11.10 m high and 26.28 m long.

5.2.3 The water head differences obtained from the centrifuge tests are used to setup the left side and right side boundary condition. They are the head differences 6.49 m for 30 g simulation and 0.216 m for 1g simulation to observe the particle size effect and stress levels effect due to scaling law.

5.3 Behavior of LNAPL migration for different pattern of containment

The numerical simulations are performed to examine LNAPL migration behavior comparing between the models with containment in case of flow and no flow conditions. Several patterns of containment are simulate which are single and double wall containment. The two-dimensional sections of the numerical models are generated to replicate the cross sections of the centrifuge models. Gasoline is used as LNAPL to represent the field contamination. According to the results of numerical models, the appropriated pattern of containment will be recommended for field construction.

RESULTS AND DISCUSSION

In this study, the works were divided into 4 parts which consist of suction test, small tank model test, centrifuge test and numerical simulation.

1. Suction Test

According to suction test, the relationship between suction and volumetric water content of sandy soil and soil cement samples is show in Figure 48. The SWCC fits of soil and soil cement using the mathematics models proposed by van Genuchten (1980) as shown in Figure 49. As the results, soil type and particle size of soil affect the soil suction. If the particle size of soil is smaller, the suction is higher. The suction of soil in drying process is greater than wetting process because when the water is drained out in drying process, the water content decreases and suction increases; while when the water infiltrates the soil in wetting process, the water content increases and the suction decreases. SWCC of soil cement samples is more slope than sandy soil. It shows if the soil pore is smaller, the suction is higher and it is corresponding to previous researches.

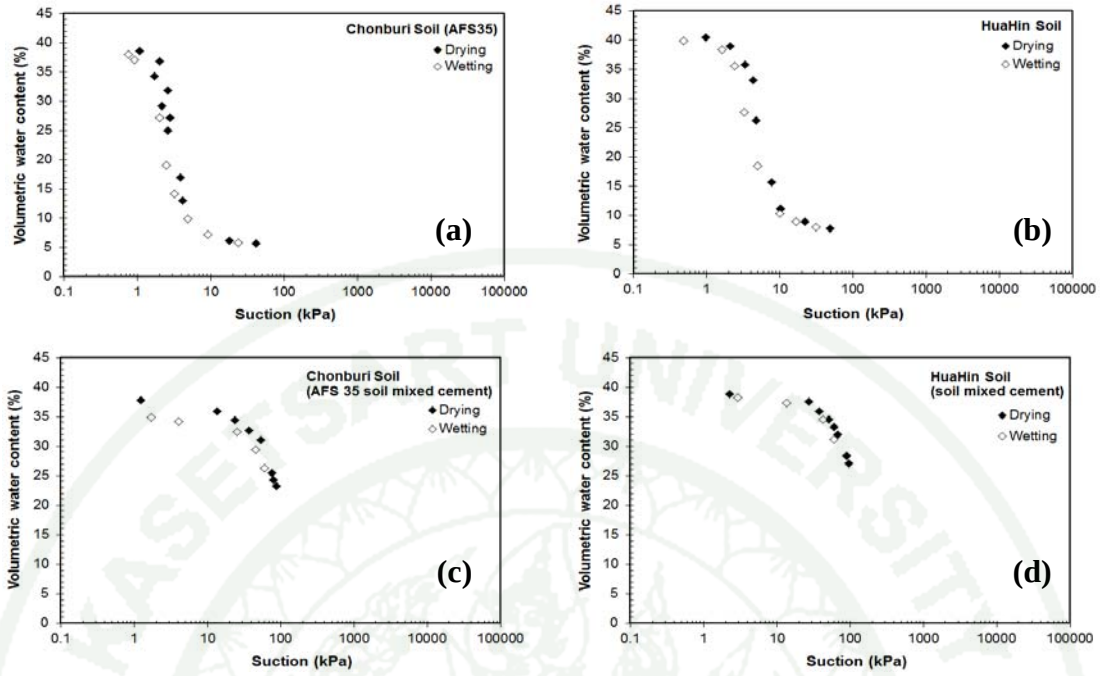

Figure 48 Relationship between suction and volumetric water content

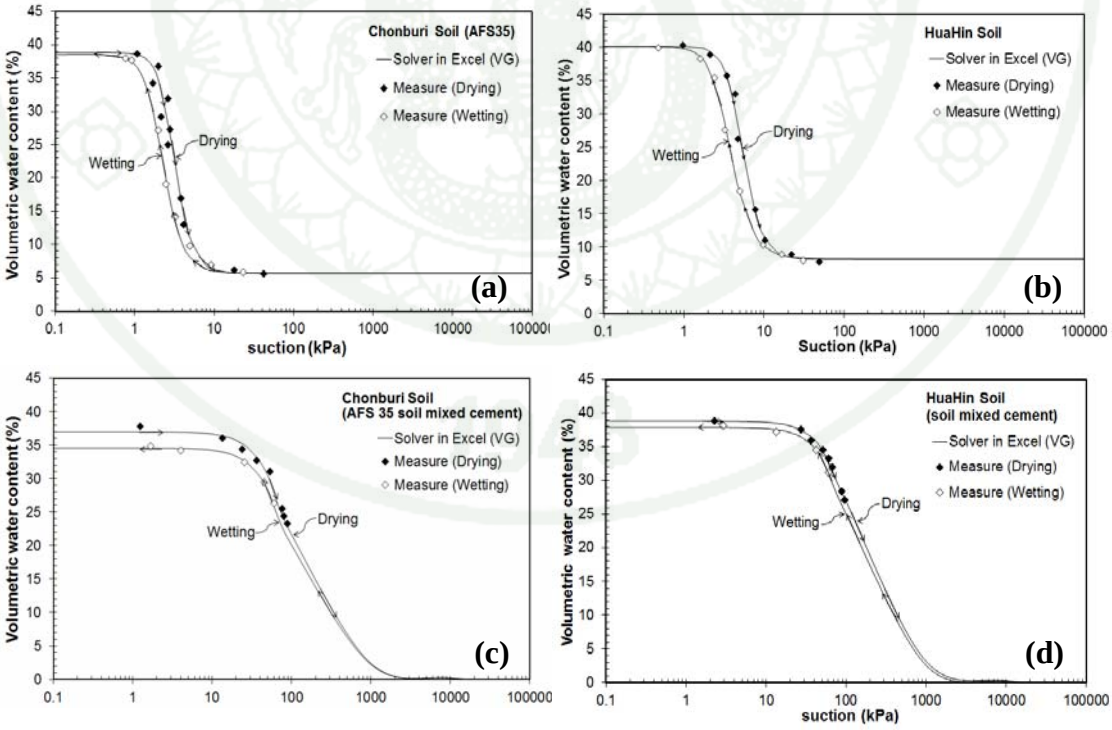

Figure 49 Soil water characteristic curves of sandy soil and soil cement

SWCCs (or S-P relationships) are used to estimate the permeability function curves (k-function) using Jackson formula (1972) as shown in Figure 50.

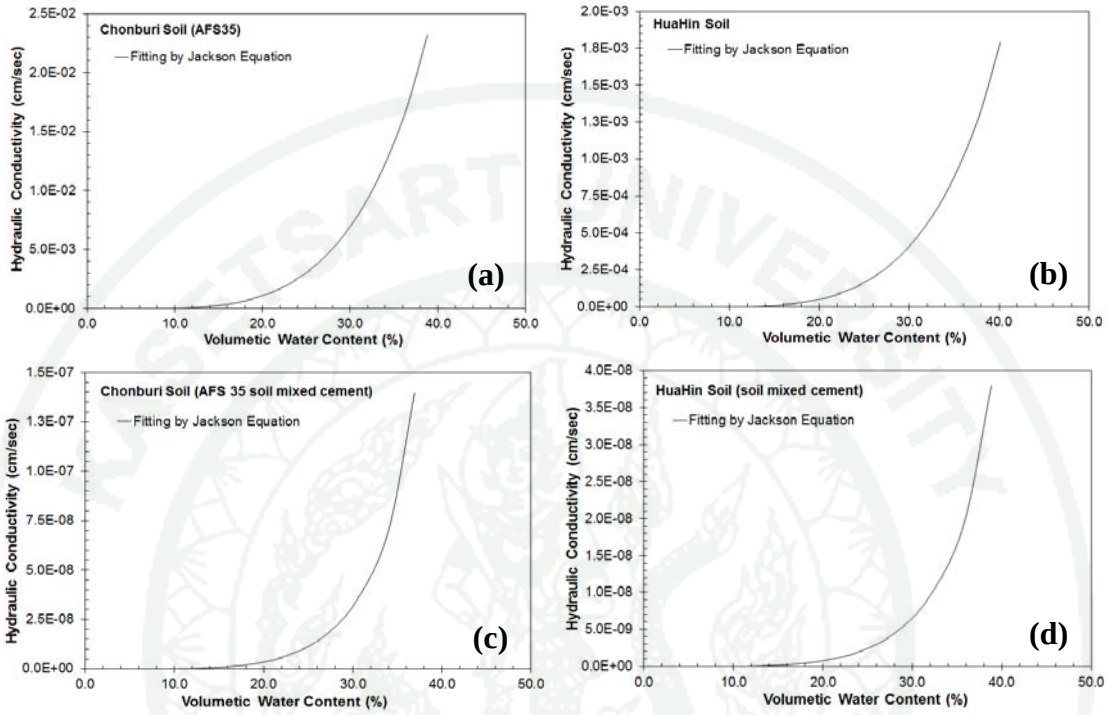

Figure 50 Permeability function curves of sandy soil and soil cement

Both SWCC and the permeability function curves can be used to determine the model parameters which are used to numerical simulation for LNAPL migration.

2. 1g Model Test

2.1 The contour plots of the gasoline plume migration

During experiment, images of the tank containing gasoline plume were taken using digital camera under constant lighting condition. The saturation of the gasoline plume measured with the image analysis which using Adobe Photoshop CS3 program to determine the concentration of gasoline and show the contour plots of gasoline saturation using AutoCAD Program. The contour plots of the gasoline plume at 210 minutes and 900 minutes for Chonburi soil and Huahin soil respectively, are

shown in Figure 51. Figures 51(a) and (c) show the gasoline plume migration in case of without containment for Chonburi soil and Huahin soil, respectively. Figures 51(b) and (d) show the gasoline plume migration in case of with containment for Chonburi soil and Huahin soil, respectively. The water levels below ground surface for Chonburi soil and Huahin soil are 14 cm and 20 cm, respectively. At the beginning of spill, the gasoline moved in both vertical and horizontal directions and the plume was narrow and oblong. This shows that the gravitational potential gradient was higher than the spilled head and capillary force and the flow was mainly gravitational. The gasoline plume continued its migration until it reached the capillary fringe due to soil particle and capillary force called suction, and began to spread out laterally above the saturated zone. For the case without a barrier, the width of the plume in the Huahin soil was small compared with the plume in the Chonburi soil because the Huahin soil has finer percentage than the Chonburi soil but the entrapment of gasoline in Huahin soil was larger than that of the Chonburi example. For the case with a barrier, the behavior of migration was same as previous case but the gasoline plume did not migrate outside the barrier in both sandy soils. After finish experiments, the sample of soil cement wall which containing gasoline was taken to measure the concentration of benzene by using gas chromatography / mass spectrometry (GC/MS) method at department of science service, ministry of science and technology, Thailand. As the results, the concentration of benzene within the wall is 0.025 mg/kg which less than the standard value of 6.5 mg/kg (Announcement of National Environmental Board No.25, 2004). This confirms that soil cement wall can be used as the containment for containing LNAPL.

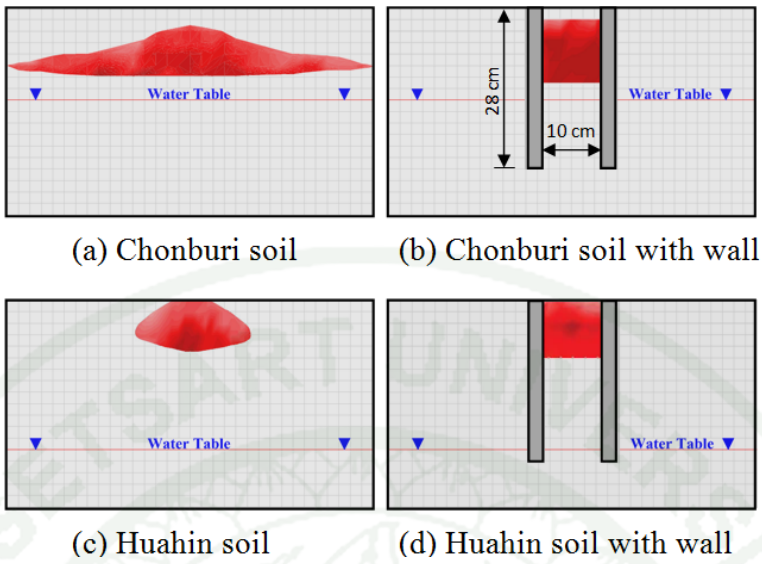

Figure 51 The contour plots of the gasoline plume at 210 minutes and 900 minutes for Chonburi soil and Huahin soil respectively

2.2 Effect of LNAPL types on LNAPL migration

Soga *et al.* (2003) investigated the movement and the entrapment of water and LNAPLs in unsaturated, layered soil deposits and compared the results to those of a numerical simulation. Two types of LNAPLs used in this study were Soltrol 220 and silicon oil. The kinematic viscosity of the silicon oil is approximately three times that of Soltrol 220. The results show that the front velocity of Soltrol was approximately three times faster than that of silicon oil during the redistribution stage. They mention that the movement of the LNAPL front is dictated by the LNAPL viscosity and density. The observed difference in velocity is directly related to the difference in kinematic viscosity.

Kamon *et al.* (2006) described that both liquid paraffin and benzene are LNAPLs. Liquid paraffin consists mainly of a mixture of saturated straight-chain hydrocarbons. It is a substance that in its pure form is white, odorless and translucent and has the approximate chemical formula of $C_{20}H_{42}$. Benzene is a volatile aromatic hydrocarbon and is known to be a human carcinogen. Thus, liquid paraffin was used

as a substitute LNAPL sample for experiment. Result from the column test, they found that the residual saturation of liquid paraffin was fitted to 0.5. Actually, the residual saturation of benzene in the in-situ contaminated subsurface should not be so large due to its much lower viscosity.

The result from 1g model show the effect of LNAPL types on LNAPL migration which is corresponding to the past study by Soga *et al.* (2003) and Kamon *et al.* (2006). The contour plot of the liquid paraffin plume at 210 minutes is as shown in Figure 52. It depicts that the plume in both vertical and horizontal directions are smaller than the gasoline plume migration because the viscosity of the liquid paraffin is larger than the gasoline. The comparison of the vertical and horizontal movement and the area of plume migration between the gasoline and the liquid paraffin are as shown in Figures 53 and 54, respectively. The results from this experiment can predict the distance of migration in sandy soils.

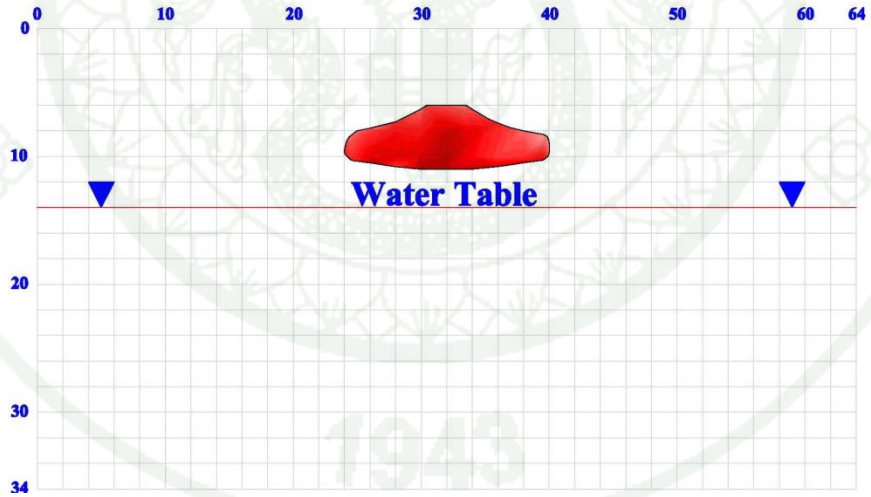

Figure 52 The contour plots of the liquid paraffin plume at 210 minutes for Chonburi soil

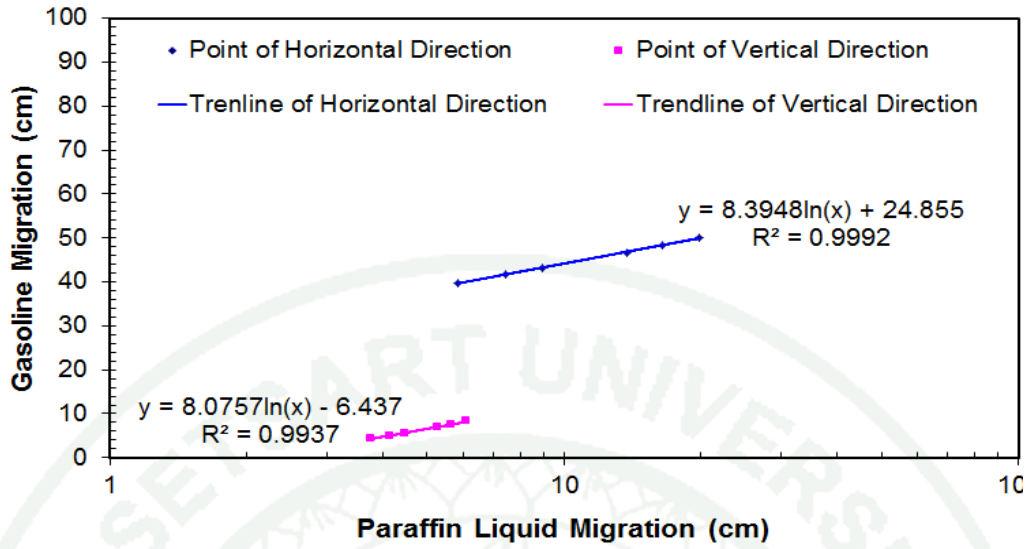

Figure 53 The comparison of the vertical and horizontal movement between the gasoline and the liquid paraffin

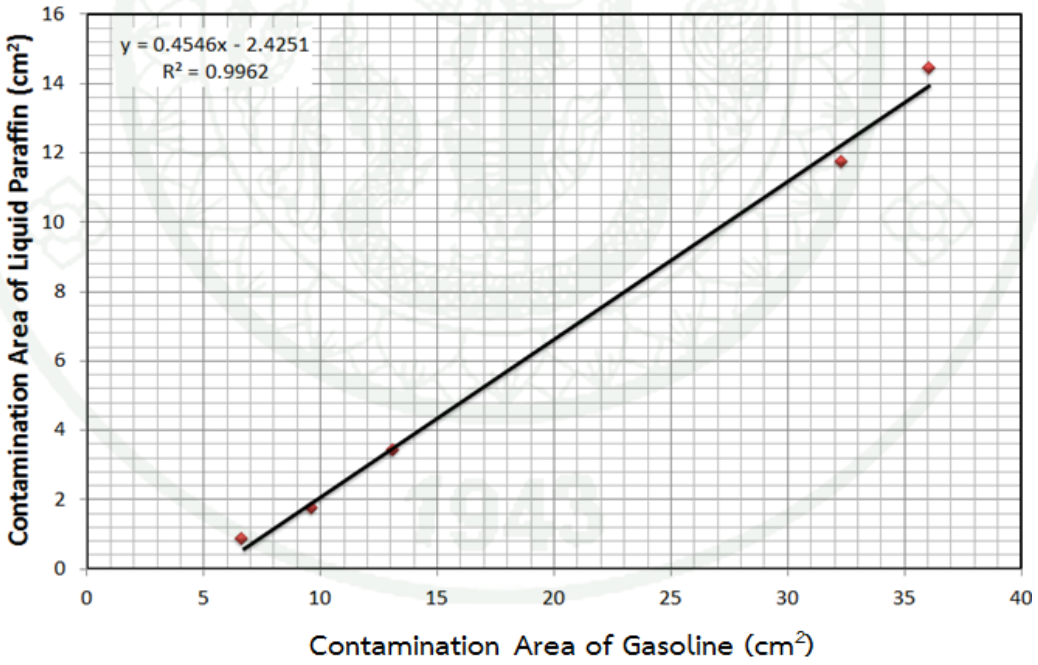

Figure 54 The comparison of the contaminated area between the gasoline and the liquid paraffin

3. Centrifuge Test

Tests 1 and 2 were under no groundwater flow conditions at different water levels. The phreatic surface of groundwater at 3.63 m and 1.81 m below the soil surface for tests 1 and 2, respectively, is presented in Figure 55. It shows that the levels of the phreatic surface at various locations are the same level which confirms the condition of no groundwater flow. The phreatic surface was developed from water pressure measured by pore pressure sensors at various locations in the model.

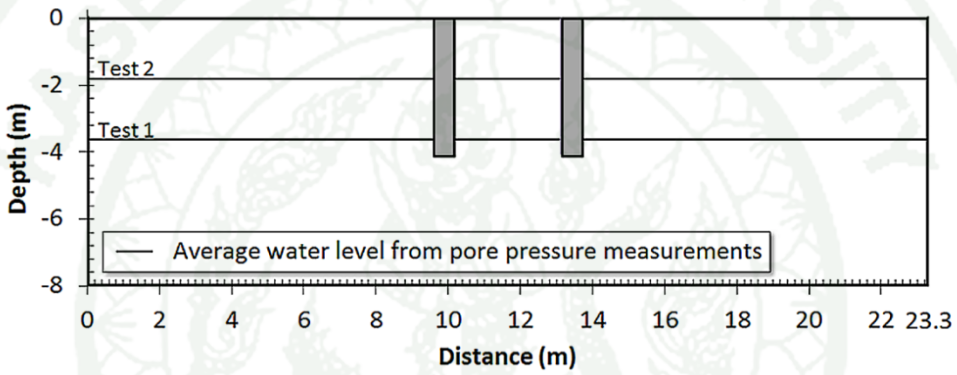

Figure 55 The phreatic surface of groundwater for tests1and 2 from pore pressure measurements (prototype unit)

Tests 3 and 4 were performed under groundwater flow conditions at 3.67 m and 6.49 m which are the difference in head pressure, respectively and the depth of water level below the soil surface at the middle of the container was 2.20 m for test 3 and 2.72 m for test 4. The head difference used in this study simulate for the case of the underground storage tank located near the water resource or the pumping well which is the extreme case. The phreatic surfaces simulated by TMVOC, which were comparable with the measured value from pore pressure sensor measurements, are presented in Figures 56 and 57. They show that the measured values are corresponding to the results from numerical modeling. Moreover, the flow net shows effects of the walls on the behavior of water flowing. These reveal that the pore water sensors are effective for using as the instrument in centrifuge model test. More

information regarding the TMVOC simulator is included in the numerical simulation section.

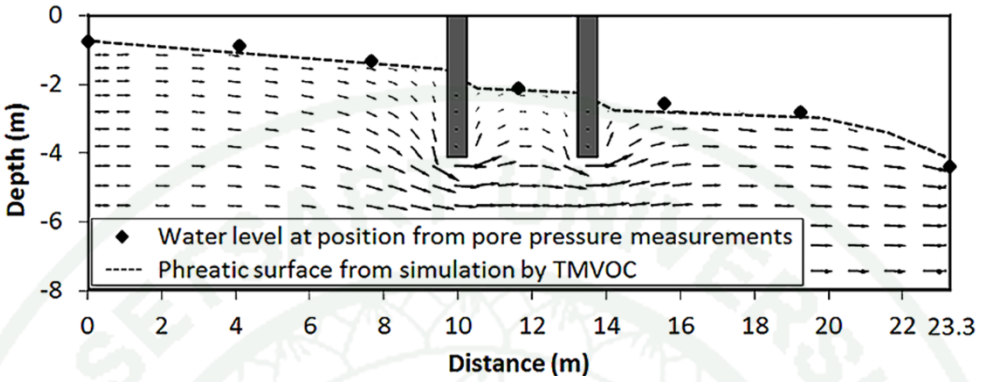

Figure 56 The phreatic surface determination for Test 3 comparing between numerical simulation (TMVOC) and pore pressure measurements

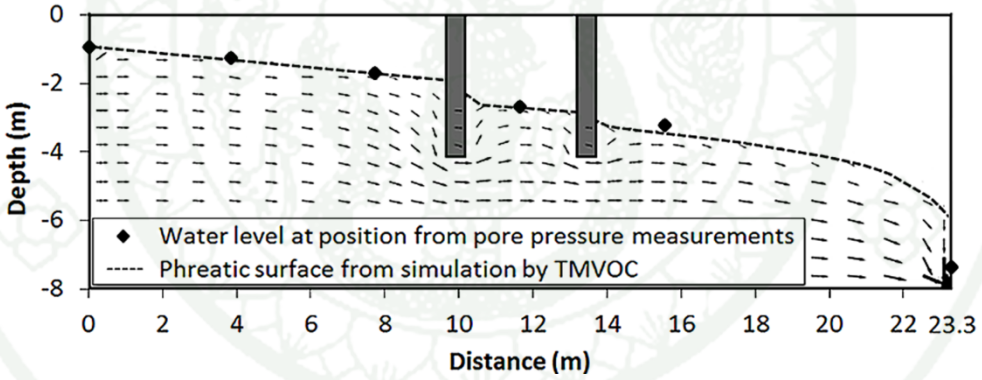

Figure 57 The phreatic surface determination for Test 4 comparing between numerical simulation (TMVOC) and pore pressure measurements

3.1 LNAL plume migration

The LNAPL was released to the soil surface at the center of the model and it rapidly spread over the surface of the model between the containment walls. The LNAPL then moved downward into the soil layer and was observed through the Plexiglas wall of the model container. In this study, the LNAPL migration was modeled as a 2D line source based on the observations during the centrifuge tests. This

assumption was confirmed from the model dissection after the centrifuge test, where a consistent distribution of LNAPL migration was observed throughout the cross section of the model.

Results from the centrifuge modeling and the numerical simulation of the LNAPL plume distribution at the end of all four experiments are shown in Figure 74. The LNAPL plume migration of test 1, which there was no groundwater flow, is shown in Figure 58(a). The LNAPL plume migrated underneath the wall with a symmetrical plume distribution. In this case, the water level was significantly depressed due to the large volume of LNAPL confined between the walls that resulted in a high positive pressure build-up, as observed from the pore water pressure measurement. As a result, the depth of the wall was inadequate for confining the LNAPL migration. The LNAPL plume migration of test 2, which there was no groundwater flow, is shown in Figure 58(b). Similar to test 1, the LNAPL plume migrated below the water level with a symmetrical plume distribution, but in this case, the depth of the wall was adequate for confining the LNAPL migration. The front of the LNAPL plume remained stable at the depth of 1.25 m below the water level.

The LNAPL plume migration of tests 3 and 4 with groundwater flow are shown in Figures 58(c) and 58(d), respectively. The LNAPL plume migrated below the water table with an asymmetric plume distribution. The LNAPL accumulated above the water level at the higher pressure side of the model, whereas the LNAPL plume migrated underneath the wall at the lower pressure side of the model. The depression of water table was found to be larger in the case of water flow due to a hydraulic gradient effect. Comparing tests 3 and 4, the amount of the LNAPL plume migration underneath the wall increases as the pressure head difference increases. These results indicate that the depths of the soil cement wall below the groundwater level should be no less than 1.50 m for no groundwater flow and 2.50 m for groundwater flow. The results from experiments in case of groundwater flow with containment are corresponding to the study of Hayashi and Allersma (2004).

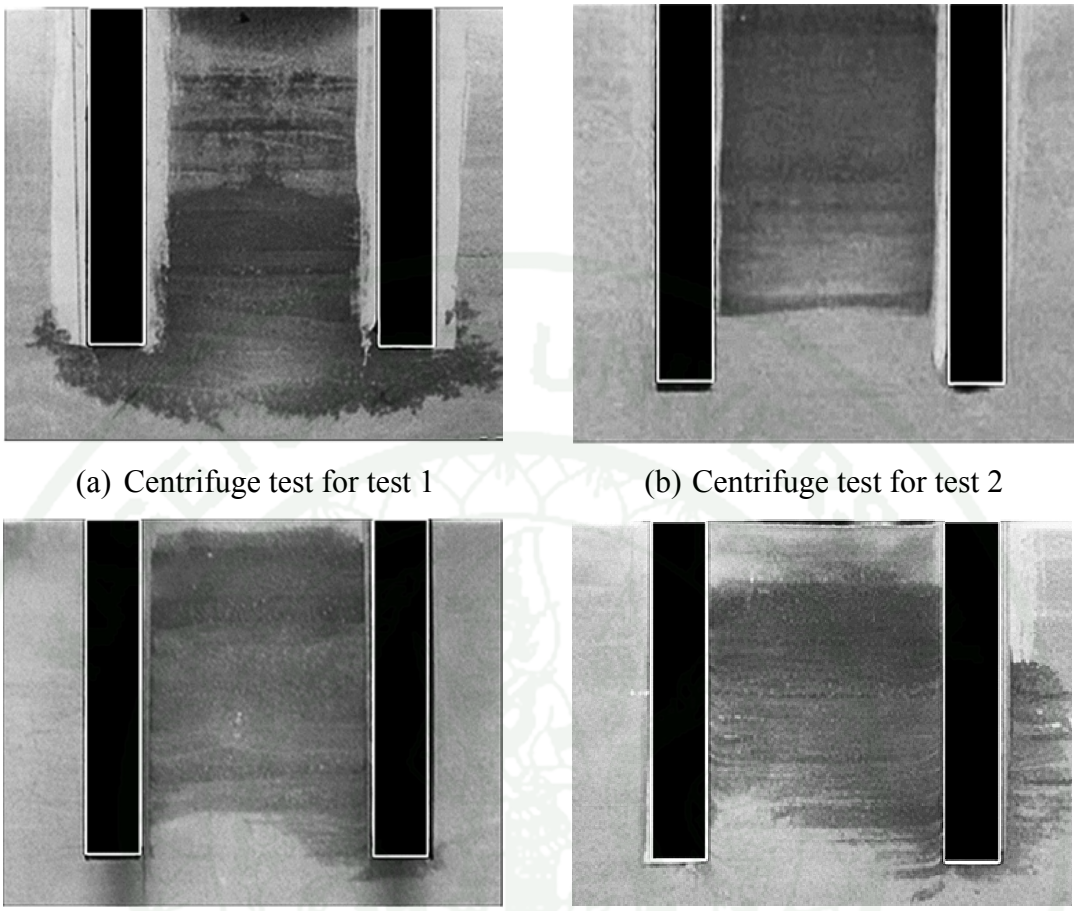

(a) Centrifuge test for test 1 (b) Centrifuge test for test 2

(c) Centrifuge test for test 3 (d) Centrifuge test for test 4

Figure 58 LNAPL plume migration at the end of centrifuge tests

3.2 Pore Pressure Measurement

Variations of pore water pressure at different depths within the soil layer are presented in Figure 59. During tests 1 and 2 (no groundwater flow), the water level decreased slightly at a constant rate because of the evaporation. The evaporation was not observed in tests 3 and 4 (groundwater flow) because the pumping system was capable of supplying water during the test.

Plots of the pore pressure change versus time for the condition of no groundwater flow are presented in Figures 59(a) and 59(b). For test 1 [Figure 59(a)], the water level was maintained near the wall tip. The LNAPL front reached sensor A1,

followed by sensors C1, A2, B2 and pressure decreased after the LNAPL passed these sensors. Once the LNAPL reached sensor A3 located at the wall tip (4.05 m below the soil surface), the water pressure increased and remained constant. This indicates that the water level was depressed due to LNAPL migration near the wall tip. As a result, the LNAPL could migrate underneath the wall and spread laterally, which was observed from video recording. In this case, the depth of the wall below the water level was inadequate. In test 2 [Figure 59(b)], the LNAPL front reached all of the sensors but never reached the sensor B2 indicating that the LNAPL was stable above this location. The water level was depressed to a depth of 1.2 m corresponding to the location of the sensor B1, where the pore pressure increased and remained constant. In this case, the depth of the wall was adequate to contain the LNAPL migration. The pore pressure measurements agreed with the observations from video recording. In addition, there were no observations of pore pressure change outside the wall indicating that the wall can act as an effective LNAPL containment barrier.

Plots of the pore pressure change with time for the condition of groundwater flow are present in Figure 59(c) and 59(d). For test 3 [Figure 59(c)], the average water level within the containment was comparable to the water level in test 2. However, in test 3 the water level was depressed to 2.07 m, corresponding to the location of sensor A11. The depth of water depression in test 3 was greater than in test 2, and the observation from video recording shows that the LNAPL plume migrated underneath the wall at the lower pressure side of the model. In this case, the depth of the wall was inadequate. In test 4 [Figure 59(d)], an increased head difference resulted in a higher flow velocity and a slightly lower water pressure in the containment. It was observed that the LNAPL front reached sensor A12, followed by sensors A11 and A3. In this test, the water depression was observed to be 2.9 m, resulting in the LNAPL migrating underneath the wall at the low pressure side. The behavior observed in test 4 was similar to test 3, but the quantity of LNAPL that migrated underneath the wall was greater than that in test 3. In addition, the pore pressures at sensors A13, A14 and A15 fluctuated due to the high velocity of the groundwater flow. The pore pressure measurements provide a more detailed insight into the LNAPL migration behavior.

Results from these measurements agreed well with the observations from the video recording.

All plots of the pore pressure change versus time are the same approach by Soga *et al*. (2003) for presenting the migration of LNAPL. Moreover, these data can be also used to evaluate the vertical velocity of LNAPL movement.

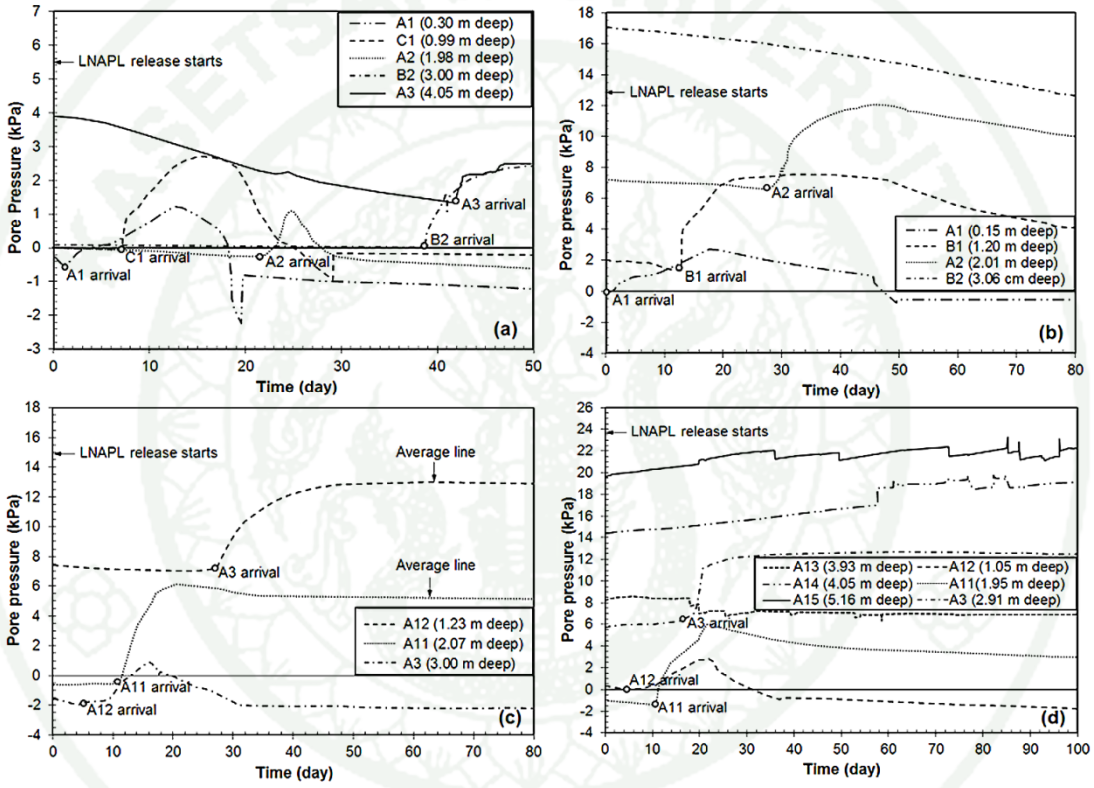

Figure 59 Change in pore water as a function of time for (a) test 1; (b) test 2; (c) test 3; and (d) test 4 (prototype unit)

3.3 Contours and Velocity of the Plume Movement

This section is focused on a comparison between cases of no groundwater flow (test 2) and groundwater flow (test 3). Snapshots of the plume migration obtained from the video recording at different times and each snapshot was processed using graphical software (PhotoShopCS3). The digitized perimeters of the plume were

extracted to construct the contour of LNAPL distribution with time, as shown in Figure 60. This technique was used by Esposito *et al*. (1999), Esposito *et al*. (2000), and Soga *et al*. (2003). Velocity of the front, measured from pore pressure sensors, was calculated from the locations of the sensors and times when the plume movements reached the sensors, as presented Figure 59. For test 2 [Figure 60(a)], the LNAPL plume reached the water level at 1.81 m below the wall within 20 days and the LNAPL was stable at approximately 0.99 m above the wall tip. For test 3 [Figure 60(b)], the LNAPL plume reached the higher pressure side water level at 1.93 m below the wall within 6 days. It shows that the groundwater flow accelerates the movement of LNAPL. Consequently, sixty days after the LNAPL was released, the LNAPL plume migrated underneath the wall at the lower pressure side.

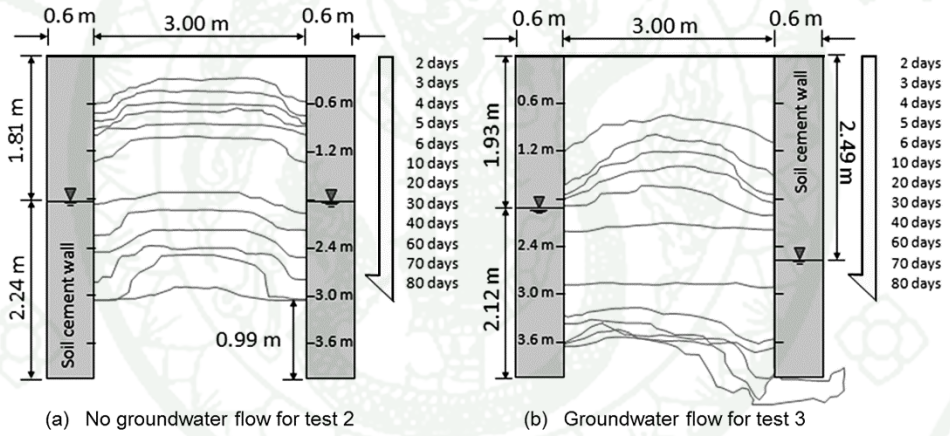

Figure 60 Contours of LNAPL movement in tests 2 and 3 (prototype unit)

The LNAPL plume distributions for both cases were examined from the vertical LNAPL movement versus times at the centerline and near the walls, as shown in Figure 61. The LNAPL moved symmetrically downward for the case of no groundwater flow [see Figure 61(a)]. The LNAPL moved slightly faster near the walls than at the centerline, and eventually, the front of LNAPL plume near the walls and at the centerline were the same level. For the case of groundwater flow [Figure 61(b)], the LNAPL moved asymmetrically downward and faster than the case of no groundwater flow. The LNAPL near the wall at the lower pressure side migrated

faster than near the wall at the higher pressure side due to the groundwater flow direction.

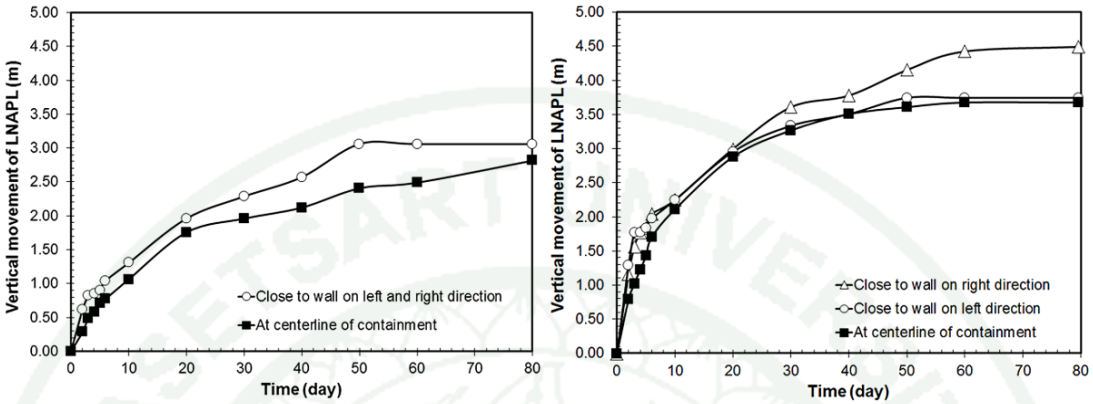

Figure 61 Comparison of LNAPL movement at centerline and near the wall (prototype unit)

The distance at the centerline of the vertical plume movement at different times was used to calculate the velocity of the LNAPL migration and is presented in Figure 62. The velocities of the front measured from the pore pressure sensors were calculated from the sensor locations and the times at which the plume reached these locations, as plotted in Figure 59. These velocities were compared with the velocities obtained from the image analysis presented in Figure 60. The results from the pore pressure measurements were shown to be in general agreement with the image analysis. Some differences were observed for the case of groundwater flow and may be due to the asymmetrical plume migration distribution. Overall, the plume velocity decreased with depth for both cases when approach the saturated zone, and the plume velocity in the groundwater flow case was faster than that in the case with no groundwater flow because the depth of unsaturated zone in test 3 is deeper than that in test 2. Moreover, the plots in Figure 62 show the velocity of LNAPL movement is proportional to the depth.

According to all centrifuge model tests, the appropriated depth of the containment for containing the contaminant migration must be considered two factors which are the self-weight of the contaminant and the effect of groundwater flow.

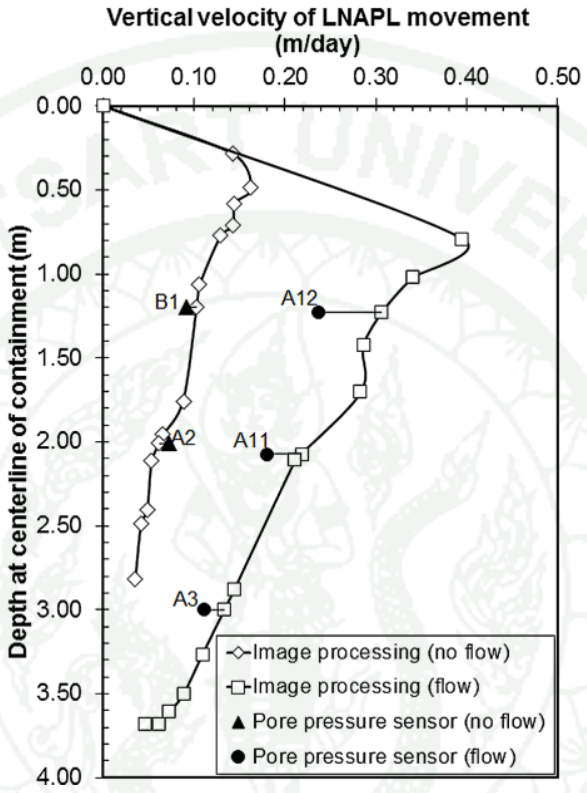

Figure 62 Comparison of plume velocity (prototype unit)

4. Numerical Simulation

4.1 Input Model Parameters

The static two-phase S-P relationships of the soil and soil cement (NAPL-water and air-NAPL) were estimated from air-water S-P relationships using a scaling factor method proposed by Leverett (1941) and Parker *et al*. (1987), as shown in Figure 63. The model parameters for the soil and soil cement were determined by the use of the van Genuchten model (1980) and Parker model (1987) to estimate the k-S-P relationships, as reported in Table 17. The applied boundary conditions which advise by

A.Battistelli are listed in details in Table 18. The initial conditions were determined by running the model to steady state governed by gravity and capillary equilibrium under the assigned boundary conditions. Model parameters tested sandy soil and soil cement for simulation in both 1g model experiments and centrifuge model experiments are the same because the grain size distribution curves of both soils are similarly. Therefore, the SWCCs of both soils also are similarly.

Table 17 Model parameters for tested sandy soil and soil cement

Description	Sandy soil	Soil cement
Relative permeability parameters for the Parker's model (1987)		
Limiting saturation S_m	$0.345^{(F1)}$	$0.345^{(F1)}$
Fitting parameter, n	$3^{(A)}$	$3^{(A)}$
Capillary pressure parameters for the van Genuchten's model (1980)		
$\lambda = m = 1\text{-}1/n$	$0.770^{(C1)}$	
Residual water saturation, S_{lr}	$0.146^{(F2)}$	
$1/P_0 = \alpha/\rho_w g$ $(1/Pa^{-1})$	$3.400x10^{-4\ (C1)}$	
Maximum value for capillary pressure, P_{max} (Pa)	$4.215x10^{-4\ (M)}$	
Satiated water saturation, S_{ls}	$1^{(F2)}$	
Capillary pressure parameters for the Parker's model (1987)		
Limiting saturation, S_m		$0^{(F2)}$
Fitting parameter, n		$2.068^{(F2)}$
Strength parameter for air-NAPL, $\alpha_{an} = \alpha \times \beta_{an}$		$0.330^{(C2)}$
Strength parameter for NAPL-water, $\alpha_{nw} = \alpha \times \beta_{nw}$		$0.217^{(C2)}$

Strength parameter is the parameter describing the shape of the saturation-capillary head curve. α is a curve fitting parameter; β_{an} $(= \sigma_{aw}/\sigma_{an})$ is scaling factor for air-NAPL; β_{nw} $(= 1/(1\text{-}1/\beta_{an}))$ is scaling factor for NAPL-water; F1 is a curve fitting parameter of k-function curve; F2 is a curve fitting parameter of S-P curve; A is recommended by Rasmusson, 2009; C1 is calculated from van Genuchten curve

fitting parameter (n); M is measured from a suction test; C2 is calculated from a fitting parameter multiply by a scaling factor (Rasmusson 2009)

Table 18 Boundary conditions applied to simulation

Boundary	Pressure (Pa)	Condition
Top (z=0 m)	P_{atm}= $1.013x10^5$	Gas Only (Temp=20°C, Mole fraction=0.99, Fixed state)
Bottom (z=depth of model)	Impervious	Impervious
Left (x = 0 m)	$1.013x10^5$	Gas and Water, Above Water Table (Temp=20°C, water sat. = 0.20, Fixed state)
	$1.013x10^5$+ 9789z	Water Only, Below Water Table (Temp=20°C, Fixed state)
Right (x = width of model)	$1.013x10^5$	Gas and Water, Above Water Table (Temp=20°C, water sat. = 0.20, Fixed state)
	$1.013x10^5$+ 9789z	Water Only, Below Water Table (Temp=20°C, Fixed state)

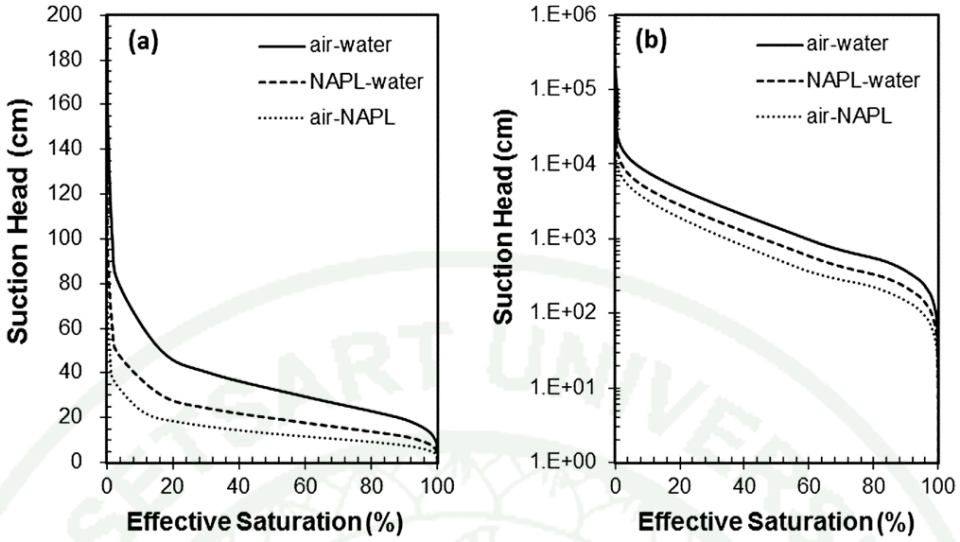

Figure 63 Three two-phase the scaled saturation-capillary head (S-P) relations for (a) sandy soil and (b) soil cement

4.2 Validation of numerical results compare to small tank model test results

The plots of plume migration at 210 minutes from numerical results compare to 1g model test were shown as Figure 64. The Figure 64(a) shows the plume migration of the gasoline and The Figure 64(b) shows the plume migration of liquid paraffin. Overall, the results from the numerical simulations agreed with the results from the 1g model experiments. This numerical results confirmed the performance of the simulator which can be used for simulate the gasoline and liquid paraffin migration in sandy soil layer.

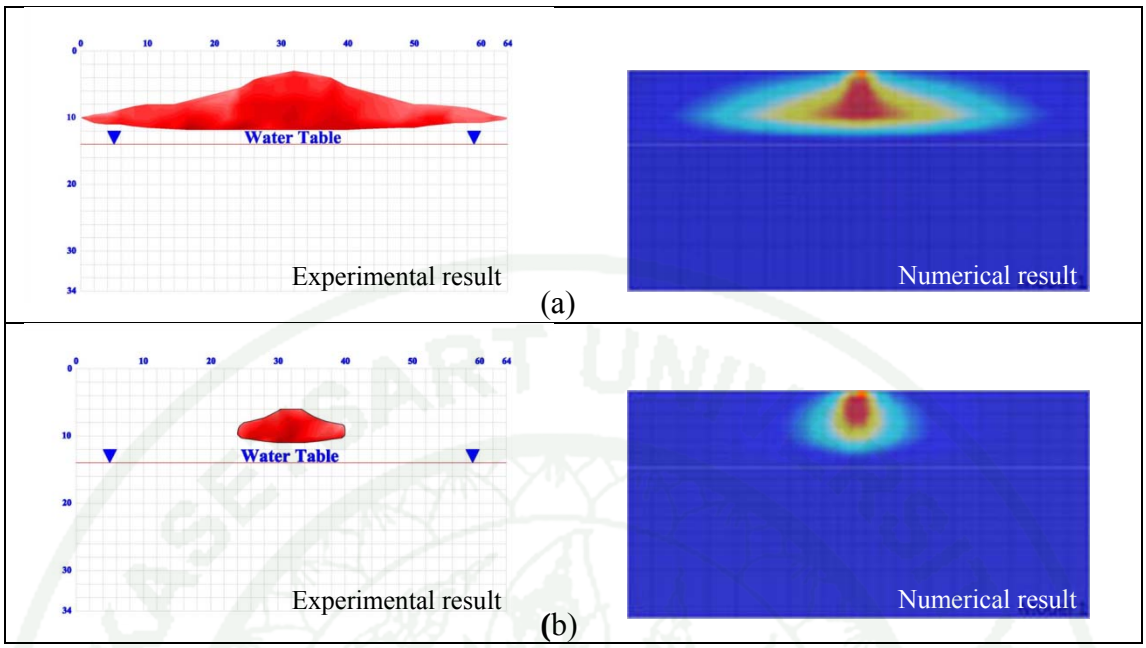

Figure 64 Numerical results compare to small tank model test results (a) gasoline migration 210 minutes (b) liquid paraffin migration 210 minutes

4.3 Validation of numerical results compare to centrifuge test results

The computed LNAPL saturation contours at the end of the testing are shown in Figures 65(a), 65(b), 65(c) and 65(d). The numerical models simulated the observed effects of the water level and groundwater flow on the plume migration distribution. The LNAPL plume distribution of test 1 for the condition of no groundwater flow [Figure 65(a)], in which case, the LNAPL can migrate underneath the wall. A large amount of LNAPL was retained above the groundwater level, and some LNAPL was trapped in the unsaturated zone. The plume migration distribution was symmetrical, similar to the results of the centrifuge test. The LNAPL plume distribution of test 2 for the condition of no groundwater flow [Figure 65(b)] where the plume migration distribution was symmetrical. The LNAPL plume can penetrate below the groundwater level to a greater extent than that observed in the centrifuge test, however, the amount of LNAPL near the wall tip was minimal. The LNAPL plume distributions of tests 3 and 4 are shown in Figures 65(c) and 65(d), respectively. The plume migration was asymmetrical, corresponding to the centrifuge test results. The

numerical simulation results show the large amount of the LNAPL accumulated at the lower pressure side near the water level, and that the LNAPL could migrate underneath the wall at the lower pressure side. In this case, the LNAPL migrated underneath the wall to a lesser extent in the numerical simulation than in the centrifuge test. The different plume migration distribution in the numerical simulation and the centrifuge test results from an uncertainty in the capillary and the relative permeability parameters, including some of the chemical properties of the LNAPL. Overall, the results from the numerical simulations agreed with the results from the centrifuge experiments. Both methods confirmed the effective performance of the soil cement wall as a containment barrier. These behaviors of LNAPL migration can be used as the data for determining the appropriated remediation or the appropriated containment as well as the further study.

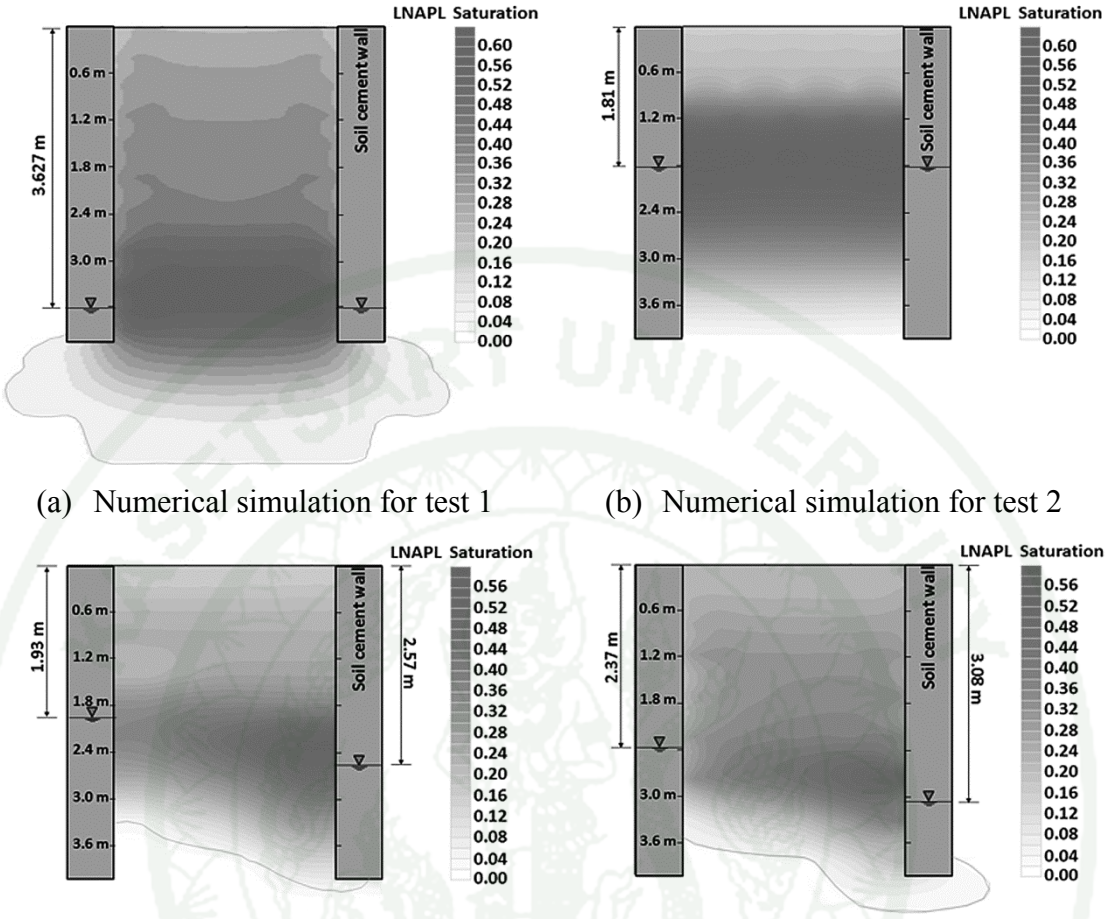

(a) Numerical simulation for test 1

(b) Numerical simulation for test 2

(c) Numerical simulation for test 3

(d) Numerical simulation for test 4

Figure 65 LNAPL plume migration from numerical simulation at the end of testing times

4.4 Effect of Particle Size on Centrifuge Test

According to scaling laws, Nevada sand was used as the soil layer in all centrifuge tests that the particle size should be scaled up but it does not increasing. Therefore, the effect of scaling law and stress level on LNAPL was observed by two dimensional seepage analysis. The results of centrifuge model in 1g, 30g with no enlarge particle size and 30g with enlarge particle size are shown in Figures 66(a), 66(b) and 66(c), respectively. All plots are compared at the same position namely points 1, 2, 3 and 4.

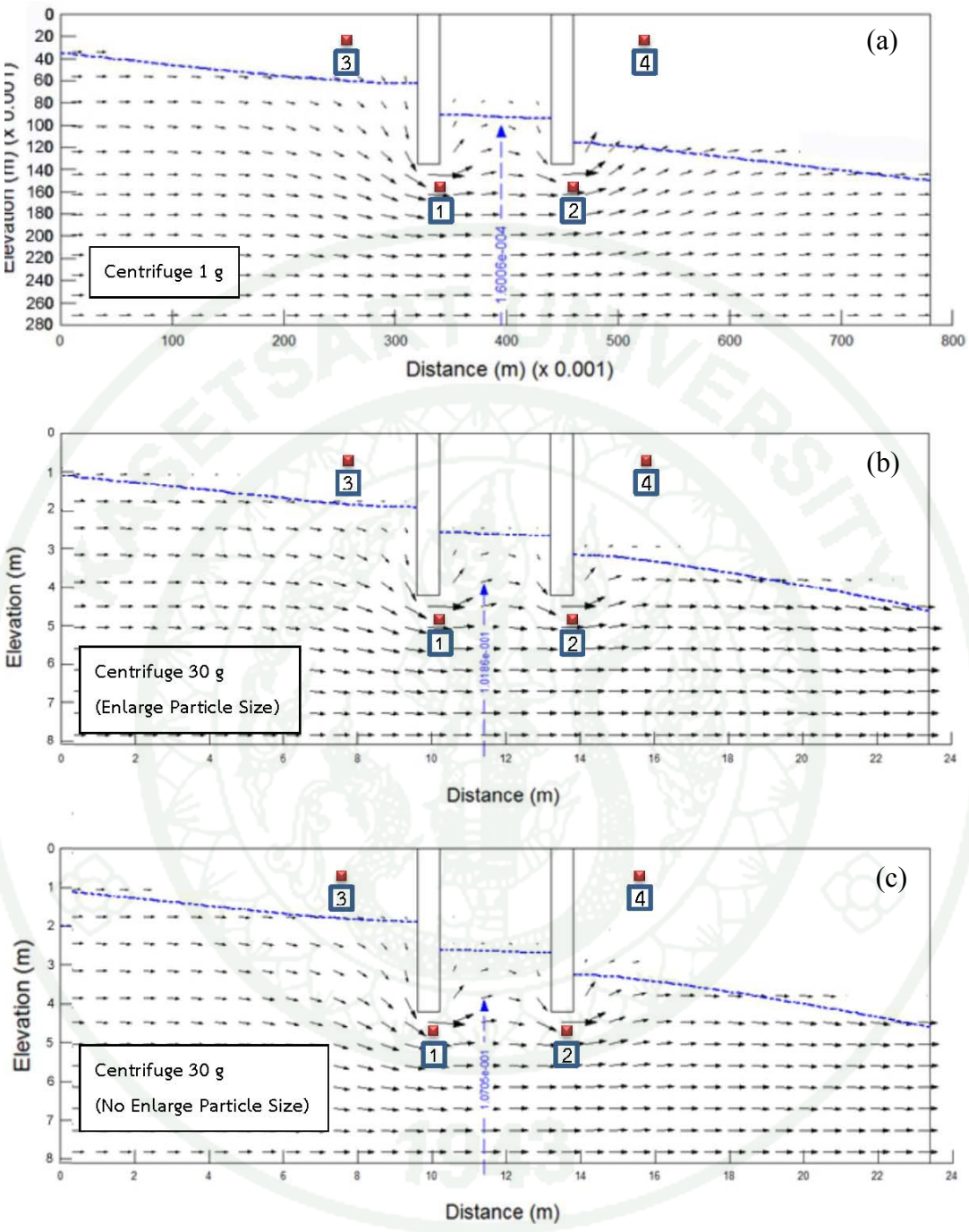

Figure 66 Flow vector from 2D seepage analysis (a) 1g in centrifuge model (b) 30g in centrifuge model with enlarge particle size (c) 30g in centrifuge model with no enlarge particle size

The comparison of the seepage between the plots in Figure 66(a) and Figure 66(b) illustrate the difference of pressure head at all points. Especially, the capillary pressure at points 3 and 4 in Figure 66(a) is more obviously than that in Figure 66(b). The direction of the flow vectors in all simulation is similarly, especially, in the saturated layer. The effect of particle size can describe by comparing between the plots of Figures 66(b) and 66(c). The quantities of the pressure head and the seepage behavior of both models (no enlarge and enlarge particle size) are similar. This would lead to a clear of particle size effect. The result of all seepage analysis shows that the behavior of groundwater flow in soil layer is similarly. Therefore, both the 1 g model and 30 g model can use to study the contaminant migration but the 1 g model has to spend longer time which compare to the 30 g model. However, the stress level and the field dimensions are the factors which are not possible to provide in the strong box. The effect of particle size does not matter in centrifuge simulation. It could therefore be concluded that the particle size must not be increased with scaling law in centrifuge modeling.

4.5 Behavior of LNAPL migration for different pattern of containment

To investigate the behavior of gasoline migration, the numerical simulations are performed on different patterns of containment. These containment patterns are considered in both flow and no flow conditions. All boundary conditions are the same as the centrifuge model in 30g. The quantities of gasoline are divided into four groups as follows: 500 liters, 1000 liters, 1500 liters and 2000 liters. The gasoline spill is modeled for 1 year with a constant rate of 0.015 ml/s. As the numerical simulations, the gasoline was contained with containment dimensions of 3 m x 4.65 m x 1 m as shown in Figure 67. In case of no flow condition, the gasoline plume migrated below the water table with a symmetrical plume distribution, but the depth of wall was adequate for containing the gasoline migration in all groups. While the gasoline migration in case of flow condition can migrate underneath the wall except the quantities of 500 liters. These results indicate that the effect of the hydraulic gradient of water within the wall affects on gasoline migration.

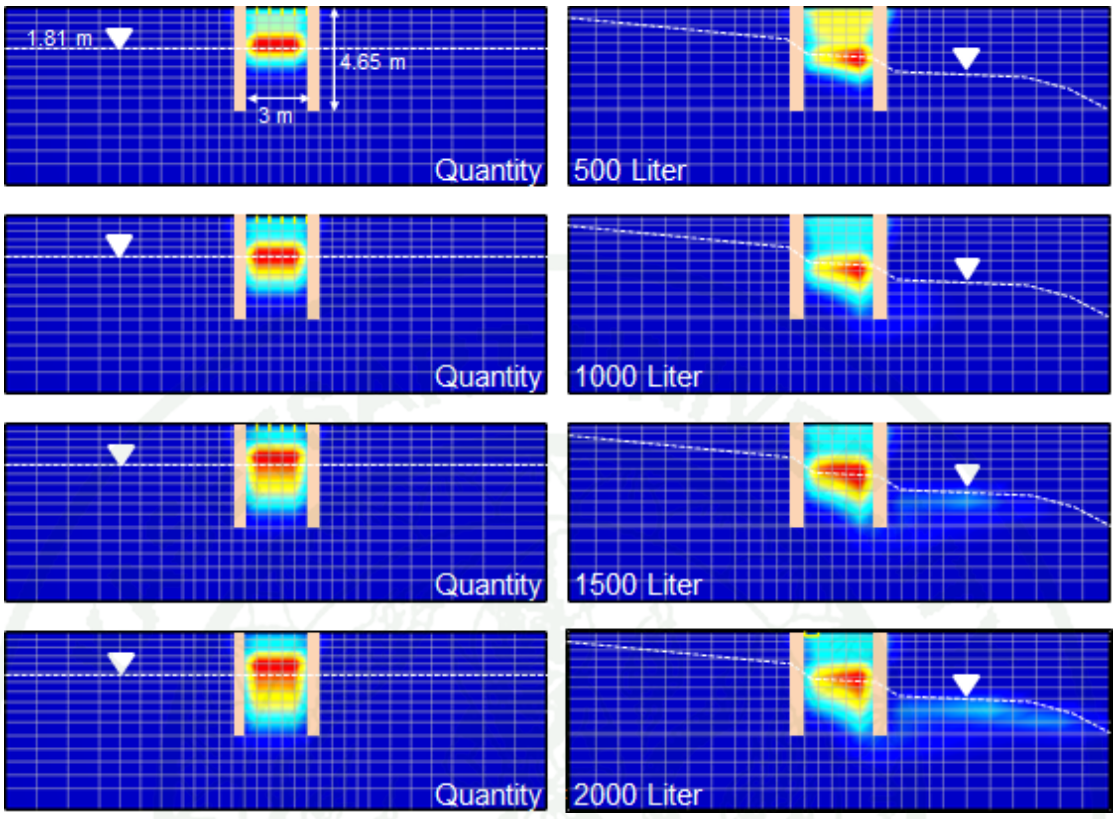

Figure 67 Gasoline plume migration which was contain with containment dimensions of 3 m x 4.65 m x 1 m after 1 year

To prevent the gasoline migration underneath the wall, the containment was extended to be the dimensions of 4.2 m x 4.2 m x 1 m as shown in Figure 68. In case of no flow condition, the gasoline plume migrated below the water table with a symmetrical plume distribution, but the depth of wall was adequate for containing the gasoline migration in all groups. While the gasoline migration in case of flow condition can migrate underneath the wall except the quantities of 500 liters. This result indicates that the increase of the width of containment cannot prevent the gasoline migration underneath the wall. The behavior of gasoline plume in case of groundwater flow corresponding to the study by Hayashi and Allersma (2004) who described that the installation of wall delayed and decreased the LNAPL transportation to the downstream; however, the contaminated area spread to deeper area. The advantage of the barrier is that it created a space in which the accumulated gasoline could be extracted from the sand layer.

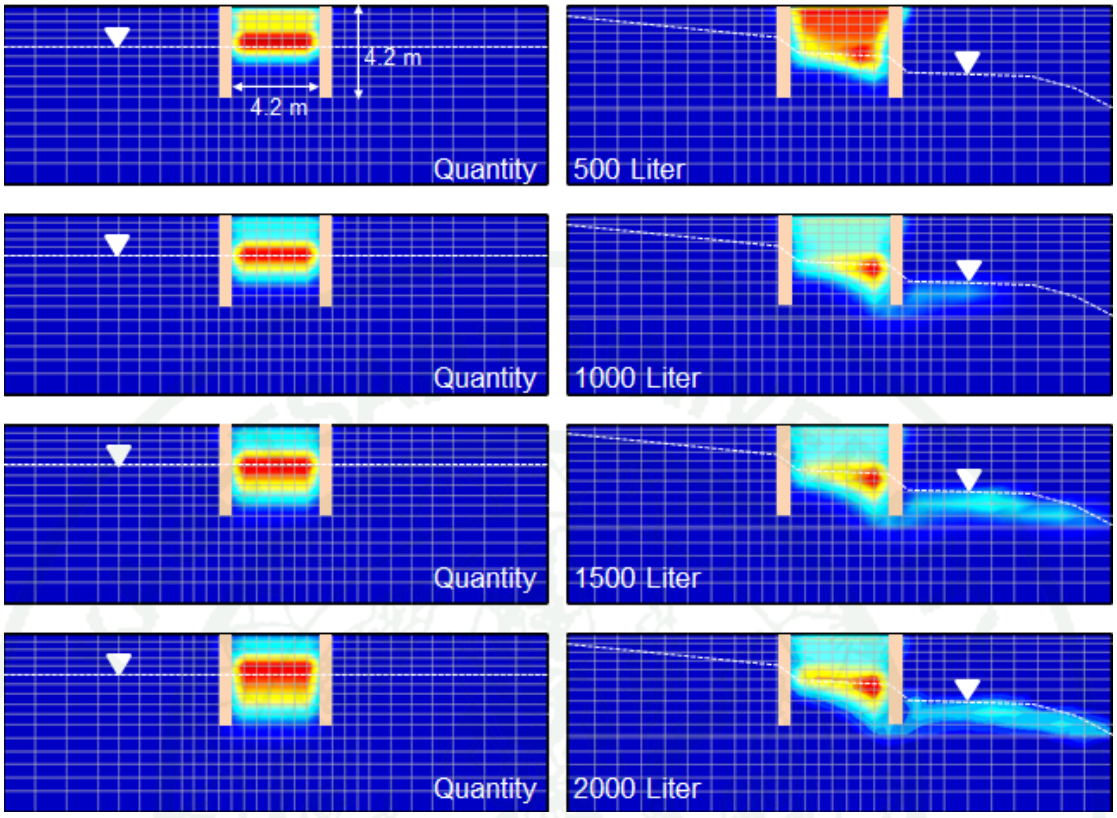

Figure 68 Gasoline plume migration which was contain with containment dimensions of 4.2 m x 4.2 m x 1 m after 1 year

Therefore, the double containment was considered for preventing the gasoline migration only in case of flow condition as shown in Figure 69. According to the numerical results, there were no observations of gasoline migration outside the wall. This illustrate that the pattern of the double containment can prevent the gasoline migrate underneath the wall in all groups because the gasoline plume moves into the strait between the walls. The contaminant can be easily remediated by pumping out from the soil. Moreover, if the direction of groundwater flow was confirmed, the double wall can be constructed only the same direction of the groundwater flows. The double wall containment from this study is under the assumptions which are the constant groundwater levels, the constant of gasoline infiltration rate and negligible dissolved phase.

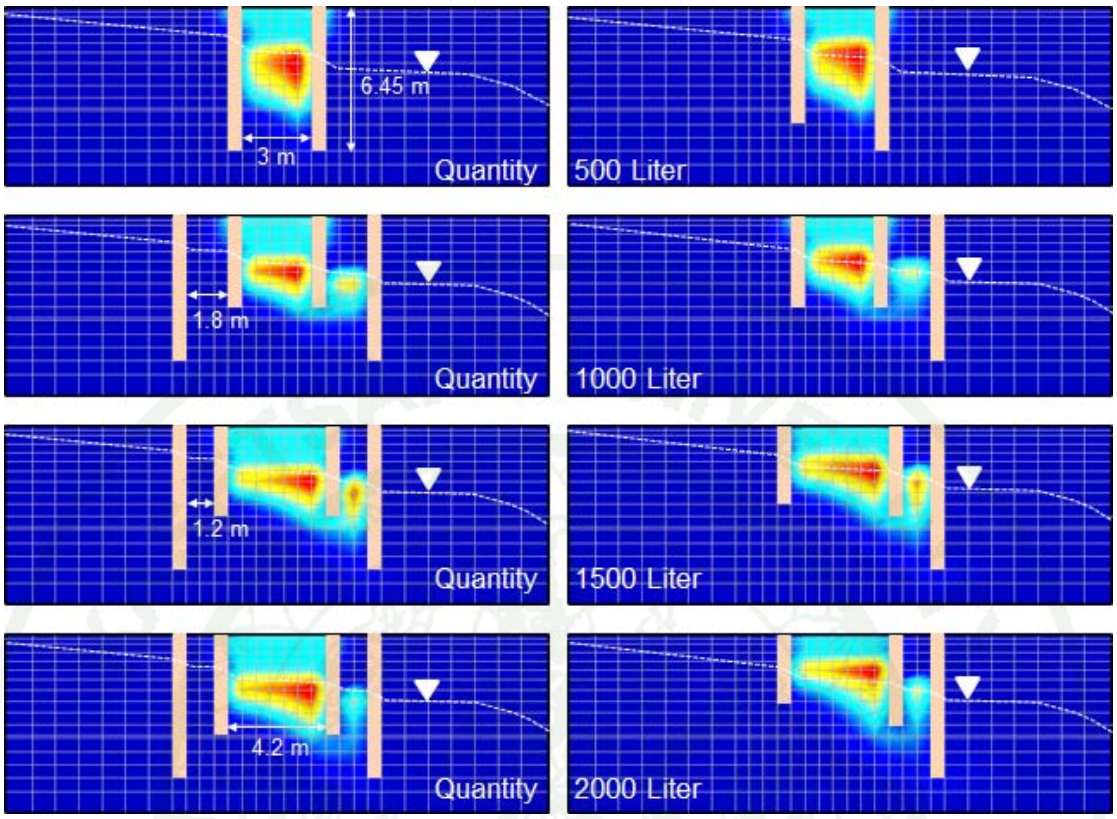

Figure 69 Gasoline plume migration which was contain with double containment after 1 year

The dimensional proportion of the double wall recommends as follows: the inner depth of the wall of 1.1B, the outer depth of the wall of 1.6 B and spacing between the inner wall and the outer wall of 0.3B, where B is the width of the containment. The tip of inner wall should be more than 1.5 m below the water table at low pressure side. The double wall appropriates to the field which has the old underground storage tank and a limitation of a construction area. For sandy soil area, the containment construction by using soil cement column has the limitation of the depth therefore the deeper installation may be not possible. The wider wall may be possible for construction but it has to use more area to avoid the effect of ground water flow including may be costly.

Notwithstanding, for the condition of no limitation of the area construction, the pattern of single wall may be used as the pattern of the containment but the distance between the wall has sufficient for containing the contaminant. For the condition of no limitation of deeper containment installation, the single wall may be used as the pattern of the containment but the depth of the containment has to sufficient for containing the contaminant.

CONCLUSION AND RECOMMENDATION

Conclusion

From the experimental results and discussion of this study, the conclusion can be drawn as follows:

1. According to the results from the small tank models, the distance of the gasoline plume migration in the poorly-graded sandy soil (SP) is higher than that in the silty sandy soil (SM) about 3.5 times in horizontal direction.

2. The gasoline and the liquid paraffin are used as LNAPL. The horizontal distance of gasoline migration can predict from the equation of G = 8.3948*ln(LP)+24.855 where G and LP represent gasoline and liquid paraffin, respectively. It was found that the plume migration can move less than that of gasoline due to its much higher viscosity. For the case with barrier, Both LNAPL plume cannot migrate through the barrier in both sandy soils.

3. The contaminated area of the gasoline is more than that of the liquid paraffin about 2.6 times. Moreover, the results from numerical simulation agreed with the results from 1g model experiment.

4. Results from centrifuge modeling, the walls were effective as a containment barrier. The depth of the soil cement wall depends on the self-weight of LNAPL and the effect of groundwater flow. The guide depth of the containment in the sandy soil layer below the water content as shown in Figure 70.

5 According to the seepage analysis, the behavior of water flowing which considers the particle size effect was investigated by using the parameters from SWCC and K-function in both 1g and 30g in centrifuge tests. The direction of the flow vectors in saturated layer of both is similarly. The seepage behavior of 30g simulation in both no enlarge and enlarge particle size is similar. Therefore, the

particle size must not be increased with scaling law in centrifuge modeling. The 1g simulation can be used to study the contaminant migration but it has to spend longer times and large dimension for represent the field condition. While the centrifuge simulation with higher g-level can reduce experiment times and scale down the dimension.

6. The double wall appropriates to the old underground storage tank and the limitation of construction area because the single wall have to use the large area and the deeper penetration is limitation by using soil cement columns in sand layer. The guide pattern for the containment in condition of groundwater flow is shown in Figure 71. The tip of inner wall should be more than 1.5 m below the water table at low pressure side. The depth of the containment depends on the limitation of the construction.

7. The model parameters used in numerical simulation are validated by comparing the behavior of LNAPL migration to the physical model test. Therefore, these parameters can be applied to numerical modeling on the contaminant migration in sandy soil, especially, the capillary pressure parameters and the relative permeability parameters.

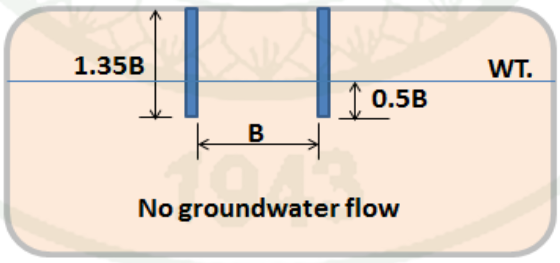

Figure 70 The guide depth of the containment below the water content

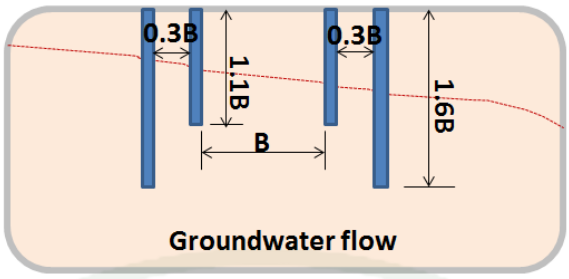

Figure 71 The guide pattern of the double wall containment

Recommendation

1. The soil cement barrier used in this study was created as the wall but the soil cement in the field was constructed as the column, therefore, the further study should be represented the soil cement column. Moreover, the overlap of each column should be considered in the simulation.

2. The fluctuation of water table can cause the drainage and imbibition of a porous medium saturated with LNAPL. Therefore, the next experiments could be to incorporate a fluctuating groundwater table as the effect of a changing groundwater table on the LNAPL distribution was shown to be of great importance in the simulation.

3. The dissolution of LNAPL is the one factor which affects the movement of LNAPL plume migration therefore, it should be considered in the further study.

4. For to cover the remediation, the further study should be combined the remediation system and the containment system.

LITERATURE CITED

Abriola, L.M. and G.F. Pinder. 1985. A multiphase approach to the modeling of porous media contamination by organic compounds, 1, Equation development. **Water Resour. Res.** 21: 11-18.

Adenekan, A.E., T.W. Patzek and K. Pruess. 1993. Modeling of multiphase transport of multicomponent organic contaminants and heat in the subsurface: numerical model formulation. **Water Resour. Res.** 29 (11): 3727-3740.

Allersma, H.G.B. and G.M. Esposito. 2000. Optical analysis of pollution transport in geotechnical centrifuge tests, pp. 3-10. *In* **Int. Symp. on Physical Modelling and Testing in Env. Geotech.** La Baule, France.

Al-Tabbaa, A. and C. Evans. 2003. **Deep soil mixing in the UK: geoenvironmental research and recent applications**. Land Contamination & Reclamation 11 (1): 1-14.

Arulanandan, K., P.Y.Thompson, B.L. Kutter, N.J. Meegoda, K.K. Muraleetharan and C. Yogachandran. 1988. Centrifuge modeling of transport processes for pollutants in soil. **J. Geotech. Eng.** 114 (2): 185-205.

Azizi, F. 2000. **Applied analysis in geotechnics**. E & FN Spon, London.

Barbour, S.L. 1998. 19th Canadian Geotechnical Colloquium: The soil-water characteristic curve: a historical perspective. **Can. Geotech. J.** 35: 873-894.

Barry, D.A., J.W. Griffioen, L. Li, I.G. Lisle, J.Y. Parlange, H. Prommer and G.C. Sander. 2001. Similitude applied to centrifugal scaling of unsaturated flow. **Water Resour. Res.** 37 (10): 2471-2479.

Battistelli, A. 2004. Modeling biodegradation of organic contaminants under multiphase conditions with TMVOCBio. **Vadose Zone J.** 3: 875-883.

_____. 2008. Modeling multiphase organic spills in coastal sites with TMVOC V.2.0. **Vadose Zone J.** 3: 875-883.

Brooks, R.H. and A.T. Corey. 1964. **Hydraulic properties of porous media**. Hydro. Paper No.3, Colorado State Univ., Fort Collins, Colo.

Bruce, D. A. 2000. **An introduction to the deep soil mixing methods as used in geotechnical applications**. Available Source: http://www.fhwa.dot.gov/pavement/pub_details.cfm?id=13, April 10, 2011.

Busby, R.D., R.J. Lenhard and D.E. Rolston. 1995. An investigation of saturation-capillary pressure relations in two- and three-fluid systems for several NAPLs in different porous media. **Groundwater** 33: 570-578.

Campbell, G.S. 1974. A simple method for determining unsaturated conductivity from moisture retention data. **Soil Sci.** 117: 311-314.

Chandrasekaran, V.S. 1988. Creation of geotechnical centrifuge facilities in India, pp. 101-102. *In* C. James and Schofield**,** eds. **Centrifuges in soil mechanics**. A.A. Balkerma, Rotterdam.

Charles, W.W.Ng. and L.K. Bruce. 2001. Proceedings of International Symposium on Geotechnical Centrifuge Modelling and Networking: focusing on the use and application in the Pan-Pacific region. *In* **International Symposium on Geotechnical Centrifuge Modelling and Networking**. 8-9 December 2001, Hong Kong University of Science and Technology, Clear Water Bay, Kowloon, Hong Kong.

Chevalier, L.R. 1998. Experimental and numerical evaluation of LNAPL lens and polluted capillary fringe thickness. **J. Env. Eng**. 124 (2): 156-161.

Clapp, R.B. and G.M. Hornberger. 1978. Empirical equations for some soil hydraulic properties. **Water Resour. Res.** 14: 601-604.

Colli Drill. 2006. **Technical Specification Jet Grouting**. Available Source: http://www.collidrill.it/catalogo_EN/scheda_a5.php, April 12, 2011.

Consoli, N.C., K.S. Heineck, J. Antonio and H. Carraro. 2010. Portland Cement stabilization of soil-bentonite for vertical cutoff walls against diesel oil contaminant. **Geotech. Geol. Eng.** 28: 361-371.

Cooke, A.B. and R.J. Mitchell. 1991. Physical modeling of a dissolved contaminant in an unsaturated sand. **Can. Geotech. J.** 28 (6): 829-833.

Corey, A.T. 2003. **Mechanics of immiscible fluids in porous media**. Water Resources Publications, Highlands Ranch, Co.

Croney, D. and J.D. Coleman. 1961. Pore pressure and suction in soils, pp. 31-37. *In* **Proc. Conf. Pore Pressure and Suction in Soils**. Butterworths, London.

Culligan-Hensley, P.J. and C. Sanvvidou. 1995. Environmental geomechanics and transports process, pp. 196-263. *In* **Geotechnical Centrifuge Technology, R.N. Taylor (edit)**, Blackie Academic, London.

_____, D.A. Barry and J.-Y. Parlange. 1997. Scaling unstable infiltration in the vadoze zone. **Can. Geotech. J.** 34 (3): 466-470.

_____ and _____. 1998. Similitude requirements of modeling NAPL movement with a geotechnical centrifuge. **ICE J. Geotech. Eng.** 131 (3): 180-186.

Dell'Avanzi, E. and J.G. Zonberg. 2002. Scaling laws for centrifuge modeling of unsaturated flow, pp. 425-430. *In* **Proc. 3th Int. Conf. on Unsaturated Soils**, (Volume 1). Recife, Brazil.

Dwyer, B.P. 1997. **Demonstration of close-coupled barriers for subsurface containment of buried waste**. Sandia Report SAND97-1193, California.

Dunn, A.M. 2005. **Air and LNAPL entrapment in the partially saturated fringe: laboratory and numerical investigations.** Ph.D. thesis, Notre Dame, Indiana.

Eckberg, D.K. and D.K. Sunada. 1984. Nonsteady three-phase immiscible fluid distribution in porous media. **Water Resour. Res**. 20: 1891-1897.

Edwards, A.L. 1972. **TRUMP: A Computer Program for Transient and Steady State Temperature Distributions in Multidimensional Systems**. National Technical Information Service, National Bureau of Standards, Springfield, VA.

Esposito, G. and H.G.B. Allersma. 1998. Centrifuge modelling of LNAPL transport in partially saturated sand, pp. 53-55. *In* **Proc., Centrifuge 98**. (Volume 2). Balkema, Rotterdam, The Netherlands.

_____, _____ and A. P. S. Selvadurai. 1999. Centrifuge modeling of LNAPL transport in partially saturated sand. **J. Geotech. Geoenviron. Eng.**, 125 (12): 1066-1071.

_____, _____, K. Soga, C. Kechavarzi and H. Coumoulos. 2000. Centrifuge simulation of LNAPL infiltration in partially saturated porous granular medium, pp. 141-148. *In* **Int. Symp. on Physical Modelling and Testing in Env. Geotech.** La Baule, France.

Fagerlund. F. and A. Niemi. 2003. **Multi-constituent modelling of a gasoline spill using the T2VOC numerical simulator.** Available Source: http://esd.lbl.gov/research/projects/tough/documentation/proceedings/2003.html, April 10, 2011.

_____ and _____. 2007. A partially coupled, fraction-by-fraction modelling approach to the subsurface migration of gasoline spills. **J. Contam. Hydrol.** 89: 174-198.

_____, _____ and T. Illangasekare. 2006a. **Modeling NAPL Source Zone Formation in Stochastically Heterogeneous Layered Media - a Comparison with Experimental Results**. Available Source: http://esd.lbl.gov/research/projects/tough/documentation/proceedings/2006.html, April 10, 2011.

_____, _____ and M. Odén. 2006b. Comparison of relative permeability –fluid saturation-capillary pressure relations in the modelling of non-aqueous phase liquid infiltration in variably saturated, layered media. **Adv. Water Resour.** 29 (11): 1705-1730.

Fredlund, M.D. and A. Xing. 1994. Equations for the soil-water characteristic curve. **Can. Geotech. J.** 31: 533-546.

_____, D.G. Fredlund and G.W. Wilson. 2000. An equation to represent grain-size distribution. **Can. Geotech. J.** 31: 817-827.

_____, _____ and _____. 2002. Use of the grain-size distribution for estimation of the soil-water characteristic curve. **Can. Geotech. J.** 39: 1103-1117.

Frydman, S. 1988. Centrifuge of soil-structureinteraction, pp. 169-181. *In* C. James and Schofield, eds**. Centrifuges in soil mechanics**. A.A. Balkerma, Rotterdam.

Gardner, W.R., D. Hillel, and Y. Benyamini. 1970a. Post irrigation movement of soil water. I. Redistribution. **Water Resour. Res**. 6: 851-861.

_____, _____ and _____. 1970b. Post irrigation movement of soil water. II. Simultaneous redistribution and evaporation. **Water Resour. Res**. 6: 1148-1153.

Garnier, J., L. Thorel, R.J. Lynch, M.D. Bolton, C. Kechavarzi, A.C.J. Treadaway, H. Coumolos, K. Soga, D. Konig, A. Rezzoug, G Heibrock, F. Weststrate, J. Van der Poel, O. Oung, R. Schrijver, R.N. Taylor, S. Robson, S. Spiessl, H. Allersma, G. Esposito, M.C. Davies, S. Burkhart, C. Merrifield and W. Craig. 1998. **NECER: network of European centrifuges for environmental geotechnic research,** pp. 33-35. *In* **Proc., Int. Conf. Centrifuge '98**, Tokyo, Japan.

Gudbjerg, J., T. O.Sonnenborg, and K.H. Jensen. 2004. Remediation of NAPL below the water table by steam-induced heat conduction. **J. Contam. Hydrol.** 72: 207-225.

Gurney, M. 2001. **Information sheets on land remediation.** May Gurney (Technical Services), Trowse, Norwich, UK.

Hamza, K.I. and A.S. Elansary. 2000. Contaminant Transport Modeling at Underground Gasoline Tanks Sites, pp. 1-9 *In* **Conference Water Resources Engineering and Water Resources Planning & Management**, Hyatt Regency Minneapolis, Minneapolis, MN, USA.

Hayashi, Y. and H.G.B. Allersma. 2003. Centrifuge modeling of LNAPL infiltration in sand deposits with an impervious sheet, pp. 305-310. *In* **Int. Symp. on Groundwater Problems related to Geo-environment; Groundwater engineering -recent advances-.** Okayama, Japan.

_____ and _____. 2004. Centrifuge modelling of LNAPL transport in sand deposite by groundwater flow, pp. 464-469. *In* **Int. Conf. on Offshore and Polar Engineering**. Toulon, France.

Heiser, J. and B. Dwyer. 1995. **Demonstration of close-coupled barriers for subsurface containment of buried waste**. Available Source: http://www.osti.gov/scitech/servlets/purl/116565, April 10, 2011.

Host-Madsen, J. and K.H. Jensen. 1992. Laboratory and numerical investigation of immiscible multiphase flow in soil. **J. Hydrol.** 135: 13-52.

Houston, W.N., H.B. Dye, C.E. Zapata, Y.Y. Perera and A. Harraz. 2006. Determination of SWCC using one point suction measurement and standard curves. **Geotechnical Special Publication**. American Society of Civil Engineers, Reston, VA 20191-4400, United States, Carefree, AZ, United States.

Hu, L.M., I.M.C. Lo and J.N. Meegoda. 2006. Centrifuge testing of LNAPL migration and soil vapor extraction for soil remediation. **Pract. Period. Hazard., Toxic, Radioact. Waste Manage.** 10 (1): 33-40.

Huang, S., S.L. Barbour and D.G. Fredlund. 1994. A history of the coefficient of permeability function, pp. 57-80. *In* **Sino-Canadian Symposium on Expansive Soils/Unsaturated Soils**, Chinese Institution for Soil Mechanics and Foundation Engineering, CEES. Wuhen, China.

Illangasekare, T.H., E.J. Armbruster III and D.N. Yates. 1995. Non aqueous phase fluids in heterogeneous aquifers. Experimental study. **J. Environ. Eng.** 121: 571-579.

_____, M. Znidarcic, Al-Sheridda, and D.D. Reible. 1991. Multiphase flow in porous media, pp. 517-523. *In* **Proc., Centrifuge 91.** Balkema, Rotterdam, The Netherlands.

Irene, M.C. Lo and L.M. Hu. 2004. Long-Term Migration of Light Nonaqueous-Phase Liquids in Two Unsaturated Soils: Clayey Silt and Fine Sand. **Prac. Period. Haz. Toxic Radio. Waste Manag.** 8 (4): 228-237.

Jackson, R.D. 1972. On calculation of hydraulic conductivity. **Soil Sci. Soc. Am. Proc.** 35: 380-382.

Johnny Xu. 2005. **DEEP CEMENT MIXING METHOD**. Available Source: www.p3planningengineer.com, April 12, 2011.

Jotisankasa, A., W. Porlila, S. Soralump and W. Mairiang. 2007. Development of a low cost miniature tensiometer and its applications, pp. 475-480. *In* **Proceedings of the 3rd Asian Conference on Unsaturated Soils**. 21-23 April 2007, Science Press. Nanjing, China.

_____ and H. Vathananukij. 2008. **Investigation of soil moisture characteristics of landslide-prone slopes in Thailand**. Available Source: http://www.gerd.eng.ku.ac.th/Paper/Paper_Other/GERD_STAFF/JotISM_withheading.pdf, April 10, 2011.

_____ and W. Mairaing. 2010. Suction-monitored direct shear testing of residual soils from landslide-prone areas. **J. Geotech. Geoenviron. Eng.** 136 (3): 533-537.

Jotisankasa, A. 2010. **Manual for user of KU tensiometer.** 2nd ed. Geotechnical Innovation Laboratory. Geotechnical Engineering Research and Development Center, GERD, Kasetsart University. Bangkok. Thailand.

Kaluarachchi, J.J. and J.C. Parker. 1989. An efficient finite element method for modeling multiphase flow in porous media. **Water Resour. Res.** 25: 43-54.

Kamaruddin, S.A., W.N.A. Sulaiman, N.A. Rahman, M.P. Zakaria, M.Mustaffar and R. Sa'ari. 2011. A review of laboratory and numerical simulations of hydrocarbons migration in subsurface environments. **J. Env. Sci. and Tech.**, 4(3): 191-214.

Kamon, M., Y. Li, G. Flores, K. Endo, T. Inui and T. Katsumi. 2006. Experimental and numerical study on migration of LNAPL under the influence of fluctuating water table in subsurface. **Annuals of Disas. Prev. Res. Inst.**, Kyoto Univ., No. 49: 383-392.

Kechavarsi, C., K. Soga and T.H. Illangasekare. 2005. Two-dimensional laboratory simulation of LNAPL infiltration and redistribution in the vadose zone. **J. Contam. Hydrol.** 76: 211-233.

_____, _____, _____ and P. Nikolopoulos. 2008. Laboratory study of immiscible contaminant flow in unsaturated layered sands. **Vadose Zone J.** 7 (1): 1-9.

Kererat, C. and C. Chaikaew. 2009a. **Suitable of soil cement mixing for containing contaminant migration.** Research Report, Rajamangala University of Technology Rattanakosin, Nakorn Pathom.

_____ and S. Soralump. 2009b. LNAPL migration through soil cement barrier with and without flow condition. **As. J. Energy Env.** 10 (3): 185-193.

Kererat, C. and S. Soralump. 2010. Modeling of organic contaminant migration through soil cement barriers using TMVOC, pp. 405-408. *In* **Proc.** 17th **Southeast Asian Geotechnical Conf.** Taipei, Taiwan.

Knight, M.A. and R.J. Mitchell. 1996. Modelling of light nonaqueous phase liquid (LNAPL) releases into unsaturated sand. **Can. Geotech. J.** 33 (6): 913-925.

Kueper, B.H., W. Abbott and G. Farquar. 1989. Experimental observations of multiphase flow in heterogeneous porous media. **J. Contam. Hydrol.** 5: 83-95.

Kunze, R.J., G. Uehara and K. Graham. 1968. Factors important in the calculation of hydraulic conductivity. **Soil Sci. Soc. Amer. Proc.** 32: 760-765.

Leverett, M. C. 1941. Capillary behavior in porous solids. **Trans. Soc. Pet. Eng. (AIME)** 142: 152-169.

Li, Y. 2005. **Mechanism of LNAPL migration in conjunction with groundwater fluctuation**. D. Eng. Thesis, Kyoto Univ.

Lenhard, R.J. 1992. Measurement and modeling of three-phase saturation–pressure hysteresis. **J. Contam. Hydrol.** 9: 243-269.

_____. 1994. Scaling fluid content-pressure relations of different fluid systems in porous media. **Hydrology days Conf.** Fort Collins, Co.

_____, T.G. Johnson and J.C. Parker. 1993. Experimental observation of non aqueous-phase liquid subsurface movement. **J. Contam. Hydrol.** 12: 79-101.

_____. and J.C. Parker. 1987. Measurement and prediction of saturation-pressure relationships in air-organic-liquid-water porous media systems. **J. Contaminant Hydrol.** 1 (4): 395-406.

Lenhard, R.J. and J.C. Parker. 1988. Experimental validation of the theory of extending two-phase saturation-pressure relations to three-fluid phase systems for monotonic drainage paths. **Water Resour. Res**. 24: 373-380.

Leong, E. C. and H. Rahardjo. 1997. A review of soil-water characteristic curve equations. **J. Geotech. Geoenviron. Eng.** 123 (12): 1106-1117.

Leverett, M.C. 1941. Capillary behaviour in porous solids. **Soc. Pet. Eng. AIME** 142: 152-169.

Lo, I. M. C. and L.M. Hu. 2004. Long-term migration of light nonaqueous phase liquids in two unsaturated soils: clayey silt and fine sand. **Pract. Period. Hazard., Toxic, Radioact. Waste Manage.** 8 (4): 228-237.

_____, _____, and J.N. Meegoda. 2004. Centrifuge modeling of light nonaqueous phase liquids transport in unsaturated soils. **J. Geotech. Geoenviron. Eng.** 130 (5): 535-539.

Lu, N. and W.J. Likos. 2004. **Unsaturated soil mechanics.** John Wiley & Sons, New Jersey.

Marshell, T.J. 1958. A relation between permeability and size distribution of pores. **J. Soil Sci.** 9: 1-8.

Mayer, A.S. and, S.M. Hassanizadeh. 2005. **Soil and groundwater contamination: nonaqueous phase liquids**. the American Geophysical Union, Washington, DC.

McCuen, R.H., W.J. Rawls and D.L. Brakensiek. 1981. Statistical analyses of the Brook-Corey and the Green-Ampt parameters across soil textures. **Water Resour. Res.** 17: 1005-1013.

Meegoda, J. N. and L. Hu. 2011. A review of centrifuge testing of gasoline contamination and remediation. **Int. J. Environ. Res. Public Health** 8: 3496-3513.

Millington, R.J. and J.P. Quirk. 1959. Permeability of porous media. **Nature** 183: 387-388.

Mitchell, J.K. 1976. **Fundamentals of soil behavior**. Wiley, New York.

Mitchell, R.J. 1991. Centrifuge modelling as a consulting tool. **Can. Geotech. J.** 28: 165-167.

_____ and B.C. Stratton. 1994. LNAPL penetration in porous media, pp. 45-349. *In* **Proc. Int. Conf. centrifuge 94**. Singapore.

_____. 1998. The eleventh annual R.M. Hardy Keynote Address, 1997: Centrifugation in geoenvironmental practice and education. **Can. Geotech. J.** 35 (4): 630-640.

Mohammadi, K., M.H. Mousavizadeh and R. Kahawita. 2003. An experimental investigation of infiltrating an immiscible organic spill in a variably saturated soil, pp. 1-6. *In* **the SPE 13th Middle East Oil Show & Conference**, Bahrain.

Mualem, Y. 1976. A new model for predicting the hydraulic conductivity of unsaturated porous media. **Water Resour. Res**. 12: 513-522.

Murphy, J.W., A.C. Bumb and C.R. McKee. 1987. **Vadose model of gasoline leak. (Unpublished Manuscript)**. Laramie, WY: In-situ, Inc. 521-540.

Nakajima, H., A. Hirooka, J. Takemura and M.A. Marino. 1998. Centrifuge modeling of one-dimensional subsurface contamination. J. Am. Water Resour. Assoc**.** 34 (6): 1415-1425.

Narasimhan, T.N. and P.A. Witherspoon. 1976. An Integrated Finite Difference Method for Analyzing Fluid Flow in Porous Media. **Water Resour. Res.** 12 (1): 57-64.

Newell, J.C., S.D. Acree, R.R. Ross and S.G. Huling. 1995. **Light Nonaqueous Phase Liquids**. EPA/540/S-95/500, Washington, DC.

Nicholson, P.J., B.H. Jasperse and M.J. Fisher. 1997. **Economic alternatives for containment barriers**. Int. Containment Tech. Conf. & Exhibit, St. Petersburg, Florida.

Nield, D.A. and A. Began. 2006. **Convection in porous media**. 3rd ed. Springer Science & Business Media, New York.

Oostrom, M., C. Hofstee, R.J. Lenhard and T.W. Wietsma. 2003. Flow behavior and residual saturation formation of liquid carbon tetrachloride in unsaturated heterogeneous porous media. **J. Contam. Hydrol.** 64: 93-112.

_____, J.H. Dane and T.W. Wietsma. 2007. A review of multidimensional, Multifluid, intermediate-scale experiments: flow behavior, saturation imaging, and tracer detection and quantification. **Vadose Zone J.** 6(3): 610-637.

Pan, H., Y. Qing and L. Pei-yong. 2010. Direct and indirect measurement of soil suction in the laboratory. **Elect. J. Geotech. Eng**. 15: 1-14.

Pantazidou, M. and N. Sitar. 1993. Emplacement of nonaqueous liquids in the vadose zone. **Water Resour. Res.** 29: 705-722.

Parker, J.C., R.J. Lenhard and T. Kuppusamy. 1987. A parametric model for constitutive properties governing multiphase flow in porous media. **Water Resour. Res.** 23 (4): 618-624.

Pruess, K., and A. Battistelli. 2002. **TMVOC, a numerical simulator for three phase non-isothermal flows of multicomponent hydrocarbon mixtures in saturated–unsaturated heterogeneous media.** LBNL-49375, Lawrence Berkeley National Lab., Berkeley, CA.

_____ and _____. 2003. **TMVOC, A simulator for multiple volatile organic chemicals**. Available Source: http://esd.lbl.gov/research/projects/tough/documentation/proceedings/2003.html, April 10, 2011.

_____, C. Oldenburg and G. Moridis. 1999. **TOUGH2 user's guide, version 2.0**. Report LBNL-43134, Lawrence Berkeley National Laboratory, Berkeley, California.

Rasmusson, K., and M. Rasmusson. 2009. **NAPL spill modeling and simulation of pumping remediation.** M. Sc. Thesis, Uppsala University.

Reible, D.D., T.H. Illangasekare, D.V. Doshi and M.E. Malheit. 1990. Infiltration of immiscible contaminants in the unsaturated zone. **Groundwater** 28: 685-692.

Reid, R.C., J.M. Prausnitz and B.E. Poling. 1987. **The properties of gases and liquids.** McGraw-Hill, New York.

Ridley, A.M. and J.B. Burland. 1993. A new instrument for the measurement of soil moisture suction. **Géotechnique** 43 (2): 321-324.

Rezzoug, A., K. Diethard and T. Triantafyllidis. 2002. Scaling laws for centrifuge modeling of capillary rise in sandy soils. **J. Geotech. Geoenviron. Eng.** 130 (6): 615-620.

Rogowski, A.S. 1971. Watershed physics: model of the soil moisture characteristic. **Water Resour. Res.** 7: 1575-1582.

Rungruang, S. and C. Kererat. 2010. **Contaminant migration behavior through soil cement barrier under full scale test**. Research Report, Rajamangala University of Technology Rattanakosin, Nakorn Pathom.

Schiegg, H.O. 1990. Laboratory set up and results of experiments on two-dimensional multiphase flow in porous media. **Technical Report PNL-74-53**. Pacific Northwest Laboratory, Richland, WA.

Schofield, A.N. 1980. Cambridge geotechnical centrifuge operations. **Géotechnique** 30: 227-268.

_____. 1995. Foreword, pp. vi-x. *In*: R.N. Taylor, ed. **Geotechnical Centrifuge Technology**. Chapman and Hall, London.

Schroth, M. H., J.D lstok, S.J. Ahearn and J.S. Selker. 1995. Geometry and position of light nonaqueous-phase liquid lenses in water wetted porous media. **J. Contam. Hydro.** 19: 269-287.

_____, _____ and J.S. Selker. 1998. Three-phase immiscible fluid movement in the vicinity of textural interfaces. **J. Contam. Hydrol**. 32: 1-23.

Schwille, F. 1988. **Dense chlorinated solvent in porous and fractured media: model experiments**. Translated from the German by Pankow, J.F. Lewis Publishers, Boca Raton, Florida.

Sillers, W.S., D.G. Fredlund and N. Zakerzadeh. 2001. Mathematical attributes of some soil-water characteristic models. **Geotech. Geologic. Eng**. 19: 243-283.

Simpson, M.M., C.S. Willson, J.W. Weaver and R.J. Charbeneau. 1997. Experimental investigation of LNAPL transport in the vadose zone: comparison with the hydrocarbon spill screening model, pp. 410-424. *In* **Proceedings of the Petroleum Hydrocarbons and Organic Chemicals in Ground Water Prevention, Detection and Remediation Conf.,** Houston, Texas.

Smith, J.E. and Z.F. Zhang. 2001. Determining Effective Interfacial Tension and Predicting Finger Spacing for DNAPL Penetration into Water-Saturated Porous Media. **J. Contam. Hydrol.** 48: 167-183

Soga, K., J. Kawabata, C. Kechavarzi, H. Coumoulos and W.A.P. Waduge. 2003. Centrifuge modeling of nonaqueous phase liquid movement and entrapment in unsaturated layered soils. **J. Geotech. Geoenviron. Eng.** 129 (2): 173-182.

Sripongphichit, W. 2006. **Investigation of fossil fuel contamination in unsaturated zone using digital image analysis**. M. Eng. Thesis, Kasetsart University.

Stankovich, J.M. and D.A. Lockington. 1995. Brooks-Corey and van Genuchten soil-water-retention models. **J. Irrig. and Drain. Eng.** 121 (1): 1-7.

Stone, H.L. 1970. Probability Model for Estimating Three-Phase Relative Permeability. **Trans. SPE of AIME** 249: 214-218.

Sutthinun, W. 2010. **Determination of Effective Strength Parameters of Soft Bangkok Clay Using Suction - monitored Unconfined Compression Tests.** M. Eng. Thesis, Univ. of Kasetsart, Bangkok, Thailand.

Tapparnich, J. 2010. **Mechanical behaviour of soil in Laplae area of Uttaradit province with applications to landslide.** M. Eng. Thesis, Kasetsart University.

The Center for Earthquake Engineering Simulation. 1989. **Centrifuge**. Available Source: http://www.nees.rpi.edu/equipment/centrifuge/, February 20, 2013

Thomson, N.R., D.N. Graham and G.J. Farquhar. 1992. One-dimensional immiscible displacement experiments. **J. Contam. Hydrol.** 10: 197-223.

Tuller, M. and D. Or. 2004. Retention of water in soil and the soil water characteristic curve, pp. 278-289. *.In* D. Hillel, ed. **Encyclopedia of Soils in the Environment**. Vol. 4. Elsevier Ltd., Oxford, U.K.,

Vanapalli, S.K., D.G. Fredlund, D.E. Pufahl and A.W. Clifton. 1996. Model for the prediction of shear strength with respect to soil suction. **Can. Geotech. J.** 33: 379-392.

Van Geel, P.J. and J.F. Sykes. 1994. Laboratory and model simulations of a LNAPL spill in a variably-saturated sand: 1. Laboratory experiment and image analysis techniques. **J. Contam. Hydrol.** 17: 1-25.

van Genuchten, M.T. 1980. A closed-form equation for predicting the hydraulic conductivity of unsaturated soils. **Soil Sci. Soc. Am. J.** 44: 892-898.

Weaver, J.W. and R.J. Charbeneau. 2000. A screening approach to fuel hydrocarbon spill assessment, groundwater contamination by organic pollutants: analysis and remediation, ASCE manuals and reports on engineering practice. **Am. Soc. Civ. Eng.** 100: 41-78.

Williams,J., R.E. Prebble, W.T. Williams and C.T. Hignett. 1983. The influence of texture, structure and clay mineralogy on the soil moisture characteristic. **Aust. J. Soil Res.** 21: 15-32.

Wipfler, E.L., M. Ness, G.D. Breedveld, A. Marsman and S.E.A.T.M. Van Der Zee. 2004. Infiltration and redistribution of LNAPL into unsaturated layered porous media. **J. Contam. Hydrol.** 71: 47-66.

Yang, D.S. 1994. The Applications of Soil Mix Walls in the United States. **Geotechnical News** December (1994): 44-47.

Yu, Y., J. Pu, K. Ugai and T. Hara. 1999. A study on the permeability of soil-cement mixture. **Soil and Foundation** 39 (5): 145-149.

Zapata,C.E., W.N. Houston, S.L. Houston and K.D. Walsh. 2000. Soil-water characteristic curve variability. **Advances in unsaturated geotechnics**. 84-124.

Zhou, J. and J.Y. Yu. 2005. Influences affecting the soil-water characteristic curve. **J. Zhejiang Univ. SCI.** 6A (8): 797-804.

APPENDICES

Appendix A

Suction Test Monitoring

Appendix Table A1 Suction test monitoring for poorly-graded sandy soil (Chonburi)

RAJAMANGALA UNIVERSITY OF TECHNOLOGY RATTANAKOSIN
WANG KLAI KANGWON COMPUS

SOIL WATER CHARACTERISTIC CURVE

Project	Thesis	**SOIL SPECIMEN MEASUREMENTS**		
Location	-	Sample Diameter	62.55	mm
Date	25/2/2010	Sample Thickness	39.70	mm
Test No.	AFS35	Natural Water Content	24.50	%
Tested By	Chusak Kererat			
Sample Depth	-			

Date	Sample	Diameter (average) (mm)	Thickness (average) (mm)	Wet Soil Mass (g)	Suction (kPa)	Void Ratio e	Degree of Saturation S_r (%)	Volumetric Water Content $\theta = V_w/V$ (%)
25/2/2010	Initial	62.55	39.70	253.19	1.08	0.707	93.20	38.60
1/3/2010	1 drying	62.55	39.57	250.80	2.00	0.701	89.20	36.80
8/3/2010	2 drying	62.55	39.43	247.63	1.69	0.695	83.60	34.30
12/3/2010	3 drying	62.55	39.03	244.37	2.62	0.678	79.00	31.90
16/3/2010	4 drying	62.55	39.45	241.46	2.15	0.696	71.10	29.20

Appendix Table A1 (Continued)

Date	Sample	Diameter (average) (mm)	Thickness (average) (mm)	Wet Soil Mass (g)	Suction (kPa)	Void Ratio e	Degree of Saturation S_r (%)	Volumetric Water Content $\theta = V_w/V$ (%)
20/3/2010	5 drying	62.55	38.97	238.75	2.77	0.675	67.70	27.30
23/3/2010	6 drying	62.55	39.46	236.41	2.62	0.697	60.90	25.00
28/3/2010	7 drying	62.55	39.27	226.61	3.85	0.688	41.70	17.00
3/4/2010	8 drying	62.55	39.28	221.81	4.15	0.689	31.90	13.00
15/4/2010	9 drying	62.55	39.48	213.53	17.85	0.697	14.90	6.10
29/4/2010	10 drying	62.55	38.82	212.81	42.15	0.669	14.10	5.60
6/5/2010	1 wetting	62.55	39.07	213.15	23.38	0.680	14.50	5.90
22/5/2010	2 wetting	62.55	39.09	214.81	9.08	0.681	17.90	7.30
23/5/2010	3 wetting	62.55	38.62	217.74	4.92	0.660	24.70	9.80
25/6/2010	4wetting	62.55	39.00	223.11	3.23	0.677	35.20	14.20
6/7/2010	5 wetting	62.55	38.89	228.85	2.46	0.672	47.40	19.00
12/7/2010	6 wetting	62.55	39.46	239.14	2.00	0.696	66.40	27.30
14/7/2010	7 wetting	62.55	38.49	249.99	0.92	0.655	93.80	37.10
16/7/2010	8 wetting	62.55	38.33	250.90	0.77	0.648	96.80	38.10

Appendix Table A2 Suction test monitoring for silty sandy soil (Huahin)

RAJAMANGALA UNIVERSITY OF TECHNOLOGY RATTANAKOSIN
WANG KLAI KANGWON COMPUS

SOIL WATER CHARACTERISTIC CURVE

Project	Thesis	**SOIL SPECIMEN MEASUREMENTS**		
Location	-	Sample Diameter	62.55	mm
Date	8/3/2010	Sample Thickness	40.30	mm
Test No.	HH	Natural Water Content	25.00	%
Tested By	Chusak Kererat			
Sample Depth	1 m			

Date	Sample	Diameter (average) (mm)	Thickness (average) (mm)	Wet Soil Mass (g)	Suction (kPa)	Void Ratio e	Degree of Saturation S_r (%)	Volumetric Water Content $\theta = V_w/V$ (%)
8/3/2010	Initial	62.55	40.30	263.86	0.97	0.684	99.40	40.40
12/3/2010	1 drying	62.55	40.17	261.92	2.10	0.678	69.40	38.90
16/3/2010	2 drying	62.55	39.62	257.41	3.39	0.655	90.40	35.80
20/3/2010	3 drying	62.55	39.88	254.39	4.35	0.667	82.70	33.10
23/3/2010	4 drying	62.55	39.62	245.85	4.68	0.656	66.40	26.30

Appendix Table A2 (Continued)

Date	Sample	Diameter (average) (mm)	Thickness (average) (mm)	Wet Soil Mass (g)	Suction (kPa)	Void Ratio e	Degree of Saturation S_r (%)	Volumetric Water Content $\theta = V_w/V$ (%)
28/3/2010	5 drying	62.55	39.62	232.93	7.74	0.656	39.60	15.70
3/4/2010	6 drying	62.55	39.67	227.35	10.32	0.657	27.90	11.10
10/4/2010	7 drying	62.55	39.69	224.73	22.10	0.658	22.50	8.90
29/4/2010	8 drying	62.55	39.27	223.17	49.19	0.641	19.80	7.70
6/5/2010	1 wetting	62.55	39.50	223.61	31.13	0.650	20.40	8.00
22/5/2010	2 wetting	62.55	39.22	224.65	16.61	0.639	23.00	9.00
23/5/2010	3 wetting	62.55	39.43	226.35	9.84	0.647	26.20	10.30
17/6/2010	4 wetting	62.55	39.50	236.24	5.00	0.650	46.80	18.40
5/7/2010	5 wetting	62.55	39.79	247.66	3.23	0.663	69.40	27.60
7/7/2010	6 wetting	62.55	39.89	257.43	2.42	0.667	88.90	35.50
12/7/2010	7 wetting	62.55	39.79	260.78	1.61	0.663	96.30	38.40
14/7/2010	8 wetting	62.55	39.86	262.71	0.48	0.666	99.80	39.90

Appendix Table A3 Suction test monitoring for Chonburi sandy soil mixed cement

RAJAMANGALA UNIVERSITY OF TECHNOLOGY RATTANAKOSIN
WANG KLAI KANGWON COMPUS

SOIL WATER CHARACTERISTIC CURVE

Project	Thesis	**SOIL SPECIMEN MEASUREMENTS**		
Location:	-	Sample Diameter	62.48	mm
Date	31/7/2010	Sample Thickness	41.47	mm
Test No.	SCC	Natural Water Content	25.20	%
Tested By	Chusak Kererat			
Sample Depth	-			

Date	Sample	Diameter (average) (mm)	Thickness (average) (mm)	Wet Soil Mass (g)	Suction (kPa)	Void Ratio e	Degree of Saturation S_r (%)	Volumetric Water Content $\theta = V_w/V$ (%)
31/7/2010	Initial	62.48	41.47	266.05	1.23	0.787	86.00	37.90
7/8/2010	1 drying	62.48	41.66	263.95	13.38	0.795	81.40	36.00
13/8/2010	2 drying	62.48	41.45	261.71	23.69	0.786	78.30	34.50
21/8/2010	3 drying	62.48	41.53	259.64	36.46	0.790	74.20	32.80
24/8/2010	4 drying	62.48	41.64	257.64	53.69	0.794	70.30	31.10

Appendix Table A3 (Continued)

Date	Sample	Diameter (average) (mm)	Thickness (average) (mm)	Wet Soil Mass (g)	Suction (kPa)	Void Ratio e	Degree of Saturation S_r (%)	Volumetric Water Content $\theta = V_w/V$ (%)
4/9/2010	5 drying	62.48	41.55	250.45	76.00	0.790	57.80	25.50
8/9/2010	6 drying	62.48	41.45	248.97	79.38	0.786	55.50	24.40
16/9/2010	7 drying	62.48	41.68	247.70	80.31	0.796	52.60	23.30
10/10/2010	1 wetting	62.48	41.56	251.53	60.31	0.791	59.70	26.40
17/10/2010	2 wetting	62.48	41.54	255.55	55.85	0.790	66.90	29.50
2/11/2010	3 wetting	62.48	41.39	259.16	14.62	0.783	74.00	32.50
7/11/2010	4 wetting	62.48	41.45	261.46	4.00	0.786	77.90	34.30
10/11/2010	5 wetting	62.48	41.53	262.34	1.69	0.789	79.10	34.90

Appendix Table A4 Suction test monitoring for Huahin sandy soil mixed cement

RAJAMANGALA UNIVERSITY OF TECHNOLOGY RATTANAKOSIN
WANG KLAI KANGWON COMPUS

SOIL WATER CHARACTERISTIC CURVE

Project	Thesis	**SOIL SPECIMEN MEASUREMENTS**		
Location	-	Sample Diameter	63.04	mm
Date	25/7/2010	Sample Thickness	39.85	mm
Test No.	SCH	Natural Water Content	26.80	%
Tested By	Chusak Kererat			
Sample Depth	-			

Date	Sample	Diameter (average) (mm)	Thickness (average) (mm)	Wet Soil Mass (g)	Suction (kPa)	Void Ratio e	Degree of Saturation S_r (%)	Volumetric Water Content $\theta = V_w/V$ (%)
25/7/2010	Initial	63.04	39.85	253.48	2.26	0.847	84.80	38.90
31/7/2010	1 drying	63.04	39.51	251.47	27.26	0.831	82.80	37.60
7/8/2010	2 drying	63.04	39.62	249.52	37.10	0.837	78.80	35.90
13/8/2010	3 drying	63.04	39.65	247.79	51.45	0.838	75.70	34.50
21/8/2010	4 drying	63.04	39.54	246.16	60.97	0.833	73.20	33.30

Appendix Table A4 (Continued)

Date	Sample	Diameter (average) (mm)	Thickness (average) (mm)	Wet Soil Mass (g)	Suction (kPa)	Void Ratio e	Degree of Saturation S_r (%)	Volumetric Water Content $\theta = V_w/V$ (%)
24/8/2010	5 drying	63.04	39.58	244.64	67.42	0.835	70.40	32.00
4/9/2010	6 drying	63.04	39.40	239.98	89.19	0.827	62.70	28.40
16/9/2010	7 drying	63.04	39.72	238.77	96.61	0.841	59.40	27.20
10/10/2010	1 wetting	63.04	39.82	243.86	63.55	0.846	68.00	31.20
17/10/2010	2 wetting	63.04	39.73	247.88	50.48	0.841	75.50	34.50
25/10/2010	3 wetting	63.04	39.35	250.84	13.39	0.824	82.40	37.20
2/11/2010	4 wetting	63.04	39.44	252.08	2.90	0.828	84.30	38.20

Appendix B

SWCC curves fitting by van Genuchten Model

Appendix Table B1 SWCC curve fitting for poorly-graded sandy soil (Chonburi)

VG Parameters		Drying Process		Wetting Process	
		Suction (cm)	VWC (%)	Suction (cm)	VWC (%)
For Drying		0.000000001	38.833051	0.000000001	38.50781
θr	0.057063471	0.1	38.833051	0.1	38.50781
θs	0.388330509	0.5	38.833050	0.5	38.50780
α	0.033415226	1	38.833041	1	38.50763
n	4.354162624	5	38.822504	5	38.41284
m	0.770334715	10	38.618862	10	37.15877
		15	37.624672	15	32.97808
For Wetting		20	35.002528	20	26.35029
θr	0.057063471	30	25.047947	30	15.34763
θs	0.385078093	40	16.039700	40	10.35527
α	0.048166043	50	11.182528	50	8.22205
n	3.894531715	80	6.917621	80	6.36477
m	0.743229720	100	6.283164	100	6.05226
		150	5.854888	150	5.81346
		200	5.762970	200	5.75294
		300	5.720882	300	5.72076
		500	5.708967	500	5.70963
		1000	5.706603	1000	5.70679
		10000	5.706347	10000	5.70635
		100000	5.706347	100000	5.70635
		1000000	5.706347	1000000	5.70635
		10000000	5.706347	10000000	5.70635

Appendix Table B2 SWCC curve fitting for silty sandy soil (HuaHin)

VG Parameters		Drying Process		Wetting Process	
		Suction (cm)	VWC (%)	Suction (cm)	VWC (%)
For Drying		0.000000001	40.13785	0.000000001	40.11051
θr	0.081492723	0.1	40.13785	0.1	40.11051
θs	0.401378465	0.5	40.13785	0.5	40.11051
α	0.019840116	1	40.13784	1	40.11044
n	4.109197168	5	40.13603	5	40.08676
m	0.756643461	10	40.10645	10	39.83128
		15	39.97252	15	38.96235
For Wetting		20	39.60587	20	37.13242
θr	0.082543841	30	37.53712	30	30.75398
θs	0.401105136	40	33.12671	40	23.69836
α	0.029168859	50	27.31816	50	18.48373
n	3.569339268	80	14.99327	80	11.74436
m	0.719836100	100	11.78640	100	10.25832
		150	9.21752	150	8.96989
		200	8.58858	200	8.59686
		300	8.27407	300	8.37534
		500	8.17478	500	8.28695
		1000	8.15223	1000	8.25987
		10000	8.14927	10000	8.25440
		100000	8.14927	100000	8.25438
		1000000	8.14927	1000000	8.25438
		10000000	8.14927	10000000	8.25438

Appendix Table B3 SWCC curve fitting for Chonburi sandy soil mixed cement

VG Parameters		Drying Process		Wetting Process	
		Suction (cm)	VWC (%)	Suction (cm)	VWC (%)
For Drying		0.000000001	40.13785	0.000000001	40.11051
θr	0	0.1	40.13785	0.1	40.11051
θs	0.369532313	0.5	40.13785	0.5	40.11051
α	0.001335811	1	40.13784	1	40.11044
n	2.045079702	5	40.13603	5	40.08676
m	0.511021503	10	40.10645	10	39.83128
		15	39.97252	15	38.96235
For Wetting		20	39.60587	20	37.13242
θr	0	30	37.53712	30	30.75398
θs	0.345244267	40	33.12671	40	23.69836
α	0.001355301	50	27.31816	50	18.48373
n	2.038083850	80	14.99327	80	11.74436
m	0.509343053	100	11.78640	100	10.25832
		150	9.21752	150	8.96989
		200	8.58858	200	8.59686
		300	8.27407	300	8.37534
		500	8.17478	500	8.28695
		1000	8.15223	1000	8.25987
		10000	8.14927	10000	8.25440
		100000	8.14927	100000	8.25438
		1000000	8.14927	1000000	8.25438
		10000000	8.14927	10000000	8.25438

Appendix Table B4 SWCC curve fitting for HuaHin sandy soil mixed cement

VG Parameters		Drying Process		Wetting Process	
		Suction (cm)	VWC (%)	Suction (cm)	VWC (%)
For Drying		0.000000001	38.82536	0.000000001	37.90781
θr	0	0.1	38.82536	0.1	37.90781
θs	0.388253645	0.5	38.82536	0.5	37.90781
α	0.001001965	1	38.82535	1	37.90780
n	2.071044892	5	38.82502	5	37.90749
m	0.517151944	10	38.82391	10	37.90644
		15	38.82200	15	37.90458
For Wetting		20	38.81926	20	37.90187
θr	0	30	38.81123	30	37.89382
θs	0.379078109	40	38.79973	40	37.88213
α	0.001073226	50	38.78469	50	37.86667
n	2.114040831	80	38.71797	80	37.79698
m	0.526972239	100	38.65528	100	37.73063
		150	38.43479	150	37.49409
		200	38.12506	200	37.15765
		300	37.25770	300	36.20563
		500	34.75293	500	33.44628
		1000	27.10068	1000	25.25578
		10000	3.27541	10000	2.68526
		100000	0.27932	100000	0.20723
		1000000	0.02372	1000000	0.01594
		10000000	0.00201	10000000	0.00123

Appendix C

k-function curves fitting by Jackson Model

Appendix Table C1 k-function curve fitting for poorly-graded sandy soil (Chonburi)

Hydraulic Conductivity (cm/s)	VWC (%)
38.833051	0.023225000
36.182915	0.016392548
32.870244	0.010507850
29.557574	0.006488131
26.244903	0.003787228
22.932233	0.002041829
19.619563	0.000981403
16.306892	0.000395343
12.994222	0.000117483
9.681552	0.000018105
6.368881	0.000000151

Appendix Table C2 k-function curve fitting for silty sandy soil (Huahin)

Hydraulic Conductivity (cm/s)	VWC (%)
40.137846	0.001792600
37.578761	0.001258301
34.379903	0.000804422
31.181046	0.000496414
27.982188	0.000290142
24.783331	0.000156968
21.584473	0.000075926
18.385616	0.000030912
15.186759	0.000009347
11.987901	0.000001482
8.789044	0.000000013

Appendix Table C3 k-function curve fitting for Chonburi sandy soil mixed cement

Hydraulic Conductivity (cm/s)	VWC (%)
36.953231	0.000000140
33.996973	0.000000070
30.301650	0.000000034
26.606327	0.000000016
22.911003	0.000000007
19.215680	0.000000003
15.520357	0.000000001
11.825034	0.000000000
8.129711	0.000000000
4.434388	0.000000000
0.739065	0.000000000

Appendix Table C4 k-function curve fitting for HuaHin sandy soil mixed cement

Hydraulic Conductivity (cm/s)	VWC (%)
38.825364	0.000000038
35.719335	0.000000019
31.836799	0.000000009
27.954262	0.000000004
24.071726	0.000000002
20.189190	0.000000001
16.306653	0.000000000
12.424117	0.000000000
8.541580	0.000000000
4.659044	0.000000000
0.776507	0.000000000

CIRRICULUM VITAE

NAME : Mr. Chusak Kererat

BIRTH DATE : March 29, 1974

BIRTH PLACE : Trang, Thailand

EDUCATION :

YEAR	**INSTITUTE**	**DEGREE/DIPLOMA**
1995	Rajamangala Inst. of Tech.	B.Eng.(Civil Eng.)
2000	King Mongkut Inst. of Tech. Thonburi	M.Eng.(Civil Eng.)
2014	Kasetsart University	D.Eng. (Civil Eng.)

POSITION/TITLE : Lecturer

WORKPLACE : Rajamangala University of Technology Rattanakosin Wangklaikangwon Campus

SCHOLARSHIP/AWARDS : The program Strategic Scholarships for Frontier Research Network for the Joint Ph.D. Program Thai Doctoral degree from The Office of the Higher Education Commission, Thailand (2007-2011)